Integrated Circuit / Microfluidic Chips for

Dielectric Manipulation

A THESIS PRESENTED

BY

THOMAS HUNT

TO

THE DEPARTMENT OF PHYSICS

IN PARTIAL FULFILLMENT OF THE REQUIREMENTS

FOR THE DEGREE OF

DOCTOR OF PHILOSOPHY

IN THE SUBJECT OF

PHYSICS

HARVARD UNIVERSITY

CAMBRIDGE, MASSACHUSETTS

MAY 2007

Abstract

Integrated Circuit / Microfluidic Chips for Dielectric Manipulation

Thomas Peter Hunt   **Advisor: Robert M. Westervelt**

This thesis describes the development of integrated circuit / microfluidic chips to move individual living cells and chemical droplets along programmable paths with dielectrophoresis (DEP). The complexity of cellular and molecular biology demands powerful research techniques. Integrated circuits (ICs) offer high bandwidth, massive parallelism, submicron features, built in programmability and superb control of local electric fields. At the same time, microfluidics provide a suitable environment for both living cells and biochemistry. Our IC / microfluidic chip is an exciting technology capable of simultaneously and independently controlling the location of thousands of objects such as cells and chemical droplets.

Dielectrophoresis is the movement of a particle in a non-uniform electric field due to the induced dipole moment of the particle relative to the surrounding medium. By applying an appropriate local electric field, any particle with a dielectric constant different than the surrounding medium can be manipulated with DEP.

We initially fabricated an array of microscale post-shaped electrodes to provide an inhomogeneous electric field at the bottom of a microfluidic channel. The voltage on each electrode was independently controlled by a computer to trap and move cells and particles in fluid above the micropost electrodes. We subsequently designed an IC chip consisting of 256 x 128 metal pixels, 11 μm square, with built in control circuits for energizing each pixel to 5 V at frequencies from DC to 1.8 MHz. The chip was built in a commercial foundry and we fabricated a microfluidic channel on its top surface. By shifting the location of energized pixels, electric fields were generated to move yeast and mammalian cells through the microfluidic channel at 30 μm per second. Complex electric field patterns were generated to simultaneously move thousands of individual cells. The chip was capable of translating, splitting, and mixing pL water droplets in oil.

In addition to the IC / microfluidic system, we have developed a PDMS microfluidic device that sorts pL drops of water in oil at 1.6 kHz with DEP and a device for separating magnetically tagged bacteria from whole blood at 10k cells per second. We have also built a DEP trap integrated into the tip of a scanning probe for cell and nanoparticle manipulation.

Table of Contents

Acknowledgements

I wish to offer my heartfelt thanks to the dozens of people that have helped me along the path to my PhD. I would not be alive to write this without the nurses and doctors at Dana Farber and the cancer researchers that preceded them.

Bob Westervelt, thank you for being an outstanding advisor. You combine a positive attitude with deep understanding and good ideas. You supported me throughout my work, and I look forward to asking your advice in the years to come.

Thanks to all of the other professors that have taken time to teach and mentor me, Donhee Ham, Kit Parker, Dave Weitz, Howard Stone, John Doyle, Don Ingber, Mike Tinkham and of course Rick Rodgers. Charles Kerbage and Shanon Xia, it was a pleasure collaborating with you.

The exceptional staff members here at Harvard helped in countless ways to make my life enjoyable and my experiment a success: Naomi, Shelia, Steve, Stan, Jim, Billy, and Ralph. Thank you for going beyond the call of duty and treating every student like a friend.

My time here spanned two generations of graduate students. It was a pleasure to learn alongside Andy, Ania, Hakho, Kathy, and Parisa. I wish the best of luck to the students that continue. Dave, Erin, Halvar, Keith, and Melaku: keep fighting the good fight. Cheers to the undergrads that I have worked with, especially Jonathan and Onjgen.

Thanks to my family, especially my new wife Lauren: your support has immeasurable value. Family Dinner in all of its myriad incarnations deserves partial credit for preserving my sanity. Finally, I would like to thank the Boston weather which kept me indoors with my experiments for nine months of each year. It is the one thing about my time at Harvard that I will never miss.

Abbreviations and Symbols

a	particle radius
AC	alternating current
AFM	atomic force microscope
C_{mem}	specific membrane capacitance
CNS	center for Nanoscale systems
CMOS	Complimentary Metal Oxide Silicon
DC	direct current
DEP	dielectrophoresis
EHD	electrohydrodynamic
$\bar{E}$	electric field vector
E_{rms}	root mean squared electric field magnitude
$\bar{F}_{DEP}$	dielectrophoresis force vector
$\bar{F}_{DEP}^{Max}$	maximum dielectrophoresis force vector
g	acceleration due to gravity
GFP	green fluorescent protein
G_{mem}	specific membrane conductance
GND	ground voltage = 0
HF	hydrofluoric acid
HGMC	high-gradient magnetic field concentrator
I/O	input / output
IC	integrated Circuit
k	Boltzmann constant
l_e	characteristic electrode length
MRI	magnetic resonance imaging
mRNA	messenger RNA
nDEP	negative (minimum field seeking) dielectrophoresis
NI	national instruments
NiFe	nickel / iron
NMOS	n-channel metal oxide silicon field effect transistor

NMR	nuclear magnetic resonance
$\bar{P}$	electric polarization vector
PBS	phosphate buffered saline
pDEP	positive (maximum field seeking) dielectrophoresis
PDMS	Poly(dimethylsiloxane)
PMOS	p-channel metal oxide silicon field effect transistor
RBC	red blood cell
Re	Reynolds number
r_{min}	minimum particle radius
S	siemen $(1/\Omega)$
S	entropy
SRAM	static random access memory
T	temperature
Ti-Au	titanium - gold
U	energy
USB	universal serial bus
UV	ultraviolet
V	voltage
V_{dd}	positive power supply voltage
V_{gs}	transistor gate – source voltage
V_{sd}	transistor source – drain voltage
V_{tm}	transmembrane voltage
$\vec{v}$	velocity vector
α	polarizability
ε_{cyto}	Cytoplasm permittivity
ε_m	real permittivity (of medium)
$\hat{\varepsilon}_p$	complex permittivity (of particle)
η	fluid viscosity
ρ	density
σ	conductivity
σ_{cyto}	Cytoplasm conductivity
τ_{mw}	Maxwell-Wagner relaxation time
ω	radian frequency

List of Figures

List of Tables

Chapter 1.   Introduction

1.1   Motivation and Background

This thesis describes the development of integrated circuit (IC) / microfluidic chips for moving microscopic objects in liquid with dielectrophoresis (DEP). We used the IC / microfluidic chip to move cells and chemical droplets along programmable paths, demonstrating versatile, parallel micromanipulation with exciting applications for biomedical science.

An IC / microfluidic chip, shown schematically in Figure 1.1, combines the power and programmability of ICs with the biocompatablity of microfluidics in a system capable of performing intricate manipulation and analysis on single cells and small chemical volumes. Integrated circuits offer high bandwidth, submicron features, built in programmability and fine control of local electric fields. At the same time, microfluidics provide a suitable environment for both living cells and biochemistry.

Microfluidic Channel — Provides an environment for living cells and pL biochemical drops

IC chip — Grants programmability, speed, parallelism, precise production and detection of electric and magnetic fields.

Hybrid IC / microfluidic chips combine the power of electronics and the biocompatability of microfluidics to create versatile, programmable experimental platforms.
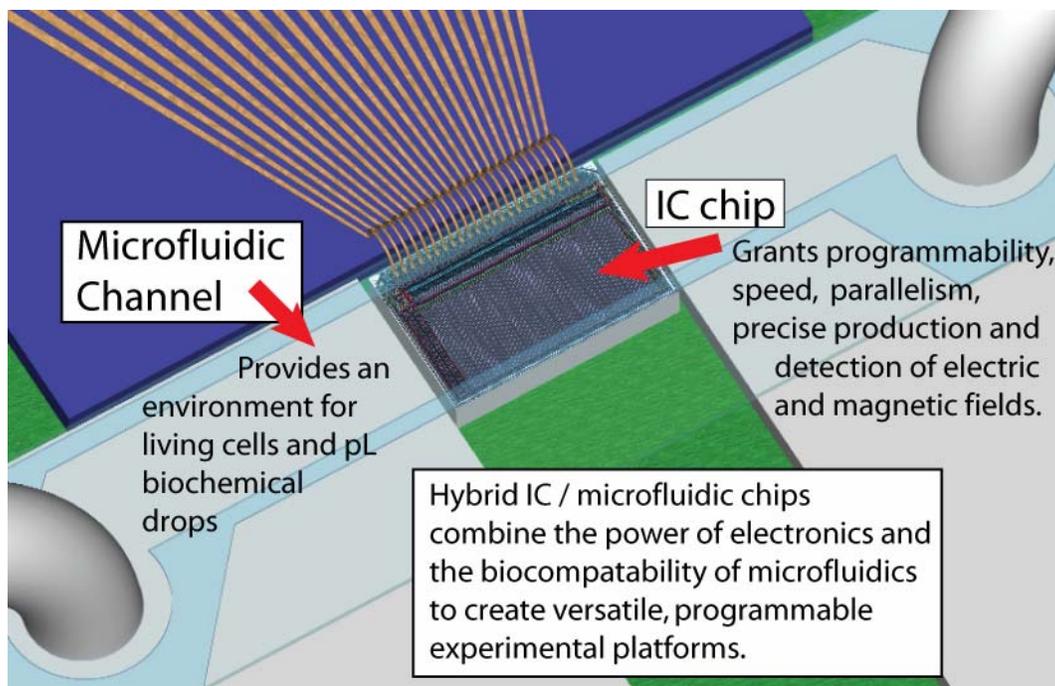
Figure 1.1 Schematic IC / Microfluidic system. The IC is located beneath the microfluidic channel where electric and magnetic fields from the IC can interact with cells or chemical droplets in the microfluidic channel. An IC can sensitively detect and precisely produce electric fields, magnetic fields, light, and heat while microfluidics provide an environment appropriate for living cells and biochemicals.

There is a clear demand in science and biotechnology for the capabilities that IC / microfludic systems can provide. High throughput DNA sequencing, synthesis, proteomics, and drug discovery all require the manipulation of thousands of pL chemical volumes. Studying statistical numbers of individual cells allows biologists to investigate the stochastic nature of gene expression and cell biology, information that is washed out with traditional methods that examine a large ensemble of cells. In addition, controlling the location of single cells allows us to assemble individual cells of different cell types into sheets of tissue, providing a platform for the study of cell-cell interaction and cellular differentiation.

Microfluidics seeks to address the challenge of parallel, small volume fluid manipulation necessary for genomics, proteomics, drug discovery and basic bioscience (Whitesides, 2006). Thousands of continuous flow microfluidic devices have been built for various biological experiments; one impressive recent example is a fully integrated on-chip DNA sequencer (Blazej et al., 2006). Droplet based microfluidics are an improvement over continuous flow microfluidics (Ahn et al., 2006), confining diffusion to within the droplet and increasing the effective concentration of analyte molecules. Programmable microfluidic systems have been developed with external control electronics for droplet manipulation with electrowetting (Lee et al., 2002; Pollack et al., 2002) and dielectrophoresis (Vykoukal et al., 2001).

Adding ICs directly to microfluidics can greatly enhance the capabilities of microfluidic systems (Lee et al., 2007). The steady miniaturization of transistors since the invention of the IC has made it possible to buy a chip for just a few dollars with nearly one billion 65 nm wide transistors switching at GHz speeds. ICs are capable of detecting and producing micropatterned electric fields, magnetic fields, heat, and light. Hundreds of wires and over a thousand transistors in a modern IC chip can fit in the 10 μm x 10 μm area beneath a single cell or pL chemical droplet. Combining ICs and microfluidics opens up the possibility of programmable detection and manipulation of thousands of individual cells and chemical drops on a single chip. A schematic IC / microfluidic chip is shown in Figure 1.1. An IC is mounted at the bottom of a microfluidic channel, where it can electrically, magnetically, thermally, and optically interact with biological systems in the microfluidic channel.

Several interesting IC / microfluidic chips have been demonstrated in the past few years. IC / microfluidic chips have been built for magnetic manipulation (Lee et al. 2005 & 2006), sensitive electric readout from thousands of cultured neurons (Eversmann et. al, 2003), monitoring live cells as biosensors (DeBusschere and Kovacs, 2001), DEP of cells (Manaresi et al., 2003), capacitive and optical cell detection (Manaresi et al., 2003), droplet manipulation on a surface (Current et. al, 2005), and DNA detection (Thewes et al., 2002).

Out of all of the possibilities for IC / microfluidics systems, we have chosen to develop a DEP manipulator chip. Dielectrophoresis is a versatile manipulation scheme that is well suited for realization in an IC / microfluidic

4

system. By varying the local electric field in space and time, any particle with a dielectric constant different than the surrounding medium can be manipulated with DEP. Dielectrophoresis has been shown to move cells (Pohl and Crane, 1971), nanoparticles(Green and Morgan, 1997), viruses (Green et al., 1997), and single molecules (Hölzel et al., 2005). We used the IC / microfluidic system to move individual cells and drops of water in oil.

Almost all DEP chips rely on a small number of hand-wired electrodes capable of performing a set task, for example, droplet sorting (Ahn et al., 2006). Our vision is to replace the small set of single purpose electrodes with a large array of programmable pixels built into an IC. With an array of programmable pixels, the electric field above the chip surface can be versatile and complex, simultaneously moving thousands of individual particles across the surface of the chip and while adaptively changing the field pattern at any time. Some of the possibilities presented by our IC / microfluidic DEP manipulator chip are shown schematically in Figure 1.2.
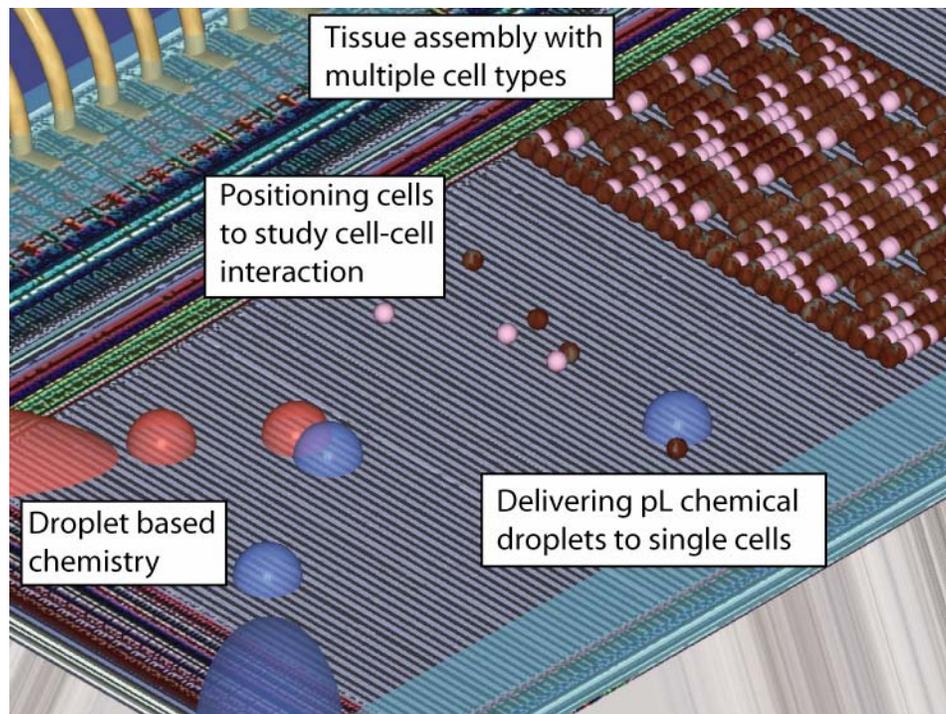
Figure 1.2 IC / Microfluidic DEP manipulator applications. This schematic shows the DEP manipulator chip being used to move and combine chemical droplets, to control the distance between cells for studying cell-cell interaction, to apply pL chemical drops to a single cell, and to assemble tissue from multiple cell types.

IC chips are an excellent electric field source for DEP. Fundamentally, IC chips are designed to generate complex patterns of electric fields. Electric fields produced by IC logic are normally used to modulate the gates of transistors, but these intricate field patterns are equally capable of moving cells and particles with DEP. DEP relies on strong electric field gradients which are easily produced by the submicron spacing between IC electrodes held at different voltages.

On the path to building a CMOS / microfluidic system, we initially fabricated an array of microscale post-shaped electrodes to provide an inhomogeneous electric field at the bottom of a microfluidic channel (Figure 1.3e). The voltage on each electrode was independently controlled by a computer to trap and move cells and particles in fluid above the micropost electrodes. After this successful demonstration, we designed a CMOS chip (Figure 1.3f) consisting of 256 x 128 metal pixels, 11 μm square, capable of being energized to 5 V at frequencies from DC to 1.8 MHz. The chip was built in a commercial foundry and we subsequently fabricated a microfluidic chamber on its top surface. By shifting the location of energized pixels, the array traps and moves cells and particles along programmable paths through the microfluidic chamber. Complex electric fields patterned in space and time were generated to simultaneously move thousands of individual cells at 30 μm per second. The chip was also used to translate, split, and mix pL water droplets in oil.

In addition to the DEP manipulator chip, we constructed several microfluidic devices to address specific biomedical needs. We describe a magnetic separator for removing bacteria from whole blood at 10k cells per

second (Figure 1.3b). Devices based on our magnetic separator could be used to diagnose and treat disease, for example, sepsis. We developed a PDMS microfluidic sorting system to change the path of pL drops of water in oil at 1.6 kHz (Figure 1.3a). The drop sorter was designed to be integrated into a larger droplet-based device for high speed combinatorial chemistry. We constructed DEP tweezers: electrodes that produce a strong field gradient at the tip of a scanning probe for cell and nanoparticle manipulation with DEP (Figure 1.3d). DEP tweezers are useful for precisely positioning single cells in three dimensions, with applications for in vitro fertilization, cell-cell interaction, cell adhesion, embryology, microbiology, stem cell research, and single cell transfection. DEP tweezers on the end of an AFM tip (Figure 1.3c) are designed for pick and place manipulation of nanoparticles in fluid.
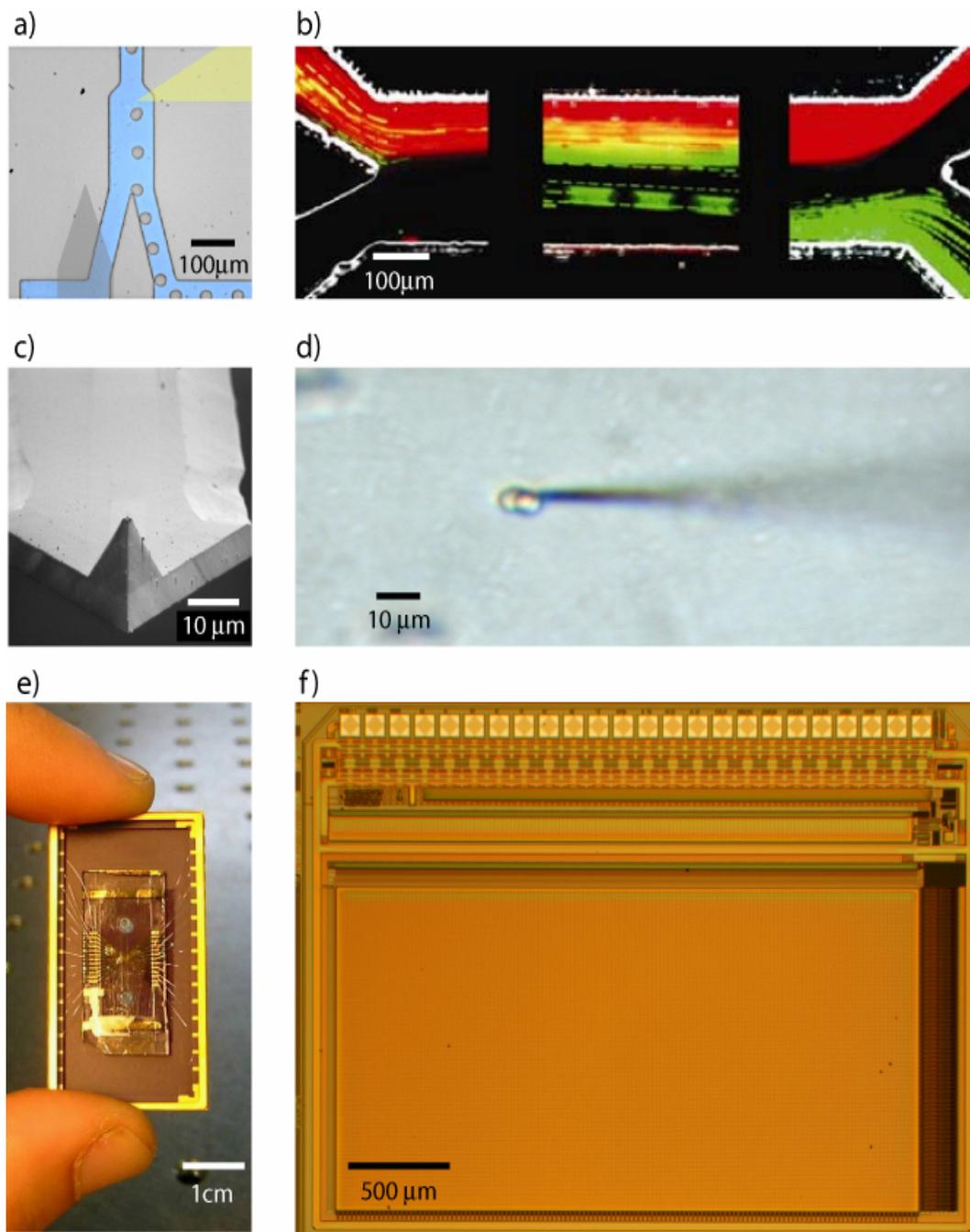
Figure 1.3 Accomplishments described in the thesis. a) high speed DEP drop sorter (Chapter 3), b) micromagnetic separator to remove bacteria from blood (Chapter 3), c) AFM DEP tweezers (Chapter 4), d) DEP tweezers for cell manipulation (Chapter 4), e) Micropost electrode array (Chapter 5), f) IC / microfluidic DEP manipulator chip (Chapters 6 & 7)

1.2   Objectives

This thesis demonstrates the potential of systems that bring together integrated circuits and microfluidics. By combining the power and programmability of integrated circuits with the biocompatibility of microfluidics we hope to pave the way for a new generation of advanced biomedical experiments. Specifically, we have produced a hybrid IC / microfluidic system to move cells and drops of water in oil along programmable paths in a microfluidic chamber. This programmable microfluidic system goes beyond common microfluidic devices that serve a single purpose with a fixed channel geometry. We describe other microfabricated devices for specific applications in biomedicine: a device to separate magnetically tagged bacteria from whole blood, a device for sorting droplets at high speed in a microfluidic system, and a DEP micromanipulator for moving individual cells and nanoparticles.

1.3   Overview of the Thesis

In Chapter 2, we describe the theory behind DEP. We discuss specific considerations for DEP applied to biology and fundamental limitations to particle trapping and manipulation. Chapter 3 describes a device that we constructed to remove magnetically tagged bacteria from blood, and a high speed DEP drop sorter. DEP tweezers for cell and nanoparticle manipulation are covered in Chapter 4. Chapter 5 discusses an array of electrodes for DEP manipulation, built in the CNS cleanroom. Chapter 6 explains the design of the IC / microfluidic system for DEP. Chapter 7 presents the manipulation of yeast cells, mammalian cells, and water drops with our IC / microfluidic chip. The thesis concludes, and future research directions are illustrated in Chapter 8.

Chapter 2.   Theory of Dielectric Manipulation

Dielectrophoresis (DEP) is the movement of a particle in a non-uniform electric field due to the induced dipole moment of the particle relative to the surrounding medium (Pohl, 1978). DEP is best implemented in microsystems which produce high electric field gradients and manipulate particles at low Reynolds numbers. In this chapter, we will discuss the theory and scaling of DEP for particle manipulation, as well as fundamental limitations of DEP and specific considerations for DEP in biology.

2.1   Overview of Dielectrophoresis

The force on an electric dipole in an electric field is:

$$\vec{F}_{DEP} = (\vec{P} \cdot \nabla)\vec{E} , \qquad\qquad (2.1)$$

where $\vec{P}$ is the dipole moment of the particle relative to the surrounding medium and $\vec{E}$ is the external electric field.

Assuming a linear dielectric particle with polarizability ($\vec{P} = \alpha \vec{E}$) in an AC field, the DEP force time averaged over the AC cycle is:

$$\vec{F}_{DEP} = \frac{\alpha}{2}\nabla E_{rms}^2 , \qquad\qquad (2.2)$$

where E_{rms} the root mean squared magnitude of the electric field. Note that the DEP force does not act along electric field lines, but rather in the direction of the gradient of the electric field squared.

There are several important reasons to use AC fields for DEP. In a conductive medium, AC fields of sufficient frequency (> 10 kHz) do not suffer from ionic screening or electrode polarization: ions cannot move fast enough to screen the applied field. The movement of particles due to net charge (electrophoresis) will time average to zero in an AC field and electroosmotic flow of the double layer along liquid – solid boundaries is eliminated. Another benefit of AC fields is to reduce the voltage across the capacitive membrane of a cell which we will discuss in Section 2.3.2.

The DEP force will act to move a particle in liquid against fluid drag. In microsystems, inertia is very small compared to viscous forces: typical Reynolds numbers are on the order of 10^{-3}. For laminar flow, (Re < 2000), the drag on a sphere is

$$\vec{F}_{drag} = 6\pi \eta \, a \, \vec{v} \, , \tag{2.3}$$

where η is the dynamic viscocity of the medium, a the radius of the sphere and v the velocity of the sphere relative to the medium. Low Reynolds number also allows us to ignore particle acceleration in our equations of motion because particles typically reach terminal velocity on a timescale of a few µs.

To determine the movement of a particle from Equation 2.3 and 2.4, we need to take a closer look at the polarization of a spherical particle relative to the surrounding medium. Particles and media with finite conductivity σ have complex permittivity $\hat{\varepsilon}$ that changes with frequency ω: $\hat{\varepsilon} = \varepsilon - i\sigma/\omega$

Solving the Laplace Equation for a conductive sphere in a conductive medium (Jones, 1995),

$$\bar{F}_{DEP}(\omega) = 2\pi\varepsilon_m a^3 CM(\omega)\nabla E_{rms}^2 , \qquad (2.4)$$

where a is the radius of the particle, ε_m is the medium permittivity, and $CM(\omega)$ is the Clausius-Mossotti factor, a relation between the frequency dependent complex permittivity of the particle and the medium.

$$CM(\omega) = \text{Re}\left[\frac{\hat{\varepsilon}_p - \hat{\varepsilon}_m}{\hat{\varepsilon}_p + 2\hat{\varepsilon}_m}\right], \qquad (2.5)$$

$\hat{\varepsilon}_p$ and $\hat{\varepsilon}_m$ are the complex permittivity of the particle and medium respectively.

$CM(\omega)$ can vary between -0.5 and 1 with important physical implications shown in Figure 2.1. When $CM(\omega) < 0,$ the fluid is more polarizable than the particle, and the particle is pulled toward the local minimum of the electric field. This is called negative DEP (nDEP). Positive DEP (pDEP) occurs when the particle is more polarizable than the fluid, $CM(\omega) > 0$, and the particle is pulled to the maximum of the electric field.

At low frequency, $CM(\omega)$ is dominated by conductivity, while at high frequency permittivity dominates $CM(\omega)$. The relevant interfacial Maxwell-Wagner relaxation time is

$$\tau_{mw} = \frac{\varepsilon_p + 2\varepsilon_m}{\sigma_p + 2\sigma_m} \, .$$

(2.6)

By controlling the electric field frequency, fluid conductivity, and electric field distribution, it is possible to trap a given particle with either nDEP or pDEP.

To trap a particle with nDEP, planar electrodes require confinement in the Z-direction. Confinement can be produced by image charges from a conductive coverslip, a physical boundary, or by gravitational force on the particle. The force due to gravity is $F_{gravity} = \frac{4}{3}\pi(\rho_p - \rho_m)a^3 g :\sim 0.1\,\text{pN}$ for cells.
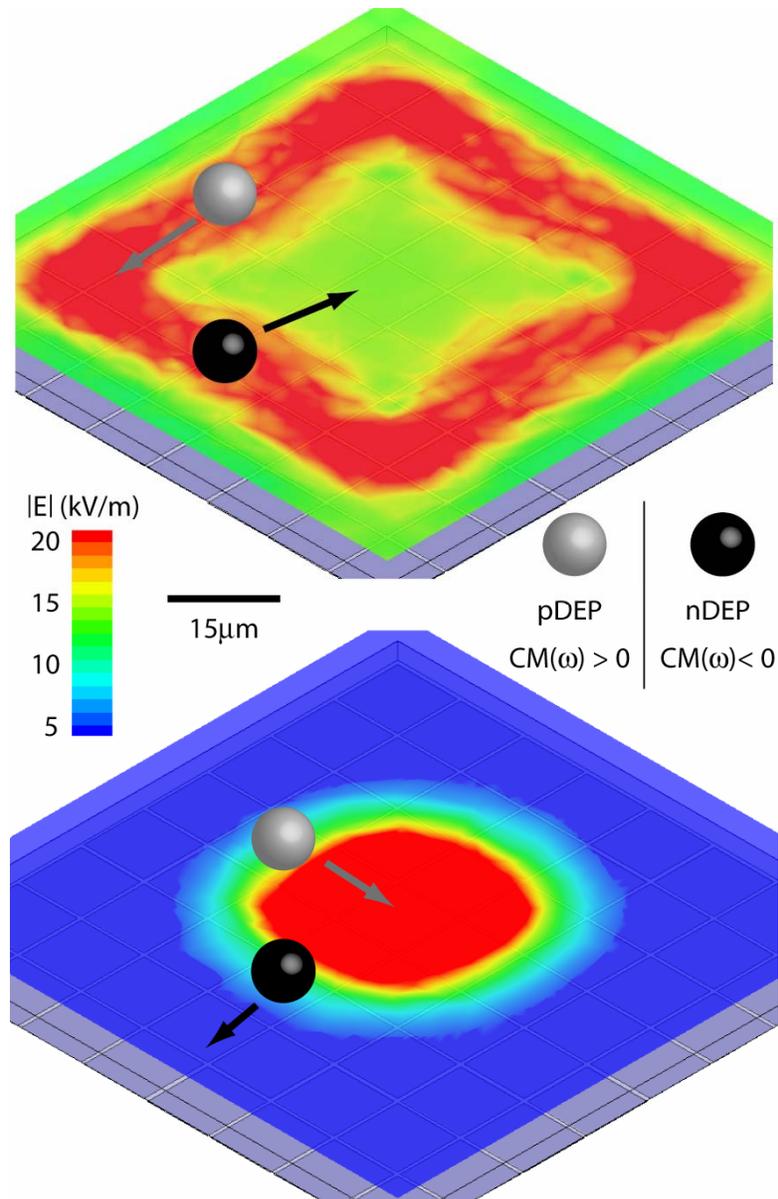
Figure 2.1 Electric field simulations of nDEP and pDEP traps. When CM(ω) > 0 a particle (gray) undergoes pDEP and is attracted to the maximum of the electric field. When CM(ω) < 0 , a particle (black) undergoes nDEP and is attracted to the minimum of the electric field. The upper and lower electric field simulations show trap geometries appropriate for nDEP and pDEP trapping, respectively.

We are interested in manipulating not just uniform particles, but also cells. The capacitive cell membrane has a significant effect on the dielectric function of a cell. We include a thin cell membrane in our model of the CM factor of a cell (Jones, 1995), obtaining the effective complex permittivity of the cell $\hat{\varepsilon}_p$

$$\hat{\varepsilon}_p = \frac{a\hat{C}_{mem}\hat{\varepsilon}_{cyto}}{a\hat{C}_{mem} + \hat{\varepsilon}_{cyto}}.$$
(2.7)

The complex membrane capacitance, $\hat{C}_{mem} = C_{mem} - iG_{mem}/\omega$, with C_{mem} the specific membrane capacitance, G_{mem} the specific membrane conductance, and $\hat{\varepsilon}_{cyto}$ the complex permittivity of the cytoplasm.

Table 2.1 shows the parameters used in our model to calculate the CM factor of mammalian cells. A plot of the calculated CM factor is shown in Figure 2.2.

Table 2.1 Model Parameters Used to Calculate the DEP Force on Mammalian Cells.

Cell radius	a	5 μm
Specific membrane conductance	G_{mem}	$1.2 \times 10^5 \, S/m^2$
Specific membrane capacitance	C_{mem}	$1 \times 10^{-2} \, F/m^2$
Cytoplasm permittivity	ε_{cyto}	$75 \, \varepsilon_0$
Cytoplasm conductivity	σ_{cyto}	0.5 S/m
Medium permittivity	ε_{medium}	$80 \, \varepsilon_0$
Medium conductivity (experimental)	σ_{medium}	$1.8 \times 10^{-2} \, S/m$
Electric field frequency (experimental)	ω	$2\pi \times 10^6 \, Hz$
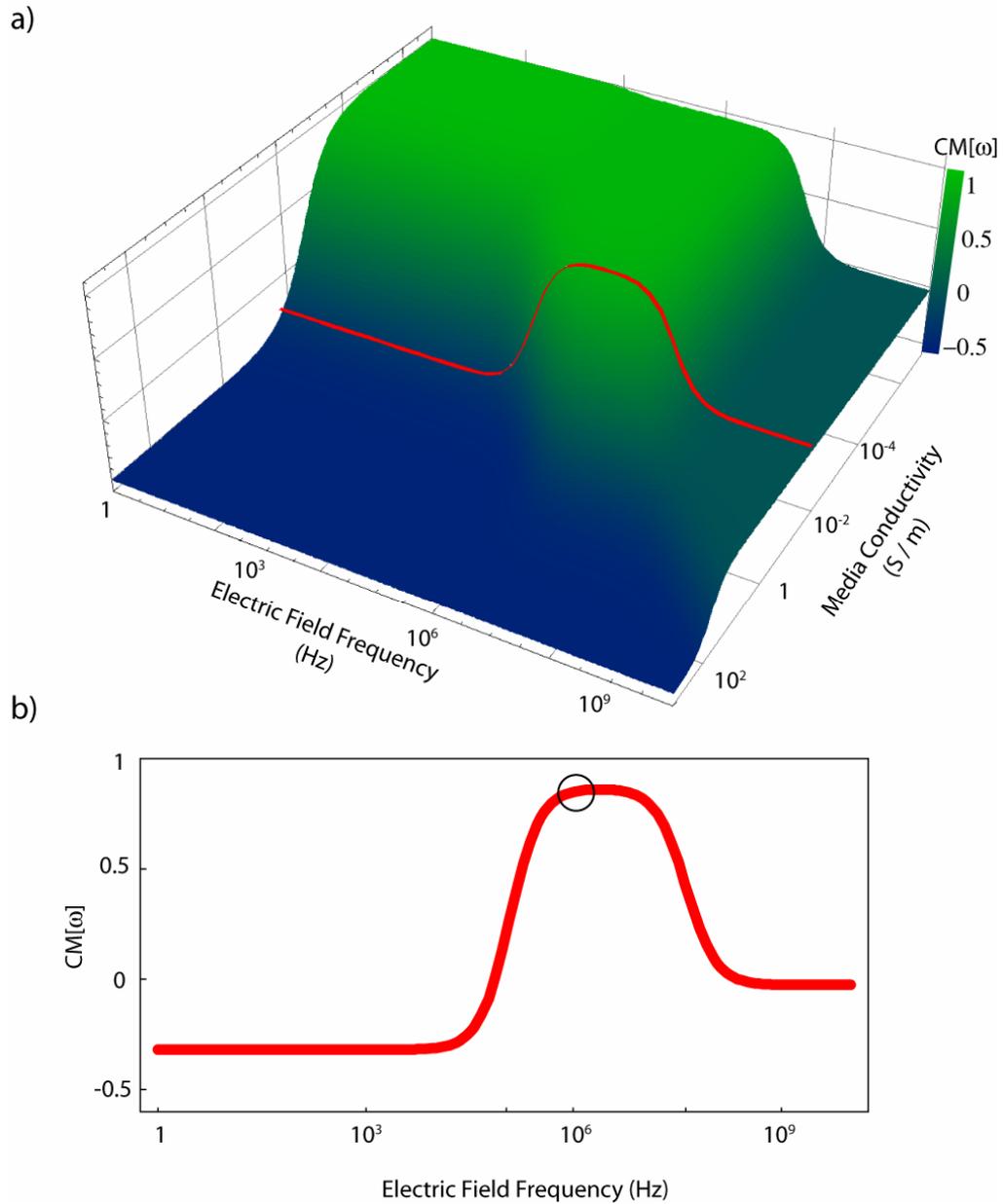
Figure 2.2 CM Factor calculations for Mammalian Cells. a) The theoretical CM factor for mammalian cells according to the parameters in
Table 2.1. The red line shows the CM factor for media conductivity of 0.018 Siemens per meter realized in our experiments. b) Theoretical plot of CM factor vs. frequency for mammalian cells in our experiments. Our IC / microfluidic chip operated at a DEP frequency of 1 MHz, corresponding to the black circle.

We now have equations that describe the DEP force on a particle or cell in a given electric field distribution. It is usually too complicated to solve analytically for the electric field produced by an experimental electrode geometry. To find experimentally relevant electric field distributions, we use finite element modeling (FEM) software. We run electrical FEM simulations on the experimental geometry with either Comsol Multiphysics or Maxwell 3D (Ansoft) as described in Appendix B. After solving for electric fields, we extract the DEP force on the particle of interest for a given electrode configuration and determine how fast the particle will move against fluid drag. The framework of theory and FEM simulations developed in this section has allowed us to optimize the design of DEP microelectrodes before investing the effort and expense to build and test a DEP / microfluidic system.

2.2 Scaling Relations of DEP Manipulation

From Equation 2.4, the DEP force is proportional to the volume of the particle and the gradient of the electric field squared $\vec{F}_{DEP} \propto a^3 \nabla E^2$. The gradient of the field squared can be approximated (Bahaj and Bailey, 1979) by the applied voltage V and the characteristic length of the electrodes l_e: $\nabla E^2 \propto V^2 / l_e^3$. Matching the characteristic length of the electrodes with the radius of the particle to be manipulated we find: $\vec{F}_{DEP} \propto V^2$. In water, with dielectric constant 81 ε_0, the maximum DEP force on a particle produced by electrodes of matching size is proportional to the applied voltage squared, $\vec{F}_{DEP}^{Max} \lesssim 1 \text{ nN} / \text{V}^2$. The relation between the maximum DEP force on a particle and the actuation voltage shows

18

that DEP may not be practical for applying large forces to macroscopic objects. Nonetheless, DEP is a good manipulation scheme for applying pN - μN forces in microsystems.

For microscopic electrodes, the DEP actuation voltage is limited by the dielectric breakdown electric field of the medium or the particle. A good dielectric can withstand 10^7 -10^8 V/m. In water, 1 V can be applied to electrodes with 100 nm spacing without risk of dielectric breakdown, resulting in a maximum ~1 nN of force on a 100 nm particle. With 1 V on electrodes spaced 10 μm apart, a 10 μm particle would likewise be subject to a maximum 1 nN DEP force.

For larger length scales, actuation voltage is limited by experimental practicality: it is difficult to switch more than a few kV at frequencies appropriate for DEP. Thus, the maximum experimental DEP manipulation force is ~ 1 mN, which is enough force for many microfluidic applications, but may be insufficient for macroscopic manipulation.

Two other considerations imply that microsystems are well suited for DEP. The high surface to volume ratio of microfluidics allows any joule heating produced by strong electric fields to be conducted away. Laminar fluid drag experienced by a particle at low Reynolds number produces less resistance ($F_{drag} \propto v$) to DEP manipulation than turbulent fluid drag ($F_{turbulent} \propto v^2$).

2.3   Specific Considerations for DEP in Biology

The physiological fluidic environment has a conductivity ~ 1 S/m. DEP of particles in such a conductive solution faces problems with excessive heating and

electrohydrodynamic (EHD) flow. In addition, cells in an electric field will experience a potentially harmful transmembrane voltage. In general, cells exposed to electric fields of less than ~100 kV/m at frequencies > 1 MHz suffer minimal ill effects. A review of the effects of electric fields on cells is provided by Voldman, 2001.

2.3.1 Heating and EHD fluid flow

Ions in liquid move when subject to an external electric field, heating the liquid. This joule heating must be kept to a minimum to avoid heat shocking any cells that are DEP manipulation targets.

In addition, the density and dielectric constant of a liquid are temperature dependent. Thermal density gradients cause convection. EHD flow occurs when non-uniform electric fields move fluid elements which have different dielectric constants due to temperature. With temperature gradients of more than a few °C across a microfluidic system, the force of convective and EHD fluid flow on a particle can be the same order of magnitude or even greater than DEP forces.

Minimizing the ion concentration in the liquid being manipulated is an excellent method to avoid heating and EHD flow. In general, cells suffer no severe consequences from being suspended in low conductivity buffer if osmotic pressure is maintained by a non-ionic solution such as sucrose or mannitol. In our DEP experiments, we have re-suspended cells in low conductivity (typically 10^{-3} S/m) solutions buffered with appropriate concentrations of non-ionic sugars.

2.3.2 Transmembrane voltage induced by DEP

Ion pumps in a living mammalian cell maintain a transmembrane voltage of approximately 70 mV across the ~ 8 nm thick cell membrane. We expect only a small effect on cell physiology if the transmembrane voltage induced by the electric field used for DEP is less than ~10 mV. As the induced transmembrane voltage increases past 100 mV, the electric field will cause electroporation of the cell membrane. Brief periods of electroporation can be useful within an experiment for delivering drugs, DNA, or RNA that would otherwise not be taken up by the cell (Olofsson et al., 2003). In most situations electroporation should be avoided to prevent damage to the cell.

The cell membrane acts as a capacitor. The maximum induced voltage across the membrane of a spherical cell in an external electric field is (Grosse and Schwan, 1992):

$$V_{tm} = \frac{1.5\,|E|\,a}{\sqrt{1+(\omega\tau)^2}} \qquad\qquad \text{Equation 2.8}$$

Where the time constant to charge the cell membrane,

$$\tau_{mem} = a\,C_{mem}\,(1/\sigma_{cyto} + 1/2\,\sigma_{medium})\,, \qquad\qquad \text{Equation 2.9}$$

is typically on the order of microseconds. Operating at MHz or higher frequencies reduces the voltage across the cell membrane. A theoretical plot of the transmembrane voltage of a cell in a 100 kV / m electric field is shown in Figure 2.3. For cells with the simulation parameters from Table 2.1, $\tau = 1.4$ μsec, $V_{tm} = 100$ mV, and $E_{max} = 100$ kV / m.
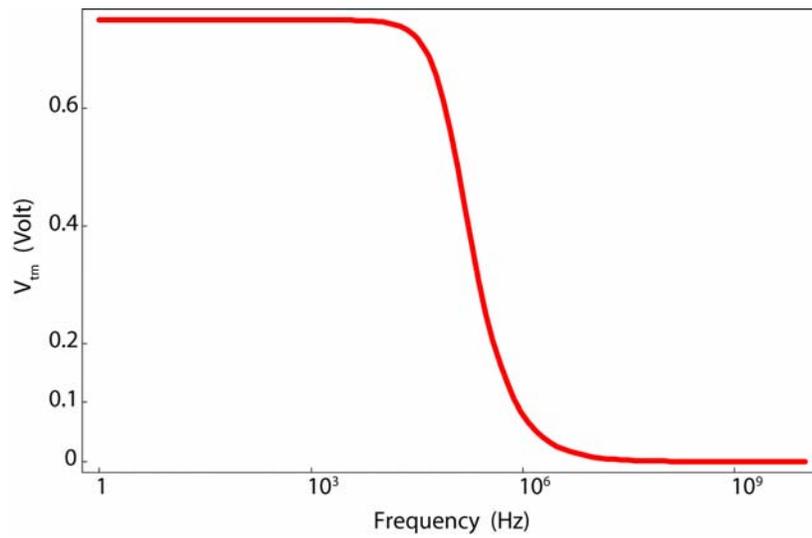
Figure 2.3 Calculated transmembrane voltage of a cell in a 100 kV/m electric field vs Frequency. Simulation parameters are given in Table 2.1.

2.4 Fundamental Limitations of Dielectrophoresis

2.4.1 Thermodynamic limits

To trap a particle against thermal fluctuations, the change in Helmholtz free energy, (U – TS), of the particle as it enters the trap must be greater than kT where T is temperature, S is entropy, and k is the Boltzmann constant. Ignoring entropy, the constraint on the smallest particle that can be trapped is

$$2\pi\varepsilon_m r_{\min}{}^3 E_{rms}^2 > kT \; , \tag{2.10}$$

with the maximum electric field set by the dielectric breakdown of both the particle and the medium. In water, we find $r_{\min} \approx 2$ nm. As the trap volume decreases, restricting the phase space accessible to a trapped particle, entropy becomes an increasingly important consideration. Nonetheless, single protein molecules of radius ~5 nm have successfully been trapped with DEP (Holzel et al., 2005).

2.4.2 Cell manipulation limits

The acceptable voltage that the electric field for DEP induces across the cell membrane limits the DEP force that can be applied to cells. With parameters from Table 2.1, and a maximum transmembrane voltage of 100 mV, we find that $F_{DEP}^{\max} \approx 70$ pN, and from Equation 2.4, $V_{DEP}^{\max} \approx 1$ cm / sec.

The geometry of planar electrodes dictates that much of the field gradient will pull the particle into the plane of the electrodes rather than moving the particle parallel to the electrodes. The maximum speed of DEP manipulation that we achieved with planar electrodes was ~30 μm/sec. Improvements in electrode

geometry and higher actuation voltages coupled with higher frequencies to reduce the voltage across the cell membrane can result in increased cell manipulation speed.

Suspending cells in drops of water in oil and using a low DEP frequency such that the ions in the water drop screen the cell from the applied external electric field may enable still faster cell manipulation speeds.

2.4.3   Drop manipulation limits

The speed of DEP manipulation of drops of immiscible liquids is limited by the strength of surface tension that prevents a drop from breaking into smaller drops. DEP requires a non-uniform field. If the gradient of the field changes significantly across the diameter of the drop to be manipulated, different portions of the drop will be subject to different forces. If surface tension is insufficient to hold the drop together, the drop will split in two. In Section 3.2, we will show, without optimizing the field geometry or the surface energy of the drops, a maximum manipulation speed of several cm per second for a 17 μm diameter drop. With careful electrode design and increased surface tension, drops could be manipulated at higher speeds. The DEP manipulation limit for drops of immiscible fluids is due to drop break up. If drops are sufficiently small and surface tension sufficiently high, they may survive until the dielectric breakdown of the liquid, when the limits of 2.3.1 apply.

2.5 Summary

DEP is an excellent manipulation tool for particles in microsystems. DEP is able to move almost any particle, so long as a medium is chosen with a dielectric mismatch to the particle at a particular frequency. Cells suffer few ill effects from electric fields less than 100 kV/m at frequencies higher than 1 MHz. Our calculations show that cells can be manipulated with DEP at tens to hundreds of microns per second, and that particles on the order of 5 nm in size can be captured and held against thermal fluctuations.

Chapter 3. Microfabricated Devices for Biomedical Applications

We have designed two microfluidic devices for specific biomedical applications. Section 3.1 describes a magnetic sorter capable of pulling magnetically tagged cells and particles out of biological fluids. This technology has applications for in-field diagnosis and treatment of diseases caused by blood-born pathogens, such as sepsis. In addition, it may be useful for isolating rare cells, such as cancer cells, stem cells or fetal cells in maternal circulation.

Section 3.2 describes a high speed DEP drop sorter capable of switching the path of water drops from one channel to another in less than 1 ms. Water drops dispersed in an inert, immiscible solvent are very promising for use as well-defined, confined micro-reactors for combinatorial biochemistry. Our high-speed DEP drop sorter is a key enabling technology for droplet based microfluidics.

3.1 Magnetic Sorter to Remove Bacteria From Whole Blood

We have constructed a microfluidic device that can pull molecules and living cells bound to magnetic particles from one laminar flow path to another by applying a local magnetic field gradient, selectively removing the labeled particles from flowing biological fluids without any wash steps. A schematic of the magnetic sorting device is shown in Figure 3.1. To sort magneticly tagged objects, a microfabricated high-gradient magnetic field concentrator (HGMC) was constructed on one side of a microfluidic channel with two inlets and outlets.

When magnetic micro-or nano-particles were introduced into one flow path, they remained limited to that flow stream. When the HGMC was magnetized, the magnetic beads were efficiently pulled from the initial flow path into the collection stream, thereby cleansing the original fluid. Using this microdevice, living E. coli bacteria bound to magnetic nanoparticles were efficiently removed from flowing solutions containing densities of red blood cells similar to that found in blood. Our microdevice allows large numbers of beads and cells to be sorted simultaneously, operates in continuous flow, and does not lose separation efficiency as particles are removed, so it may be especially useful for separations from blood or other clinical samples. This on-chip HGMC-microfluidic separator technology may potentially allow cell separations to be carried out in the field outside of hospitals and clinical laboratories.

3.1.1 Introduction

One of the key functions of microsystems used for biomedical applications is to separate specific cells or molecules from complex biological mixtures, such as blood, urine or cerebrospinal fluid. Biocompatible super-paramagnetic particles are widely available with surfaces modified to promote binding to various molecules and cells. Taking advantage of these beads is an excellent separation strategy: magnetic sorting can be carried out at high-throughput in virtually any biological fluid, without damaging the sorted entities (Lee et al., 2005). An excellent review of the theory of magnetic manipulation is presented in Hakho Lee's thesis (Lee, 2005).

On-chip technologies for magnetic separation of living cells from biological fluids (e.g., blood, cerebrospinal fluid) could be used to develop portable devices for in-field diagnosis or therapy of diseases caused by blood-born pathogens, such as sepsis. If effective, this same type of on-chip magnetic separation technologies may be useful for isolating rare cells, such as cancer cells, stem cells or fetal cells in maternal circulation. We have developed an on-chip HGMC-microfluidic sorter that offers very good biocompatibility, separation efficiency, and rate of clearance, while minimizing the disturbance on normal blood cells and biomolecules. Figure 3.1 shows a schematic of our microfabricated on-chip HGMC-microfluidic system that permits efficient separation of magnetic micro-and nano-particles, either alone or bound to living bacteria, under continuous fluid flow.
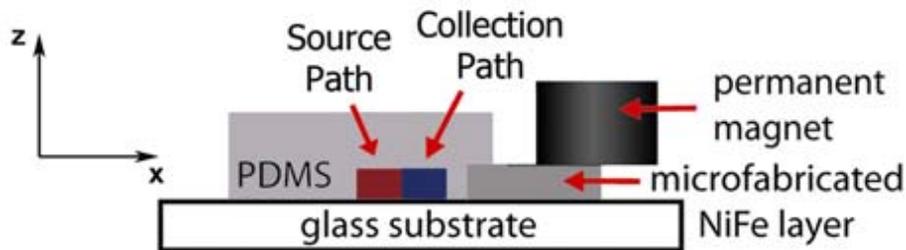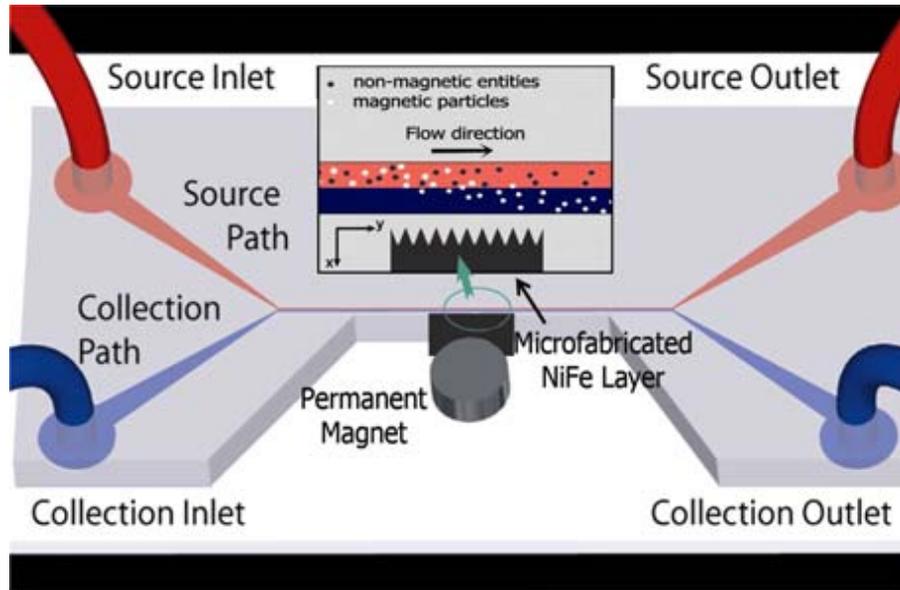
Figure 3.1 Micromagnetic / microfluidic separation device. A microfabricated layer of soft magnetic NiFe material is adjacent to a microfluidic channel with two inlets and outlets; both 3D (top) and cross-sectional (bottom) views of the microdevice are illustrated. Inset shows how magnetic beads flowing in the upper source path are pulled across the laminar streamline boundary into the lower collection path when subjected to a magnetic field gradient produced by the microfabricated NiFe layer located along the lower side of the channel.

3.1.2 Microsystem fabrication

The microfluidic channel was prepared by soft lithography with dimensions of 20 × 0.2 × 0.05 mm (L × W × H). A negative mold of the channel was produced in SU-8 photoresist (Microchem, Inc.). Poly(dimethylsiloxane) (PDMS) (Slygard 184, Dow Corning) was poured onto the mold, allowed to cure for 1 hour at 65°C, and peeled off. A lift-off process was used to define a base layer of evaporated metal (Ti/Au, 10 nm/50 nm) in the form of a microneedle (20 mm in X, 100 μm inY,50 μm in Z) or microcomb (3.8 mm in X, 12 mm in Y, 50 μm in Z with teeth 300 μm in X and spaced by 200 μm in Y) on a glass substrate that was then electroplated (1mA for 4hr) with a 50 μm thick layer of magnetic material (80% Ni, 20% Fe), as previously described (Rasmussen et al., 2001). The PDMS channel and the glass substrate with the NiFe layer were exposed to oxygen plasma (100 W, 60 sec) and bonded together.

3.1.3 Beads and cells

Non-magnetic red-fluorescent beads (2 μm diameter, 4.5×10^9 beads/ml, Molecular Probes) and superparamagnetic green-fluorescent beads (1.6 μm, 43% iron oxide, 3.1×10^9 beads/ml, Bangs Laboratories) were incubated in 10 × volume of 1% albumin solution for 1 hour before being combined and injected into the microfluidic channel E. coli (HB101 K-12) bacteria expressing green fluorescent protein (GFP) were grown overnight at 37∘C in LB medium containing ampicillin (100 μg/ml) and arabinose (0.1%, inductor of GFP expression), then harvested and resuspended in PBS buffer.

The E. coli (1×10^9 CFU/ml) were labeled with biotinylated anti-E. coli antibody (Virostat; mixing ratio 2 μg antibody/10^7 cells), and mixed with streptavidin-coated superparamagnetic particles (130 nm, 85% iron oxide, G.Kisker GbR) prior addition to the microfluidic system. Human red blood cells (RBCs) (75% hematocrit) were obtained from the blood bank at Children's Hospital Boston, stained with the red fluorescent dye (SYTO 64, Molecular Probes), and mixed with isotonic saline containing 0.5% albumin at a 1:3 ratio (final density $\sim 2 \times 10^9$ RBCs/ ml).

3.1.4 Microfluidic control and separation

Fluidic connections to the microfluidic channel were made with polyethylene tubing inserted through holes punched through the PDMS. Syringe pumps were used to control the flow rate at each of the inlet independently. Further details are available in (Xia et al., 2006). A disk-shaped (4 mm diameter, 2 mm high, magnetized along the z-axis) neodymium permanent magnet was used to magnetize the NiFe layer. Quantification of clearance efficiency using the fluorescent microbeads was performed using the inverted Nikon TE2000-E microscope by measuring the fluorescence intensity of the collected fluids from both outlets.

3.1.5 Results

Due to the small Reynolds number (Re) of microfluidic channels, the flow remains laminar with mixing due only to diffusion across the streamlines. A layer of magnetic material (NiFe) with the same thickness as the height of the

microfluidic channel was deposited adjacent to the channel during the microfabrication process to create an on-chip HGMC with defined geometry (e.g., needle or comb). When magnetized by an external permanent neodymium magnet, the HGMC can locally concentrate the gradient of the applied magnetic field to pull the magnetic particles that are present in the source flow path (upper path in Figure 3.1 inset) across the laminar flow streamlines and into the neighboring collection flow stream (lower path in Figure 3.1 inset); these particles will then exit through the lower collection outlet. Under the same conditions, non-magnetic particles in the source flow path should be unaffected by the applied magnetic field gradient, and thus, they will exit through the upper source outlet.
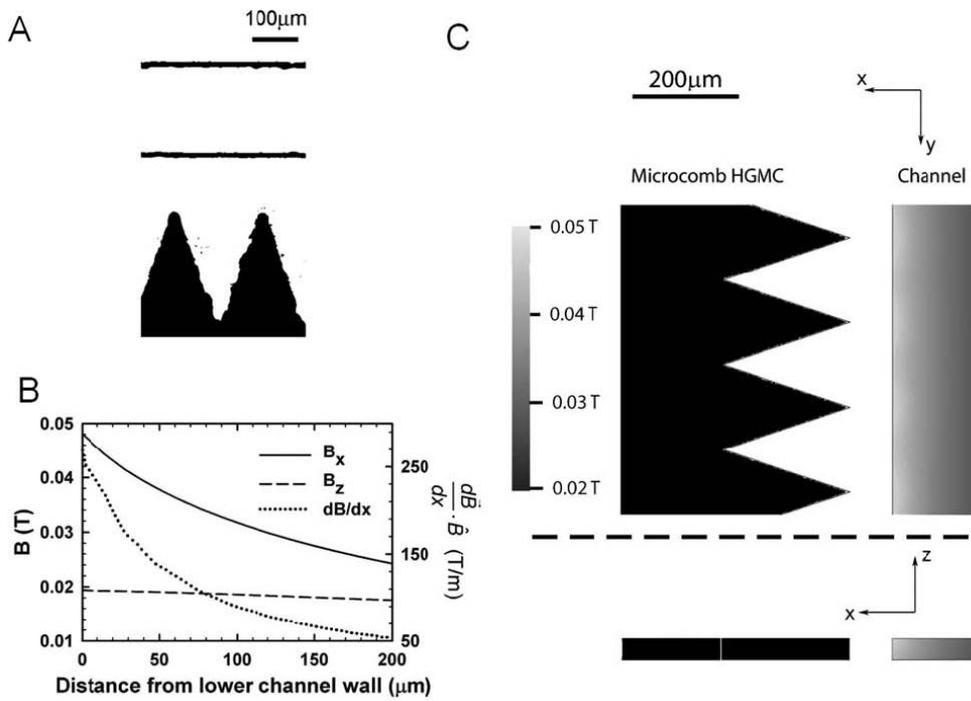
Figure 3.2 (A) Microscopic view of the NiFe microcomb. (B) The corresponding magnetic field and the magnetic field gradient are presented as a function of distance from the lower (collection stream side) channel wall.

To analyze the performance of the micromagnetic separator with the NiFe microcomb for magnetic particle separation, green fluorescent magnetic beads (1.6 μm diameter; 1.6×10^7 beads/ml) were mixed with red fluorescent nonmagnetic beads (2 μm diameter; 2.2×10^7 beads/ml) in PBS could be separated from saline containing a physiological concentration of RBCs (2×10^9 cells/ml), but the separation efficiency of E. coli at the collection outlet was 53% at a flow rate of 25 μl/hr. This decreased separation efficiency may be due to the increased viscosity of this fluid which contains RBCs, as opposed to PBS. However, the separation efficiency was greatly improved when we increased the ratio of magnetic nanoparticles to bacteria. At the same flow rate, 78% of the E. coli bacteria were retrieved through the collection outlet in a single pass when twice the amount of the magnetic particles were utilized (5×10^6 cells/ml; 1.0×10^{10} magnetic nanoparticles/ml) (Table 3.1).

Table 3.1 Results of sorting particles and cells using the combined microfluidic-micromagnetic separator with the NiFe microcomb

Sample components		Flow rate (μl/hr)[a]	Throughput (beads or cells/s)[b]	Separation efficiency (%)[c,d]	
Magnetic	Non-magnetic				
1.6 μm beads	2 μm beads in PBS	40	420	92 ± 4	86 ± 6
1.6 μm beads	RBCs in saline	25	10,000	83 ± 5	79 ± 5
E. coli + 130 nm beads	PBSe	30	80	89 ± 6	83 ± 9
E. coli + 130 nm beads[f]	RBCs in saline	25	10,000	53 ± 8	44 ± 11
E. coli + 130 nm beads[g]	RBCs in saline	25	10,000	78 ± 10	70 ± 9

a) The flow rate of source stream. Experiment run time was determined by the flow rate in order to collect enough fluid volume (at least 10 μl) for quantification.

b) Throughput was estimated based on the flow rate and cell or bead density of the sample. The magnetic nanoparticles used for labeling E. coli were not included when calculating the throughput.

c) The efficiency of separations carried out as shown in Fig. 4 were calculated in two ways: (Left column) Ic,mag/(Ic,mag + Is,mag); (Right column) Ic,mag/Is,non−,mag, where Ic,mag and Is,mag are the intensity (fluorescence or OD600 nm) of beads or cells collected at the lower outlet and upper outlet, respectively, with magnetic field turned on, and Is,non−mag is the intensity (fluorescence or OD600 nm) of beads or cells collected at the upper outlet with magnetic field turned off.

d) The amount of non-magnetic beads or RBCs collected at the lower outlet was less than 1% of the amount of non-magnetic beads or RBCs collected at the upper outlet in all the experiments.

e) For better visualization of boundary of flow path, the PBS buffer contained Texas Red-conjugated bovine serum albumin (0.1 mg/ml) in this study.

f) E. coli (5×10^6 cells/ml) + 130 nm magnetic particles (5×10^9 particles/ml).

g) E. coli (5×10^6 cells/ml) + 130 nm magnetic particles (1.0×10^{10} particles/ml).

3.1.6   Discussion

We used nanometer-sized (130 nm) magnetic particles to label the bacteria because nm beads bind more efficiently to E. coli compared to micrometer-sized magnetic beads with similar surface functionality (results not shown), possibly due to the increased steric hindrance of micrometer-sized magnetic beads. Magnetic nanoparticles also have the potential advantage that they could be used for in-line applications of this technology in the future (e.g., creating a miniaturized device for cleansing blood of biopathogens in septic patients) because they are less likely to occlude small vessels and have longer circulation times than microbeads (Gupta and Wells, 2004).
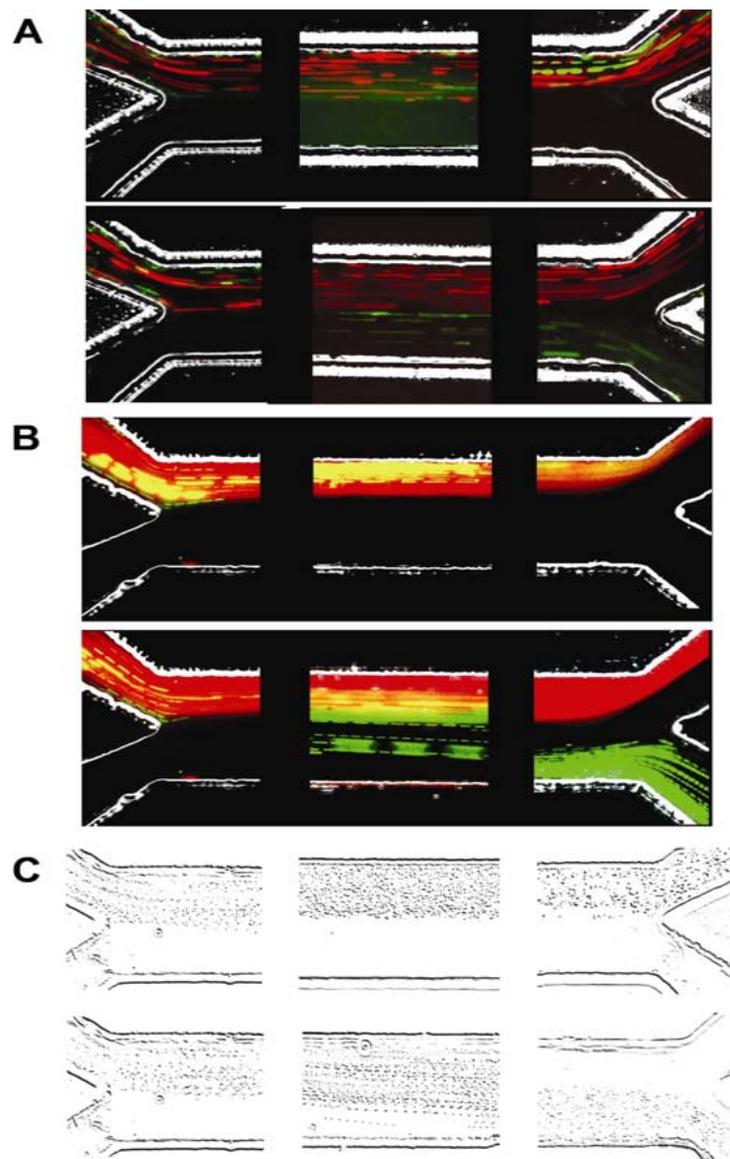
Figure 3.3 Magnetic separations using the microfluidic/micromagnetic separator with the NiFe microcomb. (A) Red fluorescent non-magnetic beads mixed with green fluorescent magnetic beads in PBS. (B) Green fluorescent magnetic beads mixed with red fluorescent RBCs in saline. (C) E. coli cells mixed with magnetic nanoparticles in PBS. Composite fluorescence and bright field images were generated by overlaying sequential frames of corresponding movies taken at the beginning, middle and end (left to right) of the channel, in the presence or absence of the neodymium disk magnet (bottom and top of each pair of images, respectively)

Heterogeneity in the size and magnetic properties of magnetic susceptible components in the source mixture result in a wide distribution of magnetic deviation distances in the x-direction during continuous separation. Although we occasionally observed sample trapping on the collection side of the channel wall, this effect was small, as indicated by the less than a 10% difference between the separation efficiencies of the magnetic beads and cells calculated with two methods in Table 1 (see footnote c in Table 3.1)

The separation efficiency of magnetic entities at the collection outlet ranged from 78 to over 90% at flow rates of 25 to 40 µl/hr. At low bead or cell densities (10^7 beads or E. coli/ml), a throughput of more than 80 beads or cells/s was routinely achieved using the micromagnetic separator; moreover, when sorting samples with a high cell density (10^9 RBCs/ml), the throughput of the microdevice increased to 10,000 cells/s (Table 3.1) We constructed an on-chip microfluidic-micromagnetic cell separator and demonstrated its effectiveness for continuous cleansing of contaminant bacteria or particulates from biological fluids. The ability to remove particles, cells or molecules from flowing blood using a low-cost microsystem technology amenable to multiplexing would have immense clinical significance.

3.2 High Speed DEP Drop Sorter

3.2.1 Overview

We have demonstrated a high-throughput microfluidic DEP drop sorter (Ahn et. al, 2006). Microelectrodes underneath a PDMS channel produce forces of more than 10 nN on a water drop in an inert oil, resulting in sorting rates greater than 1.6 kHz. We investigate the dependence of such forces on drop size and flow. Alternate designs with electrodes on either side of a symmetric channel Y-junction provide refined control over droplet selection.

Water drops dispersed in an inert, immiscible solvent are very promising for use as well-defined, confined micro-reactors (Song et al., 2003). In one particularly promising example, water drops in oil, or emulsions, have been used to carry out in vitro transcription and translation of single genes to create new enzymes (Tawfik, 1998). Micro-reactors can be the basis of a very efficient means of directed evolution: sorting genes under environmental pressure for improved or modified functionality and catalytic activity of new enzymes. Such directed evolution requires accurate control of femtoliter volumes, easily achieved by using micron-sized emulsion drops, to increase the effective concentration of the single gene in each drop and to enable high throughput screening of huge libraries of genes. While bulk emulsions provide the requisite encapsulation, effective high throughput screening requires a much higher degree of control, with access to individual micro-reactors. Such control of micro-reactors is best achieved using

microfluidic technology (Song et al., 2003), which enables formation of uniform drops (Anna et al., 2003) and mixing of small volumes (Song et al., 2003). However, high-speed sorting of drops in the microfluidic device is essential. For example, sorting a typical library of $10^8 - 10^9$ genes demands throughput of at least 1 kHz to be practical. Improved drop sorting speed in microfluidic systems is essential for development of high throughput micro-reactors.

In this chapter, we report high-speed sorting of water drops in microfluidic devices using dielectrophoresis. We characterize the dielectrophoretic force by measuring the dependence of the drop velocity on the drop size and the applied voltage. To further improve the sorting, we use a three electrode device that can pull drops to either side of a symmetric junction.
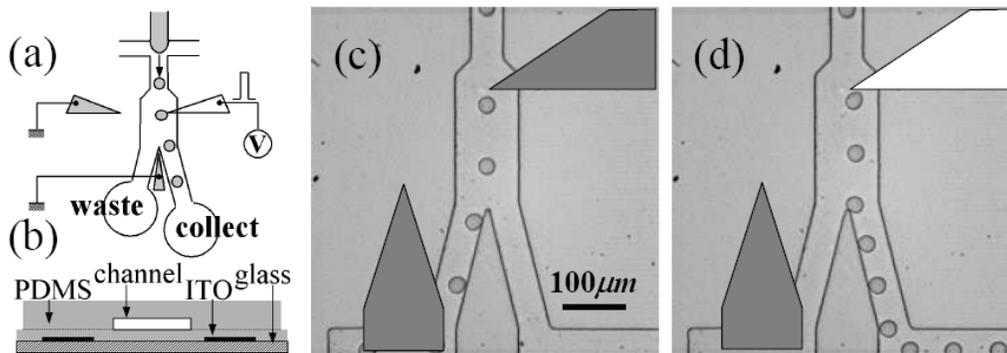
Figure 3.4 High Speed DEP Drop Sorter (a) Schematic top view of the device. Water drops formed by flow focusing in the continuous phase of oil flow into the waste channel since the resistance of the waste channel is smaller than that of the collect channel. (b) Schematic cross-section of the device. The molded PDMS microfluidic channel is aligned to the 30-micron PDMS layer which is spin-coated on the patterned ITO electrodes. (c) In the absence of an electric field, water drops flow into the waste channel. (d) Applying an electric field, the drops are attracted toward the energized electrode and flow into the collect channel. Transparent ITO electrodes have been drawn in grey for grounded electrodes and white for energized electrodes.

We form water drops in oil by hydrodynamic flow focusing (Anna et al., 2003), where two streams of oil and one of water are focused at the input of the device, as shown in Figure 3.4. The water drops flow downstream to a Y-junction. With no electric field, all drops flow into the waste channel which is shorter, and thus offers lower hydrodynamic resistance than the second, collect channel. To direct drops into the collect stream, we energize electrodes under the channel in the sorting region; the dielectrophoretic force pulls the drops into the collect stream. The electrodes are located with their tips or edges close to the center of the channel to maximize the force exerted on the drops. We use a finite element simulation (Maxwell 3-D, Ansoft) to estimate the dielectrophoretic forces on water drops for the actual device geometry; this shows that sharp edges of electrodes generate the largest field gradients and forces on the drops. Passing through the Y-junction, drops can deform and break, with each daughter drop flowing into a separate exit channel. Drops will break due to extensional flow if the capillary number, which characterizes the ratio of viscous to capillary forces, exceeds a critical value. To avoid drop breakup, we design the channel width near the Y-junction to be bigger than the diameter of the undeformed drop, preventing breakup by decreasing both velocity and extension.

3.2.2 Microsystem fabrication

The microfluidic device is fabricated using standard soft lithography methods. A channel pattern of 25 μm thick negative photoresist is produced by UV photolithography on a silicon wafer. A mixture of polydimethyl siloxane (PDMS) elastomer and crosslinker with a weight ratio of 5:1 is molded onto the channels and peeled off after being partially cured. Another mixture with a weight ratio of 20:1 is spincast at 3000 rpm to a 30 μm film on a glass substrate, on which has been patterned indium tin oxide (ITO) electrodes, and also partially cured. The PDMS mold is bonded to the PDMS-coated ITO-glass substrate and fully cured to enhance bonding between the two layers. A schematic cross section of the sorting region of the fabricated microfluidic device is shown in Figure 3.4b.

3.2.3 Drop sorting with DEP

We produce drops of water in hexadecane with the device shown schematically in Figure 3.4 (dielectric constant, $\varepsilon_{oil} = 1.8 \times 10^{-11}$ Farad/m; viscosity, $\eta_{oil} = 8.0 \times 10^{-3}$ Pa•s). We add 5 wt % surfactant (SPAN80) to prevent coalescence. The size of the water drops is controlled by adjusting flow rates of oil and water using syringe pumps (Harvard Apparatus) (Anna et al., 2003). We form water drops with radii from 2 to 30 μm using water flow rates from 1 to 6 μl/hr and oil flow rates from 100 to 1000 μl/hr. We apply AC voltage up to 2 kV across the electrodes; this avoids screening effects, which are found to weaken a DC field. Drop movement is recorded by a high-speed camera at a frame rate of 20 kHz.

In the absence of electric field, the water drops flow along the path of lower hydrodynamic resistance to the waste channel as shown in Figure 3.4c. When we turn on the voltage, the electric field elongates and displaces the drops toward the electrode located close to the drop stream (Figure 3.4d). To quantify the forces on the drops, we measure the average velocity of drops pulled in the direction perpendicular to their flow while varying the applied voltage and the drop size. The average velocity is obtained by measuring the displacement of the drops as a function of time from each frame of the movies recorded by the high-speed camera. The average velocity is proportional to the square of the applied voltage and the drop size (Figure 3.5). The velocity is determined by the dielectrophoretic force acting on a drop as described in Chapter 2. From our finite element simulations, the maximum dielectrophoretic force on a 12-μm-diameter drop at 1 kV is estimated to be 10 nN near the electrode edge, resulting in a maximum drop velocity of 1.0 cm/sec. This is in good agreement with the experimental value as shown in Figure 3.5.
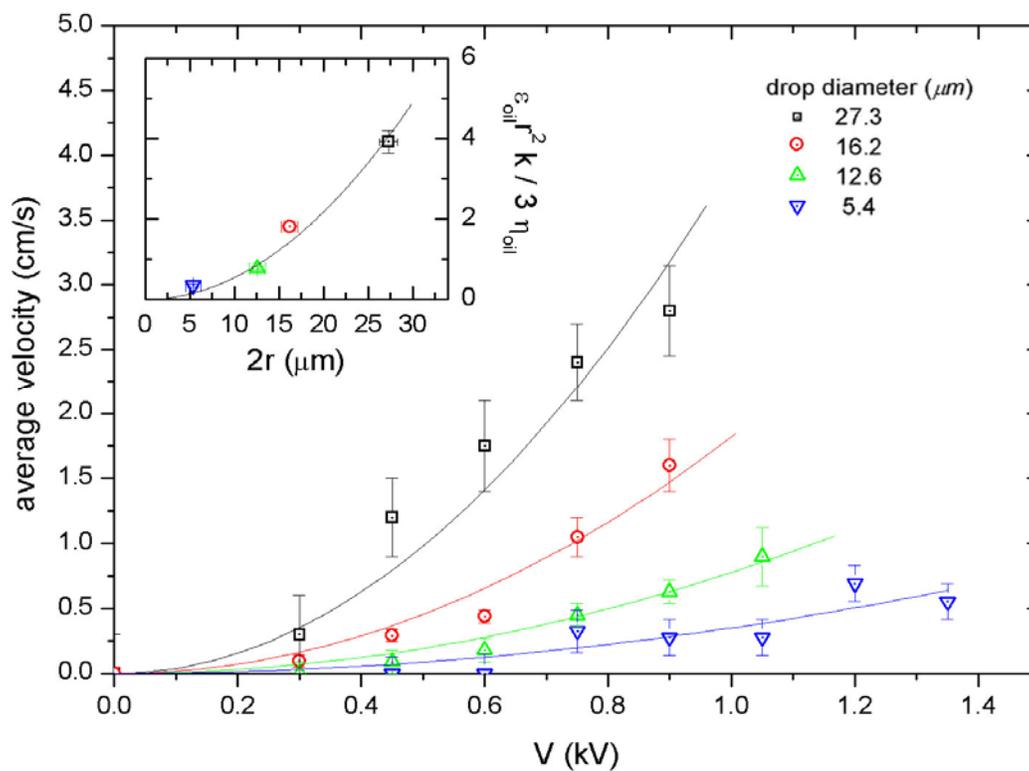
Figure 3.5 Plot of the average terminal velocity of the water drops versus the applied voltage for different drop sizes. Inset shows that the parameter $\varepsilon_{oil}\, r^2 k\, /\, 3\, \eta_{oil}$ is proportional to the square of the drop diameter.

To further refine the description of drop movement, we used a least-square fit of all the data for the velocity as a function of V, for each drop size, shown as solid lines in Figure 3.5. From these fits, we obtain values for $\varepsilon_{oil} r^2 k / 3\ \eta_{oil}$, which are plotted as a function of r in the insert of Figure 3.5. They exhibit the expected dependence on r^2 and a least-square fit gives a value for $\varepsilon_{oil} k/3\ \eta_{oil}$, from which we obtain the average geometric factor of the device, $k_{avg} = 2.9 \times 10^{11}\ m^{-3}$. This is in good agreement with values obtained from simulation, which range from $2.0 \times 10^{10}\ m^{-3}$ to $2.0 \times 10^{11}\ m^{-3}$ near the electrode. The deviation between simulation and experiment likely stems from the highly non-uniform electric field near the electrode edges or from the variation of the PDMS layer thickness at the channel bottom, which determines the distance of the water drops from the electrode and affects the electric field strength in the channel. The overall good agreement confirms that finite-element techniques can be used to help optimize electrode design for microfluidic devices.

The maximum rate of dielectrophoretic sorting depends on the force generated by DEP which determines the terminal speed of the drops. The time for the drops to attain the terminal velocity is given approximately by $t = v/(F/(\Delta\rho 4\pi/3r^3)) = 2\Delta\rho r^2/9\eta$, where $\Delta\rho$ is the density mismatch between the water and the oil. A 1 nN force acting on a 12-μm-diameter drop will accelerate the drop to its terminal velocity within 5 μs, much faster than other timescales in the system; therefore inertial effects do not limit the sorting rate. Similarly, the capacitive time constant (RC) of the circuit is small, on the order of ten nanoseconds (R ~ 200Ω, C ~ 50 pF), and also does not limit sorting rates. Instead,

for a given velocity, the sorting rate is limited by the on-time required for the electric field to displace the drops a distance, d, away from the center of the streamline into the collection channel. This distance is close to zero in the case of symmetric output channels where drop flow direction is evenly distributed into both channels. In the case of asymmetric channels, d is determined by the relative difference of the amount of liquid separated into two output channels, which is proportional to the relative difference of the length of the two output channels. Therefore, $d \sim w\Delta l/l$, where w is width of the channel, l is the total length of the collection and waste channel, and Δl is the difference between the channels. In our device, $d \sim 6$ μm; since the dielectrophoretic force moves 25 μm-diameter drops at $v = 4$ cm/sec, drops can be sorted in 250 μs. The time scale to displace the drops can be shortened by increasing V or improving the device design. However, an excessively sharp localized field gradient around the electrode ultimately results in drop breakup, setting the limit for the sorting rate in this device. For 25μm-diameter drops, we use square AC pulses with an amplitude of 700 V, a frequency of 10 kHz and a duration of 500 μs; this enables us to sort a single drop into the collect channel from a continuous stream at rates of 1.6 kHz, as shown in Figure 3.6.
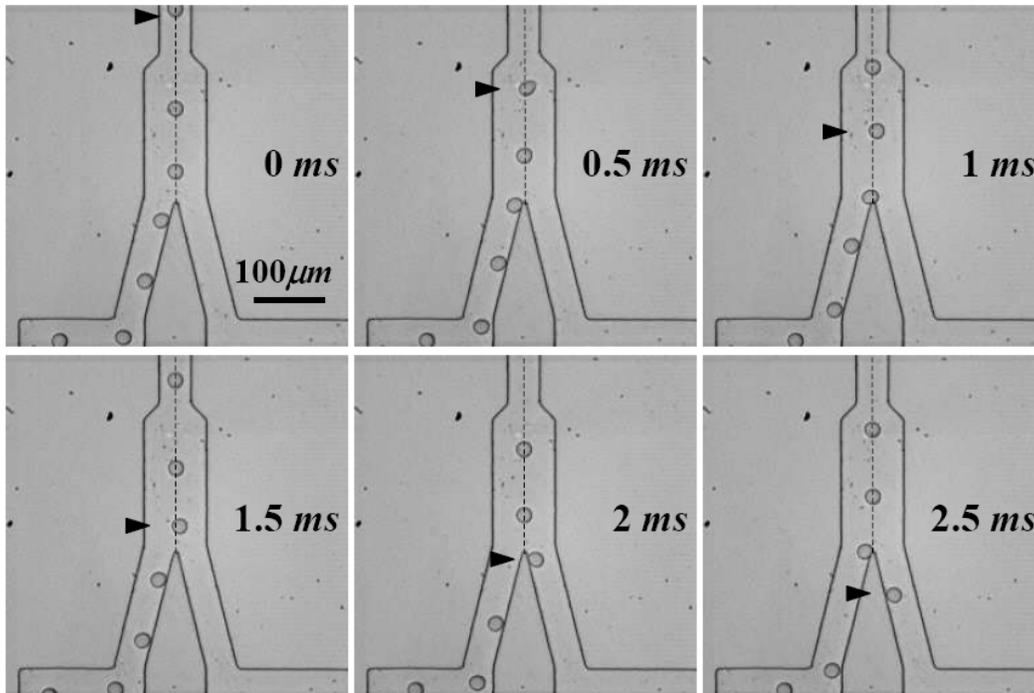
Figure 3.6 A single drop sorted out of 1.6 kHz drop flow with DEP. Images captured every 500 μs. The arrow marks the drop of interest. One drop is directed to the collect channel out of the line of drops by a 500 μs pulse of electric field. Transparent electrode location same as Figure 3.5

Improved sorting speed can be attained by decreasing d. We use a symmetric

Y-junction with equal fluidic resistance in each output channel, significantly

reducing d. However, this device requires more than two electrodes to change the

direction of electric field gradient with respect to the flow. For example, with

three electrodes in a triangular arrangement, each edge can be the highest electric

field region by choosing one of them as a cathode while the other two are

grounded. Our device for bi-directional drop manipulation has two output

channels with the same length and hydrodynamic resistance and three electrodes

aligned to the middle channel, as shown in Figure 3.7. In the absence of electric

field, drops are evenly distributed into both channels, as shown in Fig. 4a. Upon

application of a field to the appropriate electrode, drops can be directed to either

one of the two channels, as shown in Figure 3.7b and Figure 3.7c. Optimization of

such devices should further improve sorting rates.
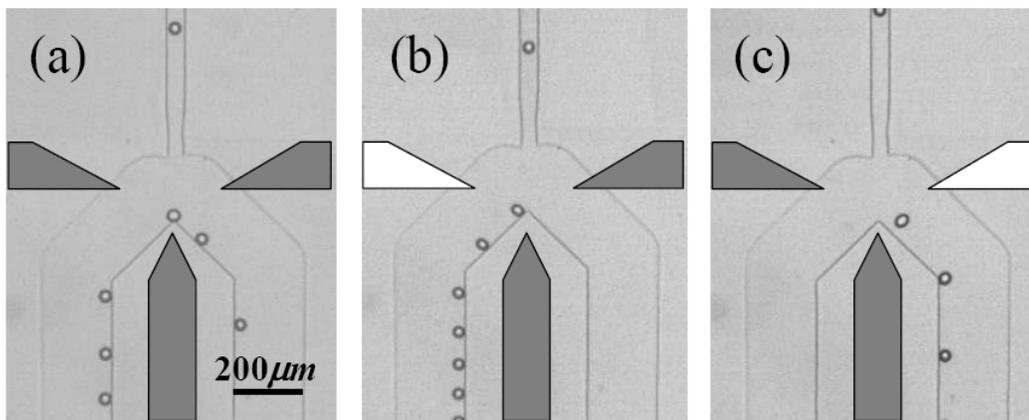
Figure 3.7 Bi-directional manipulation of drops. (a) In the absence of the electric field, two outlet channels are symmetric, the junction is an unstable equilibrium and drops flow to both directions. (b) Drops flow to the left channel with the left electrode energized. (c) Drops flow to the right channel with the right electrode energized. Transparent ITO electrodes have been drawn in grey for grounded electrodes and white for energized electrodes.

3.2.4   Conclusion

Our microfluidic drop sorting devices can be used as an essential component in a platform for high throughput screening bioassays. Dielectrophoretic forces provide high speed sorting with no moving parts, or requirements for charged droplets. We have achieved rates as fast as 4 kHz, but even this is not the ultimate limit. Sorting rates can certainly be increased further by using shorter pulses, higher fields or improved device design.

Chapter 4. DEP Tweezers: Scanning Probe DEP Traps

4.1 Overview

Positioning single cells is of utmost importance in areas of biomedical research as diverse as in vitro fertilization, cell-cell interaction, cell adhesion, embryology, microbiology, stem cell research, and single cell transfection. In this chapter, we describe DEP tweezers, a sharp glass tip with electrodes on either side, capable of trapping single cells with electric fields. Mounted on a micromanipulator, DEP tweezers can position a single cell in three dimensions, holding the cell against fluid flow of hundreds of microns per second with more than 10 pN of force. We model the electric field produced by the tweezers and the field produced by coaxial microelectrodes. We show that cells are trapped without harm while they divide in the trap. DEP tweezers offer the possibility for trapping, electroporating, and microinjecting a single cell with one probe. We have extended the basic idea of DEP tweezers to a nanomanipulation system by building coaxial electrodes on an AFM tip.

As biologists struggle to understand and manipulate living systems, they increasingly turn to single cell analysis (Brehm-Stecher and Johnson, 2004). With the advance of miniaturization, it is now possible to perform mRNA analysis on a single cell (Eberwine, 2001), transfect a single cell to change its gene expression, observe how one cell differentiates, or study how two individual cells interact. The quantum of biology is the cell, and biologists strive to reach into that world. For over one hundred years, the standard technique for single cell

manipulation has been to grasp a cell with suction through a hollow glass

micropipette tip (Barber, 1904). This manipulation process requires a very

skilled operator and can easily damage the cell membrane or cytoskeleton

(Fleming and King, 2004). Optical tweezers are an alternative, requiring intricate

optics and producing limited manipulation force. Microactuators for physically

holding cells are possible to build but have not been widely adopted. Local

magnetic fields can be used to move cells (Lee et al., 2004) if the cells are tagged

with magnetic beads. A micromanipulator based trap has the advantage of being

able to arbitrarily position single cells in three dimensions. Here we present

dielectrophoretic (DEP) tweezers shown in

Figure 4.1 (Hunt and Westervelt, 2006). DEP tweezers use electric forces

to hold single cells at the end of a micromanipulator. This technique is simple,

robust, label free, and does not damage cells. DEP tweezers on AFM tips

described in Section 4.5 could be useful tools for manipulating nanoparticles or

macromolecules.

Figure 4.1a is an illustration of how DEP tweezers work. Two electrodes

a few µm apart provide a non-uniform electric field which polarizes a nearby cell

and produces DEP force on the cell as described in Chapter 2.
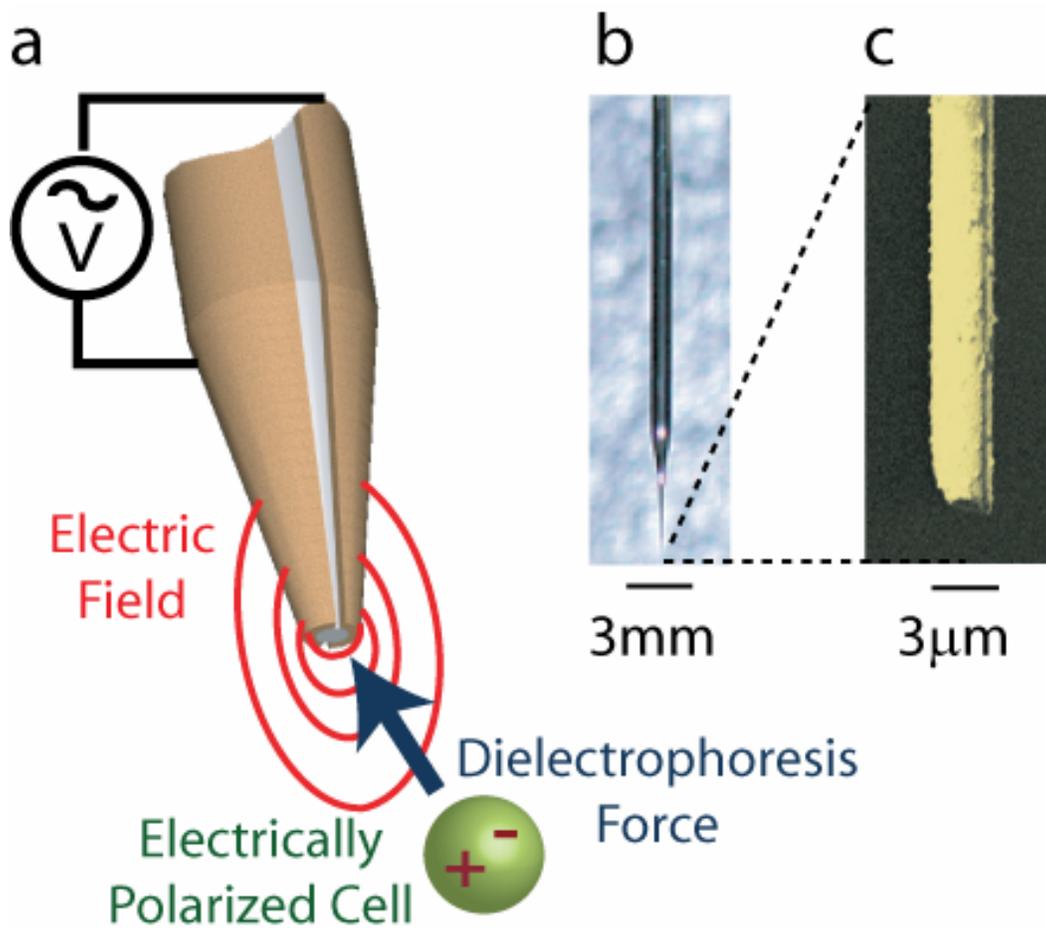
Figure 4.1 DEP tweezers for cell manipulation. (a) Schematic of DEP tweezers in operation. A voltage across two electrodes on either side of a sharp glass tip creates an electric field which polarizes a cell and pulls the cell into the field maximum at the end of the tip. (b) Photograph of DEP tweezers. (c) SEM image of the tweezer tip. Electrodes appear light while the insulating gap between electrodes is dark.

4.2   Experimental design

A photograph of the DEP tweezers is shown in

Figure 4.1. The first step to fabricate DEP tweezers is a standard method for fabricating micropipettes (Fleming and King, 2003). A 1 mm diameter glass rod is pulled to a sharp tip in a pipette puller that controllably heats the center section of the rod and pulls on either end until the rod tapers and breaks. To produce uniform, repeatable tips with a desired radius, the tapered tip was examined under a microscope and fractured at the correct radius.

To deposit electrodes, the sharpened glass rod was placed in a high-vacuum thermal evaporator. 7 nm Ti and 20 nm Au were evaporated on one side of the rod, the rod was flipped, and Ti-Au deposited on the opposite side. Most electrode pairs produced with this method were electrically isolated. If a small metal bridge connected the two electrodes, applying a few volts between the electrodes burned out the thin film of metal that caused the short.

To use the DEP tweezers, a micromanipulator was mounted on top of an inverted microscope. Spring steel clips coated with soft indium held the DEP tweezers on the micromanipulator and made electrical contact to the electrodes on either side of the tweezers. A function generator provided voltage for the electrodes with adjustable frequency and amplitude.

Figure 4.1c is an electron micrograph of the tweezer tip. We manufactured tweezer tips 3 μm in diameter to manipulate yeast cells approximately 6 μm in diameter. Sharper tips produce higher field gradients than broad tips for a given electric field. However, if a tip is much sharper than the

size of the cell being trapped, the electric field gradient produced by the tip will decay significantly across the diameter of the cell, resulting in reduced trapping force. Our tip diameter was chosen to maximize the trapping force by producing a high electric field gradient across the entire diameter of the cell.

4.3   Simulation

Figure 4.2 shows a finite element simulation of the electric field at the tip of the tweezers with an applied voltage of 10 V peak to peak. The simulation software (Maxwell 3D, Ansoft) solves Poisson's equation on a mesh of tetrahedrons optimized to fit the actual tip geometry.
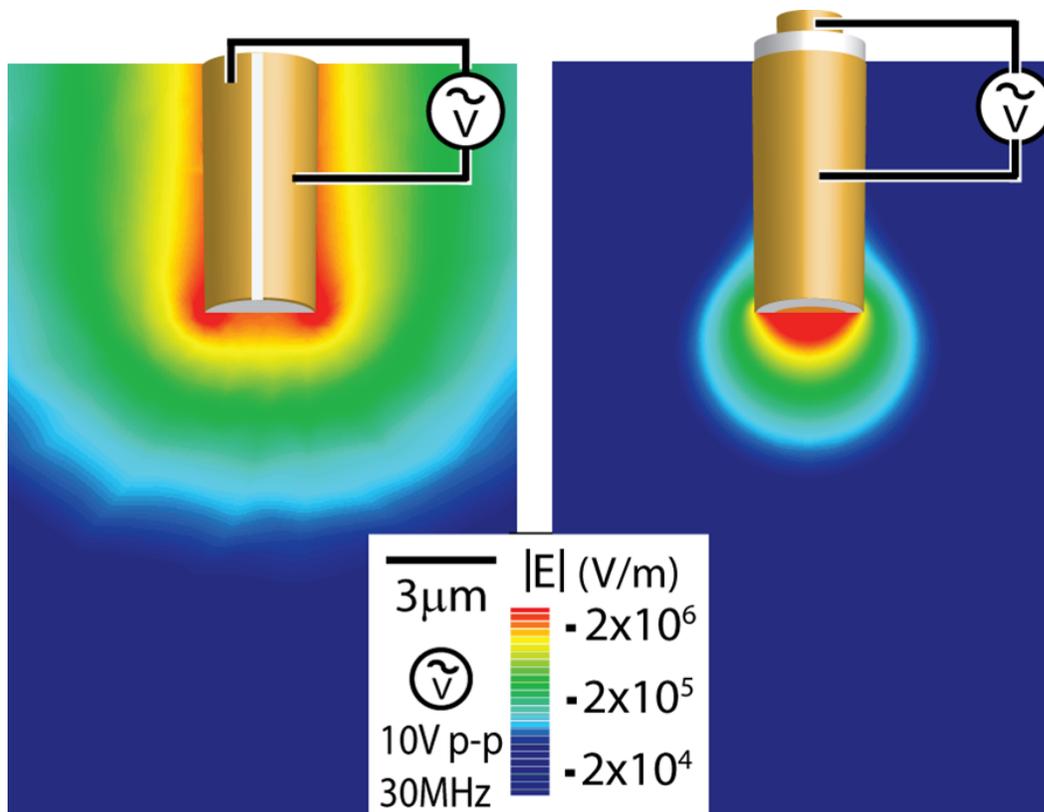
Figure 4.2 Electric field simulations near the DEP tweezer tip. Finite element model shows the field magnitude produced by DEP tweezers in a plane through the axis of the tweezers. (a) DEP tweezers as fabricated. (b) Field produced by a coaxial tweezer.

The simulation included a glass cylinder 3 μm in diameter with dielectric constant 5.5 ε_0 immersed in water with dielectric constant 81 ε_0. Two metal electrodes wrap 170 degrees around the cylinder with 10 degree gaps between the electrodes. The electric field maximum is approximately 2×10^6 V/m and dies away to 10^4 V/m within a distance to the tweezer tip, r < 20 μm. The electrodes can be approximated as two parallel wires forming a dipole, with a field that drops off with $1/r^2$. It is possible to produce a more concentrated electric field distribution with coaxial electrodes, simulated in Figure 4.2b.

A 1 μm diameter inner conductor is surrounded by an insulating glass layer and a 3 μm diameter, 100nm thick outer conductor. The coaxial geometry produces a very high field gradient that dies off with $1/r^3$ and provides strong trapping forces close to the tip. The outer conductor also serves to shield the surrounding liquid from electric field everywhere except at very end of the tip, which reduces joule heating and the resulting convection of liquid. However, the sharper field distribution of coaxial electrodes results in a reduced trap radius compared to the fabricated DEP tweezers (Figure 4.2a).

Modeling a yeast cell (Kotnik and Miklavcic, 2000) trapped at the tip of the tweezers in Figure 4.2a, with 10 V at 30 MHz applied to the electrodes, the induced voltage across the cell membrane is less than 40 mV. To further decrease the voltage across the cell membrane when the cell is trapped at the tweezer tip, the voltage on the tweezers can be reduced so that the electric field provides only the necessary trapping force for a particular manipulation.

4.4   Manipulation of yeast cells

Trapping a single yeast cell at the end of the tweezers is shown in the micrograph sequence in Figure 4.3a. Baker's yeast, (*Saccharomyces cerevisiae*) were suspended in standard yeast growth medium (yeast peptone dextrose broth, BD Inc.) with electrical conductivity 29 mSiemen/m. The tweezers were energized with 10 V peak to peak at 30 MHz and a nearby yeast cell was pulled into the maximum of the field at the tip of the tweezers. By moving the micromanipulator, the trapped cell could be translated through the fluid at hundreds of microns per second without escaping from the tweezers. Stokes drag yields an estimate of the DEP force pulling a yeast cell toward the tip of the tweezers. For a spherical cell in laminar flow, $F_{drag} = 6\pi\eta a v$, where η is the viscosity of water, a is the radius of the cell (~3 μm), and v is either the maximum velocity of a cell as it is pulled onto the tweezer tip (~0.2 mm/s) or the maximum velocity that the tweezers can be translated through fluid without releasing the cell (~0.5 mm/s). A single yeast cell is trapped by DEP tweezers with 10-50 pN force.
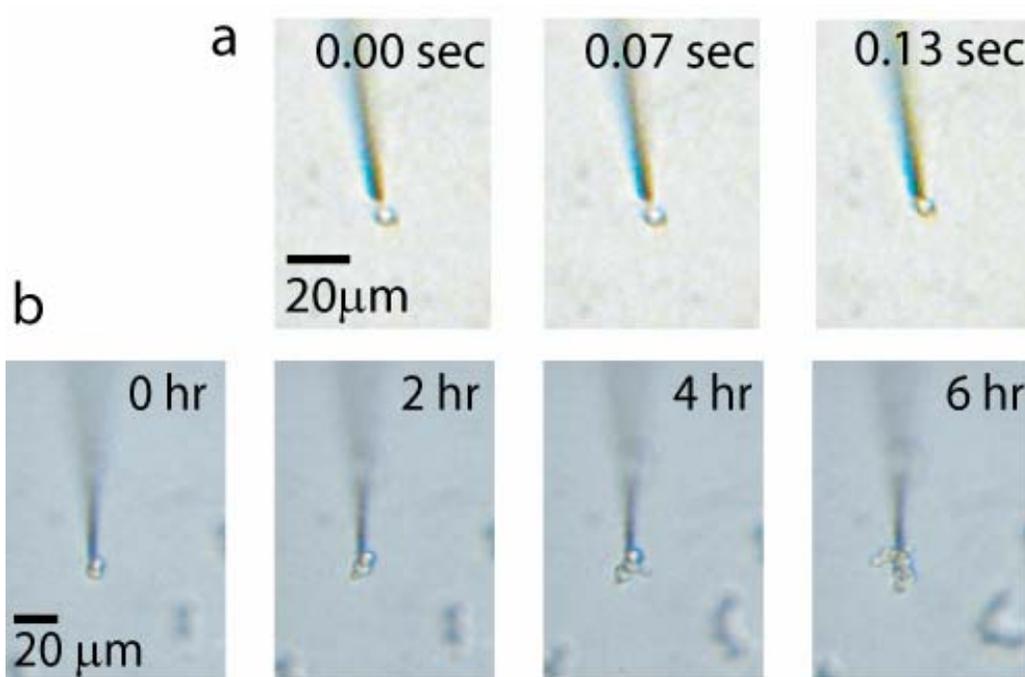
Figure 4.3 Cells held by DEP tweezers. (a) DEP tweezers capturing a yeast cell. The electrodes were energized at 0.0 sec and the yeast was rapidly pulled into the field maximum at the tip of the tweezers. (b) Yeast dividing while trapped at the tip of the tweezers.

To demonstrate that the strong electric field at the tip of the tweezers did not harm yeast cells, we trapped cells for many hours and observed them dividing in the trap. Figure 4.3b shows two yeast cells trapped by the tweezer. Both cells budded and formed daughter cells in 2 hr, producing a cell mass with many cells within 6 hr, still trapped by the field of the DEP tweezers. The voltage induced by the DEP tweezers across the cell membrane of yeast apparently does not interfere with essential cellular mechanisms necessary for growth and reproduction. To manipulate cells that are more sensitive to transmembrane potentials, it is possible to reduce the voltage on the DEP tweezers at the expense of trapping force.

4.5   Extension to AFM DEP tweezers

DEP tweezers are also a powerful tool for trapping and manipulating nanoparticles. By building DEP tweezers at the end of an AFM tip, we can use the AFM platform both to image the target nanoparticles and to position the DEP trap with nm precision.

To make AFM DEP tweezers, we fabricated an AFM cantilever with coaxial electrodes. We began with a highly doped silicon cantilever and tip. We grew 100nm of thermal oxide on the tip at 1100 degrees C in an oxygen atmosphere. The thermal oxide provided a pinhole free conformal insulating layer on the tip. We HF etched a small amount of oxide at the base of the cantilever to allow electrical contact to the silicon inner electrode, and deposited a Cr-Au outer electrode / ground shield in a thermal evaporator. We cut off the end of the tip with a FIB to produce the final tip geometry shown in Figure 4.4
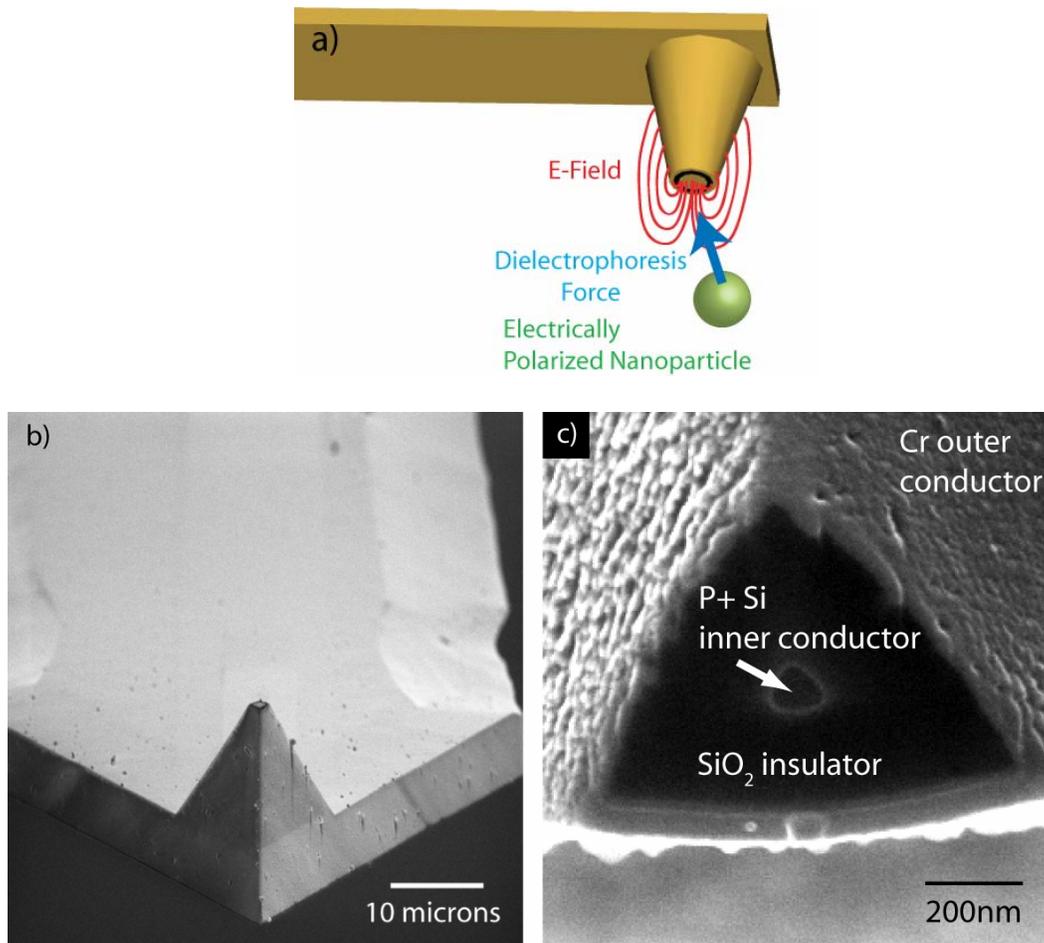
Figure 4.4 AFM DEP Tweezers. a) Schematic view of AFM DEP tweezers showing concentric electrodes. b) SEM image of AFM cantilever with DEP tweezer tip c) SEM image of tip of AFM DEP tweezers showing the center conductor, insulating layer and outer conductor.

To use the DEP tweezers, we mounted them in an Asylum MFP-3D AFM with a modified cantilever holder to make electrical contact to the inner and outer DEP electrodes. We operated on an inverted microscope for improved optical observation of our manipulation, and in fluid to minimize the surface forces on the nanoparticles. We chose fluorocarbon or hydrocarbon oil as fluid because these liquids have low dielectric constant (~2) to enable nanoparticle trapping with pDEP, and very low conductivity to minimize fluid flow due to electric fields. As a manipulation target, we used fluorescently labeled polyurethane spheres with 500nm to 10μm diameter, produced by Christian Holtze in the Weitz Group, or polystyrene beads (Bangs Labs). We applied a 10 V peak to peak sine wave at 3 MHz to the tip of the tweezers. Initial results of polystyrene bead trapping are shown in Figure 4.5.
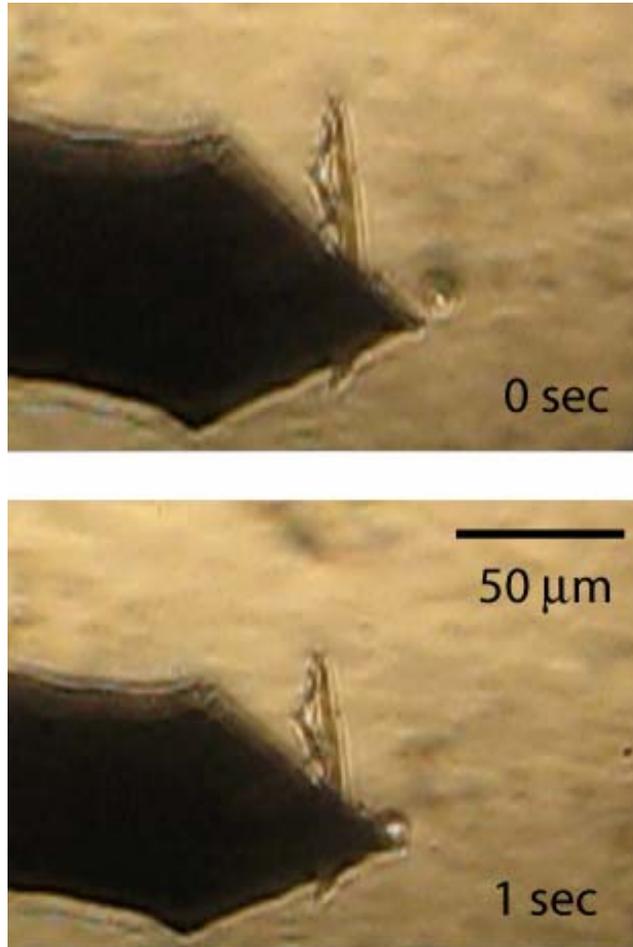
Figure 4.5 AFM DEP tweezers capturing a polystyrene bead in fluorocarbon oil. A 3 V sine wave at 10 V peak to peak has been applied between the inner and outer electrode of the AFM DEP tweezers, attracting the polystyrene bead. A piece of dust is also visible on the AFM cantilever.

4.6 Conclusion

DEP tweezers are a powerful tool for manipulating individual cells in physiological conditions: an increasingly important technique in biomedical research. It is straightforward to add electrical contacts to a suction-based micropipette micromanipulation system, allowing the use of DEP tweezers instead of suction for cell manipulation. Furthermore, by applying a high voltage pulse to the DEP tweezer electrodes, it should be possible to selectively and controllably electroporate a single cell. If the DEP tweezers are fabricated with a hollow pipette tip, it may be possible to hold a cell with electric field, electroporate the cell with a voltage pulse, and perform a microinjection with a single probe. This simple technique would greatly facilitate in vitro fertilization and single cell transfection studies. Another promising application for DEP tweezers is to trap and position nanoparticles. We have constructed coaxial electrodes on an AFM tip. This AFM DEP tweezers has trapped polyurethane spheres in fluorocarbon oil. Further applications of the AFM DEP tweezers should be able to pick and place nanowires and nanoparticles for study. By reducing the tip diameter, the electric field produced by such AFM DEP tweezers sharp tip could be increased until the field reached the dielectric breakdown strength of the dielectric liquid or the insulator between the coaxial electrodes. According to calculations in Section 2.4, it should be possible to use DEP tweezers to stably trap and manipulate objects with diameters as small as 5 nm.

Chapter 5. The Micropost Array: Microfabricated Electrodes for Moving Cells with Dielectrophoresis

5.1 Overview

Before constructing a CMOS / microfluidic DEP manipulator chip, we built a DEP chip with a 5 x 5 array of electrodes in the CNS cleanroom. The micropost electrode array (Hunt et al., 2004), shown in Figure 5.1, was capable of trapping and moving particles and cells with both positive and negative DEP. We constructed post shaped electrodes to produce high field gradients by concentrating the electric field at the top of the electrodes. In addition, the vertical separation between the top of the post shaped electrodes and the incoming leads prevented the electric field from the leads from significantly influencing the DEP fields.

As discussed in Chapter 1, an array of traps with independent, addressable electrodes provides a more flexible and powerful manipulation system than traps with fixed electric field geometries (Manaresi et al., 2003). An addressable array of closely spaced electrodes is capable of transporting cells or particles across the array (Suehiro and Pethig, 1998). Combining an array of addressable electric traps with microfluidic channels allows the creation of a programmable microfluidic system that can independently control the motion of many cells at once.

In this chapter, we describe a micropost matrix, a two-dimensional array of post-shaped electrodes at the bottom of a microfluidic channel. The micropost matrix is capable of versatile manipulation of particles and cells using DEP. Each electrode is independently addressable by an analog voltage source, which allows fine control of the trapping field inside the microfluidic channel. With the electric field produced by the micropost matrix, cells and polystyrene beads were trapped and transported inside a microfluidic channel. The union of microfluidics and a matrix of DEP traps results in a device capable of manipulation, separation, and assembly of individual cells.

The micropost matrix shown in Figure 5.1 uses post-shaped electrodes to concentrate the electric field lines under the cells in the fluid. Figure 5.1 (a) shows a micrograph of the micropost matrix, and Figure 5.1 (b) shows the layout of the microposts in three dimensions. The posts help to isolate the cells from electric fields produced by the leads. An alternative to the micropost matrix would be a chip with very close spacing between electrodes, and at least two layers of metal to allow electrical leads to address each electrode from below. The multiple metal layer alternative provides very good isolation of the chip surface from the fields produced by the leads, and was used in our CMOS chips. The micropost matrix was interesting and easier to fabricate in the CNS cleanroom. A schematic cross sectional view of the device is provided in Figure 5.1 (c). The post-shaped electrodes function as an array of monopoles that can be charged with different analog voltages - the field lines go from the posts to a conducting cover plate.
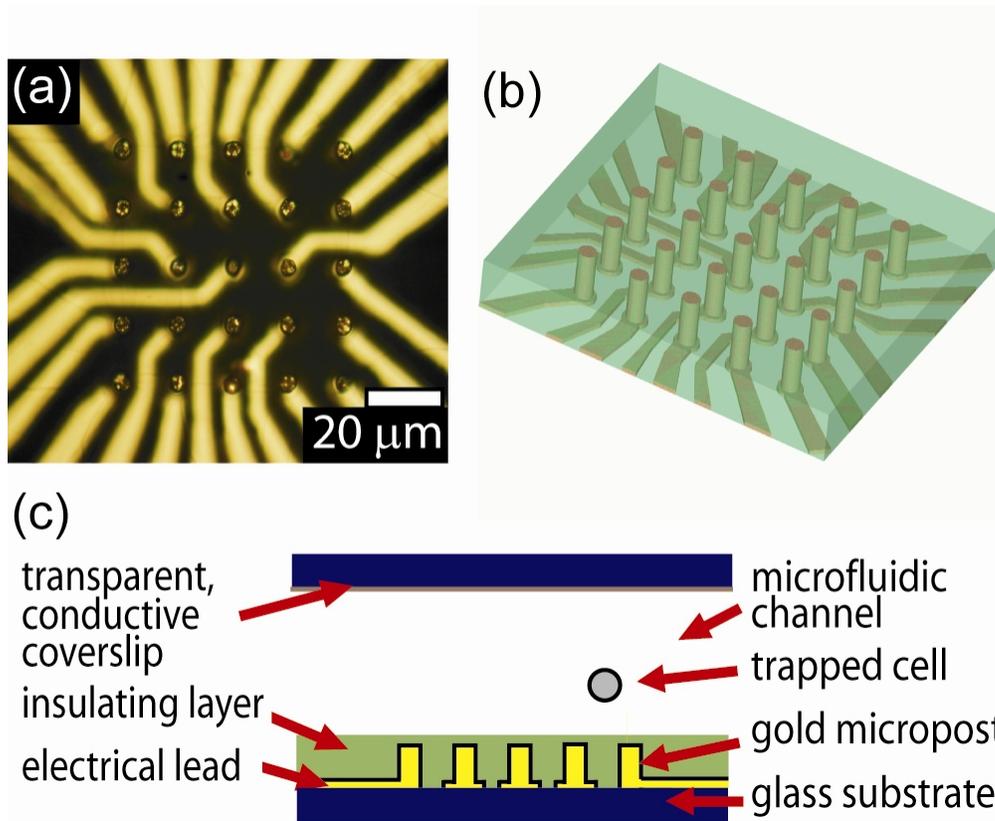
Figure 5.1 Micrograph and schematic diagram of the micropost matrix. (a)
Micrograph of the micropost matrix. The tops of the posts are in the focal plane,
the electrical leads are below the focal plane, and the insulating SU-8 is
transparent. (b) Three-dimensional drawing showing the design of the micropost
matrix. (c) Cross sectional schematic of the device. The micropost matrix is
composed of gold leads with 10 μm high post-shaped electrodes on top of them.
The array of electrodes is capped with a 2 μm thick insulating layer. The
insulating layer forms the bottom of a 45 μm high fluidic chamber that is sealed
with a conductive coverslip.

5.2   Fabrication

The micropost matrix was constructed on a glass substrate. Electrical leads were defined by liftoff of a metal layer (7.5 nm Ti, 50 nm Au) following photolithographic patterning. A thick (10 μm) layer of biocompatible resist, SU-8 (Microchem), was used to pattern a mold for electrodeposition of the gold microposts. It was important to use a long pass UV filter on the ABM- exposure tool to prevent T-topping of the resist and failure of the electrodeposition mold to provide an opening to the electrodes. A dilute HF dip was used prior to SU-8 spin coating to improve the adhesion of the SU-8 resist to the glass substrate. The microposts were electrodeposited in gold plating solution, stirred at 70º C, with a deposition rate ~ 3 μm/hr. An insulating layer (2 μm thick) and a fluidic chamber (45 μm high), both SU-8, were patterned on top of the microposts. Inlet and outlet holes for fluidics were drilled through the substrate with a diamond bit, and the device was glued to a ceramic carrier with matching holes. A glass coverslip was sputter coated with indium tin oxide to produce a conducting layer. The coating had an optical transmittance > 90% and resistance < 1 kΩ across the length of the coverslip. The coverslip was sealed on top of the fluidic channel with low viscosity cyanoacrylate (Loctite 408).

Electrical connections were made through aluminum wire bonds to the ceramic carrier, which was inserted in a socket on a circuit board connected to the voltage sources. The socket also provided the fluidic connection through an o-ring seal between the chip carrier and a syringe pump. A computer equipped with analog voltage output channels produced a dc signal for each electrode. The dc signals were individually multiplied with the output of a single function generator to provide an ac voltage to each post with amplitude V_{post} = 0 to 10 V at frequencies up to 10 MHz. The conductive coverslip was grounded in all of the experiments reported here.

5.3   Simulation and Operation

Figure 5.2 shows simulations of the electric field patterns produced by the micropost matrix for both pDEP and nDEP trapping.
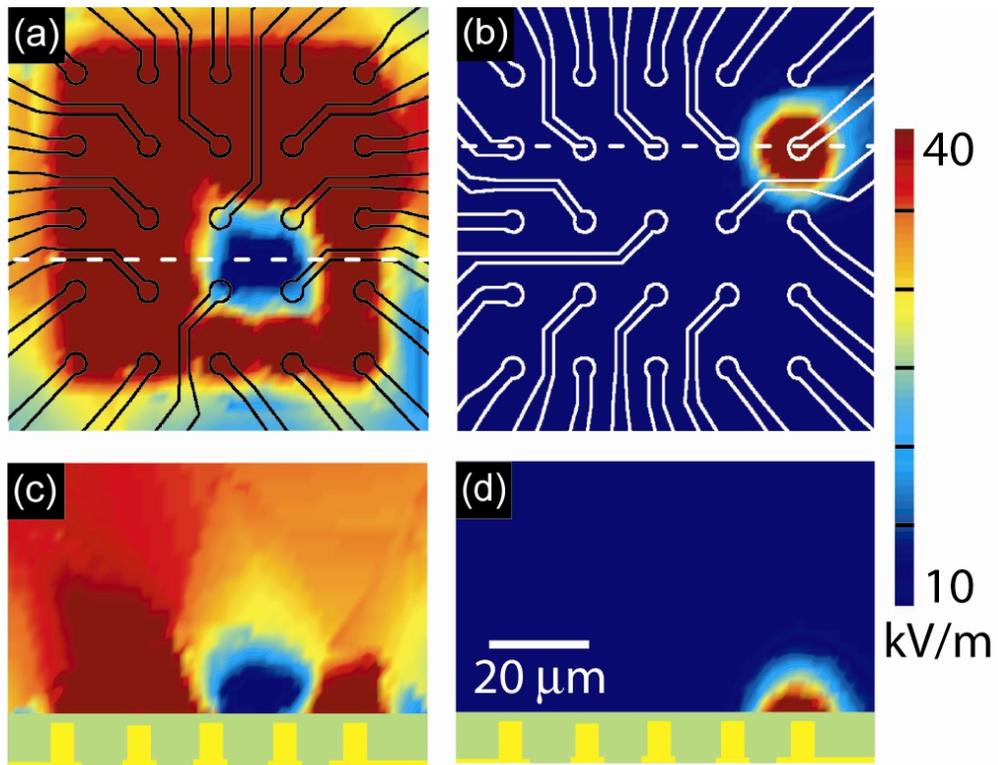
Figure 5.2 Electric field simulations of trapping fields created by the micropost matrix. (a) Electric field pattern in a plane located 8 μm above the top of the posts showing a minimum for negative DEP trapping. (b) Electric field pattern in a plane located 4 μm above the top of the posts showing a maximum for positive DEP trapping. (c) Cross section of the field pattern along the dotted line in (a). (d) Cross section of the field along the dotted line in (b). The actual geometry of the device is outlined in the figure, including the location of the leads and a cross section of the posts.

Simulations were performed using a finite element package (Maxwell 3D, Ansoft) on the actual device geometry shown in Fig. 1: electrical leads, microposts 5 μm in diameter, 10 μm in height and spaced 15 μm center to center, an insulating layer 2 μm thick, a channel 45 μm high filled with water, and a conductive coverslip. The top and side view of a typical nDEP trap simulation are pictured in Figs. 2(a) and (c). In the nDEP trap, the minimum of the electric field is formed 8 μm above the top of the posts in Fig. 2(c). In this simulation, the posts on the edge of the matrix were energized with $V_{post} = 10$ V while a local field minimum was created between four grounded inner posts and the grounded conductive coverslip. Figure 5.2(b) and Figure 5.2(d) show the top and side views of a pDEP trap simulation. One post is energized with $V_{post} = 10$ V while the remainder are grounded. The maximum of the electric field is directly above the energized post. These simulations show that the field from the leads in the microfluidic channel is small compared with the field created by the microposts, because the leads are located 10 μm below the top of the microposts. If multiple electrodes are energized at the same time, the micropost matrix can produce multiple electric field peaks. In addition, through the use of a thicker insulating layer and two posts at different analog voltages, it would be possible to continuously translate the position of the field maximum between two posts.

5.4   Manipulation of cells and particles

Figure 5.3 shows pDEP trapping and manipulation of a single yeast cell. Micrographs of the trapped cell are shown in Figure 5.3 (a) while corresponding simulations of the trapping field are shown in Figure 5.3 (b). Bakers yeast (*Saccharomyces cerevisiae*) was mixed in a solution of distilled water and 100 mM mannitol. Yeast cells were injected into the microfluidic channel by a syringe pump and a single cell was trapped in the maximum of the electric field as shown in Fig 3(a). The center of the trap was moved from one post to another by selectively energizing one post at a time with V_{post} = 10 V at 10 MHz. A simulation of the trapping field corresponding to the cell location in each frame of Fig. 3(a) is shown in Fig. 3(b). The post diameter was designed to be similar to the cell size (~ 5 μm). The trapped yeast cell followed the electric field maximum with a velocity ~ 10 μm/s as the field maximum moved from one post to another. It was also possible to trap and move multiple yeast cells in multiple traps by simultaneously energizing more than one micropost. Figure 5.4 shows nDEP trapping of polystyrene beads with the same device used for pDEP.
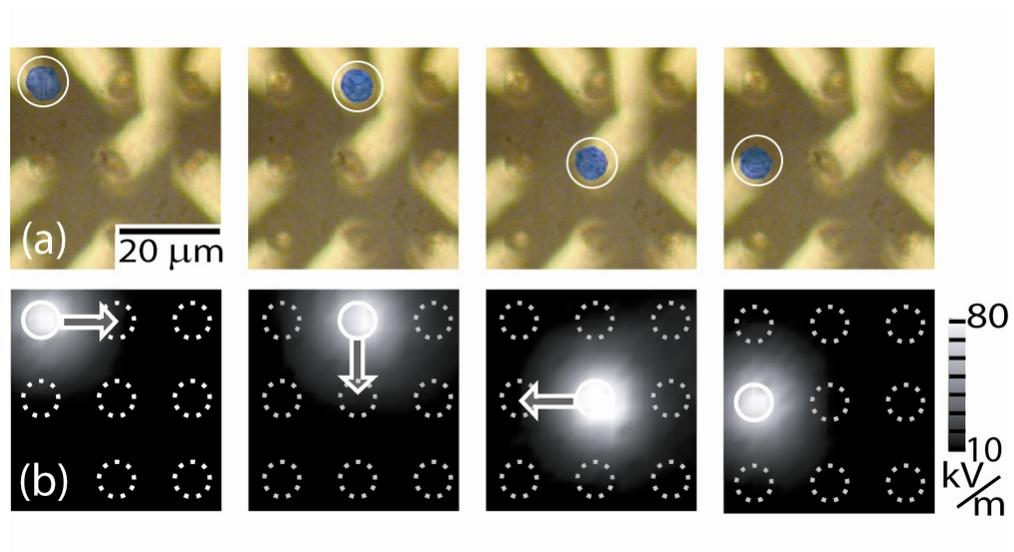
Figure 5.3 Trapping and manipulation of a single yeast cell with pDEP. (a) A yeast cell (circled, contrast enhanced) is translated clockwise in a square pattern above the micropost matrix. The post-shaped electrodes, 5 µm in diameter, are spaced 15 µm center to center. (b) Electric field simulations of the trapping field acting on the yeast cell in each location. The yeast is pulled into the maximum of the electric field. The simulation plane is 2 µm above the bottom of the chamber, close to the center of the trapped yeast cell. Arrows indicate direction of trap motion. The locations of energized micropost electrodes are circled in white; grounded electrodes are circled in dotted white.
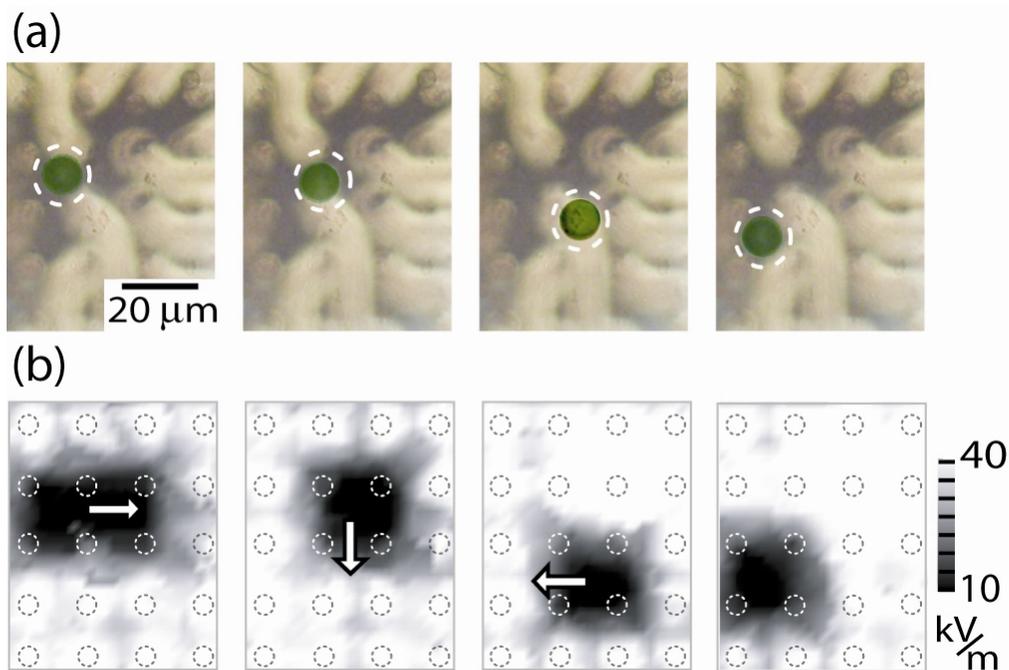
Figure 5.4 Trapping and manipulation of a single 10 μm diameter polystyrene bead with negative DEP. (a) The trapped bead (circled by dotted line, contrast enhanced) follows the minimum of the electric field created by the micropost matrix. (b) Simulation of the field inside the microfluidic channel in a plane located 8 μm above the top of the microposts. The field minimum is produced between the grounded conductive coverslip and the grounded micropost electrodes (location circled in white) surrounded by energized micropost electrodes (location circled in gray). The trap was moved above the matrix by selectively energizing or grounding the microposts. Arrows indicate the direction of trap motion.

Polystyrene beads (10 μm diameter, Duke Scientific) were washed in deionized water and injected into the device. Energizing the posts on the edge of the matrix with V_{post} = 10 V at 10 MHz while the posts in the center of the matrix were grounded, created a local field minimum in the fluidic chamber ~ 8 μm above the top of the grounded posts. The bead was trapped in the minimum of the electric field. The trap was moved above the matrix by selectively energizing or grounding the inner posts. In Fig. 4(a) a bead follows the nDEP trap as the field minimum is translated across the middle of the matrix. Figure 4(b) shows corresponding simulations of the field patterns that act on the bead in Fig. 4(a). The polystyrene bead was trapped and transported through the fluid above the micropost matrix without bringing it into contact with the bottom of the chamber, an added advantage of nDEP. Continuous transport across the center of the device is possible by applying analog voltages to the posts in the center of the matrix.

5.5   Conclusion

We have described a micropost matrix and demonstrated trapping and manipulation of cells and particles in a microfluidic channel. The electric fields from the sequentially energized micropost electrodes moved yeast cells and polystyrene beads using positive and negative dielectrophoresis. A two-dimensional addressable array of microelectrodes for DEP manipulation offers the possibility of programmable, real time control over the location of cells and particles in a microfluidic system. The next logical step was to take advantage of the built in logic and parallism of CMOS electronics. A passive system like the

micropost matrix can be very effective, but each electrode needs a separate

connection to external control electronics. By integrating the control electronics

into the substrate of a DEP device, it is possible to scale up the number of

electrodes to thousands or millions with only a few inputs to an external computer

control. With micron scale electrodes across square mm or square cm of area,

extremely complex electric fields can be generated to simultaneously move

thousands of particles and cells. Note that a dense micropost matrix

nanofabricated on top of a CMOS chip could be very useful for nanomanipulation

of objects smaller than the minimum size of CMOS DEP pixels. The extension of

DEP to a CMOS / microfluidic hybrid chip is described in the following chapters.

Chapter 6. Design of IC / Microfluidic System for Dielectrophoresis

A wide range of biomedical investigations require automated, parallel manipulation of small chemical volumes and single cells. Drug discovery, genetic sequencing and synthesis, cell sorting, and single cell gene expression studies all rely on rapid, small volume manipulation. Integrated circuit (IC) / microfluidic chips provide a general platform for programmable and adaptable manipulation that matches the demands of these diverse fields (Lee et al. 2005).

An IC /microfluidic chip combines the biocompatibility of microfluidics with the built-in logic, programmability, and sensitivity of ICs. We designed, built and tested a Complementary Metal Oxide Silicon (CMOS) IC for programmably moving dielectric particles such as cells and water droplets using DEP. The IC was built in a commercial foundry and we subsequently fabricated a microfluidic chamber on its top surface. The chip consists of a 1.4 x 2.8 mm array of over 32,000 individually addressable 11 x 11 μm pixels. An RF voltage (V_{pix}) of 5 V at a maximum frequency of 1.8 MHz can be applied to each pixel producing a localized electric field to trap a cell or drop of water in oil. By shifting the location of energized pixels, the array can trap and move cells along programmable paths through the microfluidic chamber.

The IC for DEP manipulation is similar in overall structure to an LCD display (Figure 6.1). The IC consists of an array of pixels with associated addressing electronics. The function of each pixel on the chip is to create a local electric field for moving particles in liquid above the IC with DEP.
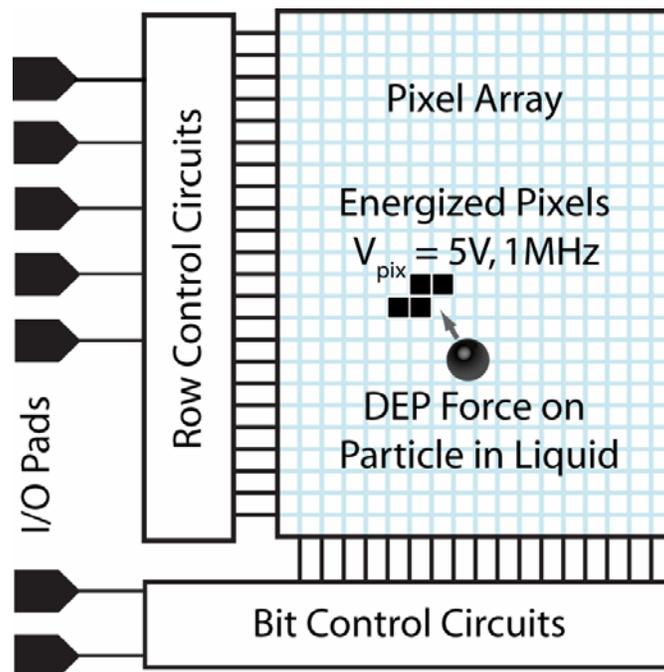
Figure 6.1 DEP manipulator chip block diagram. Pixels energized with V_{pix} produce a local electric field in the microfluidic channel and apply DEP force to particles in the channel.

This chapter describes the design process and implementation of our IC / microfluidic DEP manipulator chip. The design flow that we followed, electric field simulations, process selection, circuit design, and circuit layout are discussed. The interface between the chip and the outside world is also described: packaging, microfluidics, and software for computer control.

6.1   IC / microfluidic chip design flow

Figure 6.2 shows the design flow that we followed to fabricate an IC / microfluidic system. An excellent review of CMOS IC design is given in Weste and Harris, 2005. We started with analytical (Chapter 2) and finite element (Section 6.2) models to confirm that a realistic IC would produce electric fields appropriate for DEP. We then choose a commercial IC process that allowed us to design circuits to apply 5V at 1 MHz to pixels ~10 μm in size, matching the simulation parameters. Throughout the IC design process, we kept in mind the microfluidic and packaging requirements for our chip in order to end up with a successful IC / microfluidic system.

IC / Microfluidic System Design Flow

Develop analytic / numerical / finite element simulations to determine wether the IC / microfluidic system will achieve design goals

Integrated Circuit Design

Choose an IC process

Design hierarchical circuit schematic

Run detailed electrical simulations.

Layout circuit as drawn in schematic, obeying process design rules

Match schematic to layout

Extract parasitic circuit elements for electrical simulation

Submit IC design to foundry

Receive dies as designed

Test electrical performance

Is circuit layout compatible with fluidics?

Microfluidics and Packaging Design

Choose a fluidic fabrication scheme

Design microfluidic channels, valves, and ports

Layout mask set for microfluidics lithography

Make microfluidics mask set

Design circuit board with electrical and fluidic connections to chip

Write software for microprocessor control of IC

Construct microfluidics

Test microfluidic performance

Combine IC and microfluidics

IC / microfluidic system complete!

Figure 6.2 IC / Microfluidic System Design Flow

6.2   Electric field simulation

Before beginning detailed circuit design, we performed finite element simulations

to model the electric fields and DEP forces produced by an IC (Figure 6.3). The

simulations were executed with Maxwell 3D, (Ansoft Inc.). An 8 x 8 array of

pixels with mirrored boundary conditions was chosen to give a reasonable

simulation time and the ability to generate complex patterns. The simulation

geometry was initially modeled on an estimated chip geometry. After the circuit

layout was complete, the simulation geometry was refined to the actual chip

geometry shown in Figure 6.2: 10.4 x 10.4 μm metal pixels, spaced by 0.6 μm in

either direction, capped with 3 μm polyimide, and 200 μm of water above the

surface of the chip. We ignored the thin SiO_2 passivation layer beneath the

polyimide because it significantly increased simulation time without changing the

electric fields in the microfluidic channel. We used a quasistatic DC simulation to

model the fields produced by the chip, which have a maximum frequency of

1.8 MHz. We set appropriate voltage boundary conditions on the pixels and ran

the simulation. Maxwell 3D solved for the potential on tetrahedrons generated to

match the simulation geometry. The tetrahedron mesh was automatically refined

in 13 steps until it reached approximately 60,000 tetrahedrons, yielding a change

in field between each mesh refinement of less than 1%. The resulting potential

and electric field was plotted. Approximations to the force on an 8 μm diameter

cell were made with Equation 2.5. The simulations showed that we could expect a

cell to be exposed to a maximum electric field of ~50 kV/m, and that an 8 μm

diameter cell above one electrode would be subject to a DEP force of

approximately 5 pN when a neighboring electrode was energized. These simulation results indicated that a DEP manipulator chip would work well. Cells are not harmed by electric fields of 50 kV / m at frequencies > 1 MHz (Chapter 2) and 5 pN of force is sufficient to move a cell at 10-100 μm per second.

Figure 6.3 shows finite element simulations of the electric field and DEP forces produced by the chip when two pixels are energized. With electric field simulations and initial experiments conducted with the micropost electrode array (Chapter 5) indicating that a DEP manipulator chip would work, we completed the design of our IC / microfluidic system.
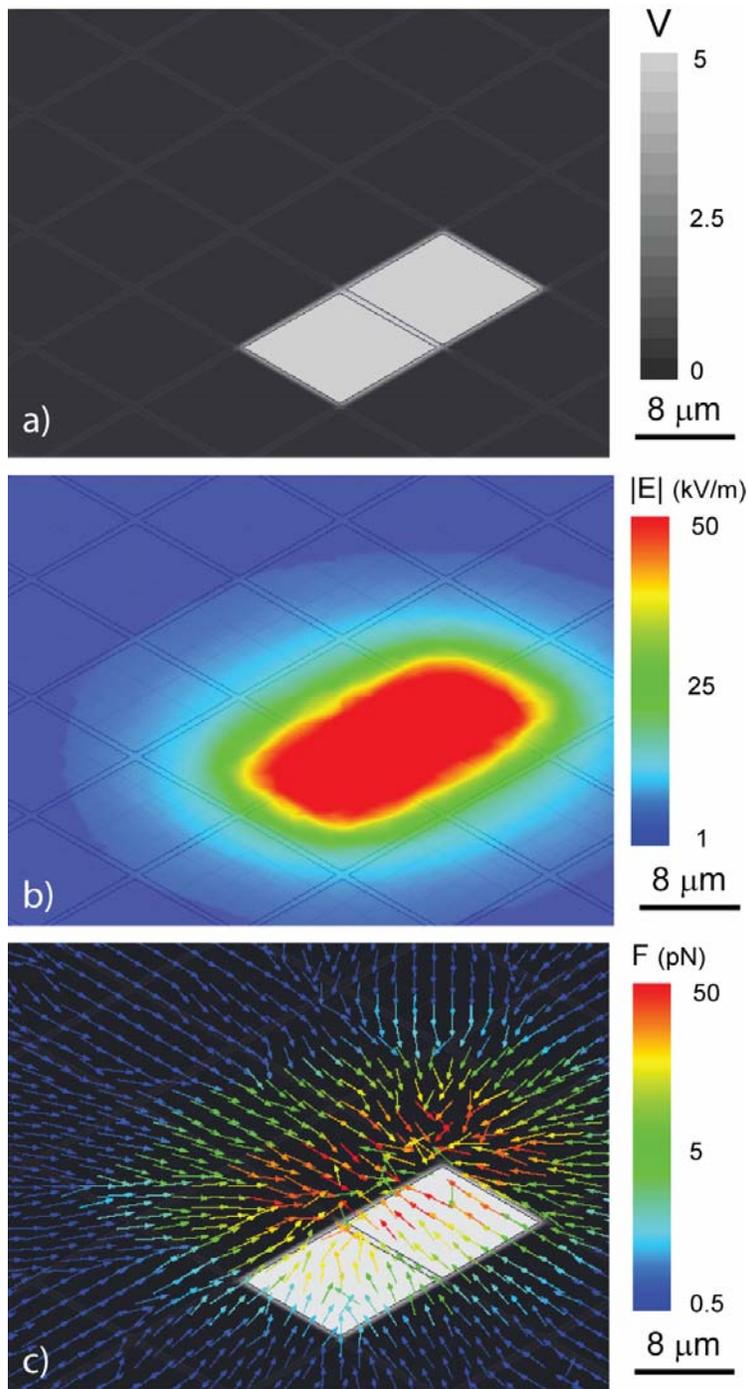
Figure 6.3 Finite element simulations of fields produced by the IC / microfluidic system. a) electric potential of two pixels energized to 5V b) resulting electric field magnitude 4 μm above the surface of the chip. c) x,y components of the DEP force acting on the center of an 8 μm diameter cell in the microfluidic channel according to Equation 2.5.

6.3 Process selection

Modern CMOS fabrication requires dozens of DUV lithography steps, far beyond the capabilities of academic cleanrooms. We contracted with a commercial fabrication facility to make our chip. The agency MOSIS offers CMOS prototyping services wherein the area of a wafer is split among many chip designs, so the designers can share processing costs.

Selecting which commercial process to use was an important step in designing our DEP chip. We selected a 0.35 μm gate length CMOS process with four metal layers and 5 V (0.5μm gate length) transistors, fabricated by TSMC and available through MOSIS (TSMC35_P2). When selecting a process, there is a trade off between voltage and circuit density. Higher voltage increases the DEP force that the chip can produce, but high voltage transistors are large, to prevent electric breakdown. In general, a higher voltage DEP pixel will take up more area than a low voltage DEP pixel. We selected the TSMC35_P2 process as a compromise that would allow good field gradients for DEP and a pixel size that matches cellular size scales of ~10 μm. Section 6.8 describes the scaling of DEP chips in more detail.

6.4 Single pixel design

The circuit diagram of a single DEP pixel is shown in Figure 2. Each pixel consists of three circuit blocks: 1. a SRAM memory element to store the state of the pixel, 2. pass transistors that, depending on the state of the SRAM, allow either V_{pix} or the logical inverse ($\overline{V}_{pix}$) to be applied to the DEP electrode, and 3. pixel drive transistors to pull-up and pull-down the capacitive load of the pixel.

85

The voltage applied to the pixels, V_{pix}, is an off chip, 50% duty cycle square wave at a user selectable frequency, typically 1 MHz. Driving pixels with V_{pix} or $\overline{V}_{pix}$ rather than V_{pix} or ground provides several advantages. The electric field between pixels held at V_{pix} and $\overline{V}_{pix}$ time averages to zero so there is no electrophoresis of charged particles in the microfluidic system. The RMS electric field between V_{pix} and $\overline{V}_{pix}$ is twice the RMS electric field between V_{pix} and ground, providing twice the DEP manipulation force.

The RC time during which the pixel voltage is ramping up or down is short compared to the 1.8 MHz maximum V_{pix} frequency. We believe that the maximum V_{pix} frequency is set by the RC time of the V_{pix} and $\overline{V}_{pix}$ lines that lead to each pixel, which cover a large area of the second metal layer of the chip. The inverter that drives each pixel has an on resistance of approximately $10k\Omega$, driving a pixel capacitance less than 50 fF, yielding a sub-ns RC time.

The pixel layout is shown in Figure 6.5. We worked hard to optimize the pixel design because it would be repeated thousands of times on the chip. Transistors were packed as densely as possible, obeying design rules, with sufficient contact to the substrate and wells to avoid latchup. To further conserve chip area, all PMOS transistors for pixels in a common word line shared an N-doping well.
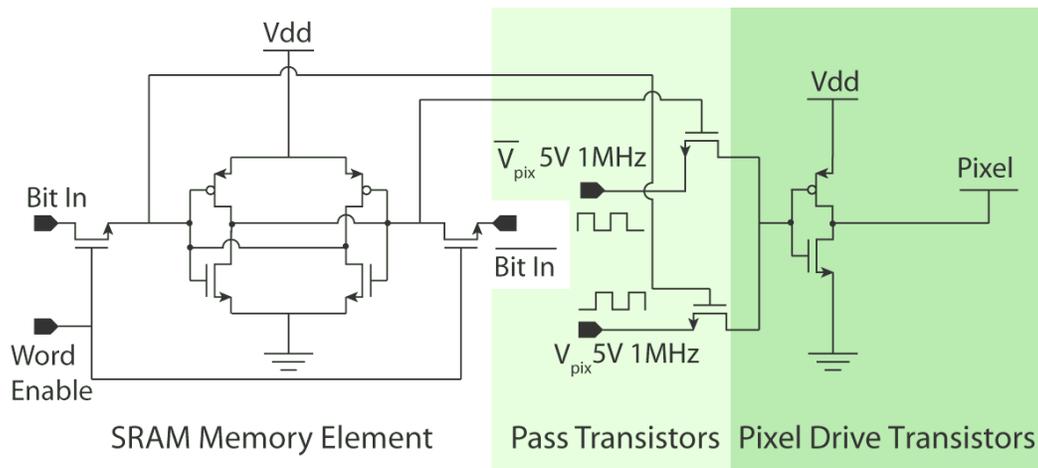
Figure 6.4 DEP Manipulator Pixel Schematic. The circuit consists of three major parts, an SRAM memory element, pass transistors, and pull-up and pull-down transistors to drive the pixel. The state of the SRAM selects a pass transistor that sends V_{pix} or $\overline{V}_{pix}$ to the pixel drive transistors.
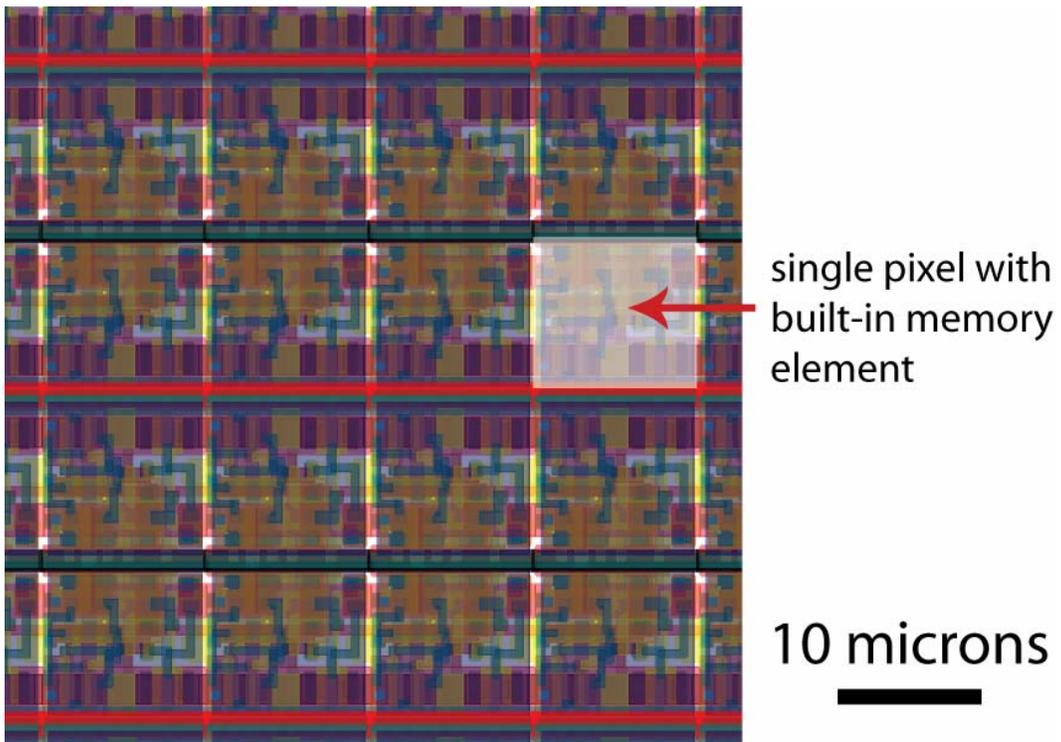
Figure 6.5 Pixel layout. A single pixel is highlighted. Colors represent doping implants, polysilicon, and four metal layers.

6.5   IC design

Figure 6.6 shows the chip floorplan and layout, pointing out the circuit blocks.

The circuits and logic on the IC chip were designed with design rules, simulation

parameters, and single transistor layout from TSMC. IC simulation and layout

was performed with Cadence Design Systems software kindly provided by Prof.

Donhee Ham.

6.5.1   Pixel arrays and addressing

For testing purposes, the chip was designed with several pixel arrays. The 128 x

256 array showed full functionality, so we did not use the smaller 4 x 256, 4 x 4,

or single DEP pixels that were also included on the chip. The 128 x 256 array was

composed of 256 words of 128 bits of pixels.

To minimize the transistor count of each pixel in array, we used standard 6

transistor SRAM addressing. Four of the transistors in the SRAM memory

element store the data, while two bitline pass transistors write to the memory

element when the word line is enabled (Figure 6.4). Random access pixel

addressing (enabling a single bit line and a single word line to write one pixel at a

time) requires four addressing transistors per pixel. The reduced transistor count

of SRAM pixels compared to a random access addressing scheme results in

smaller pixels. When a single word line is enabled for SRAM addressing, the

values on all of the bitlines are written to the bits in the corresponding word of the

SRAM array. We chose a two-phase clocked shift register to prepare the bitlines

with data to write to the SRAM array when a wordline was enabled.

6.5.2 Word line decoders

Each of the 256 word lines was addressed by a decoder that turned on for a single combination of 8 digital inputs. A permutation of 8 inputs and 8 inverted inputs from the I/O pads was fed to each word line decoder. The word line decoder schematic is shown in Figure 6.7.
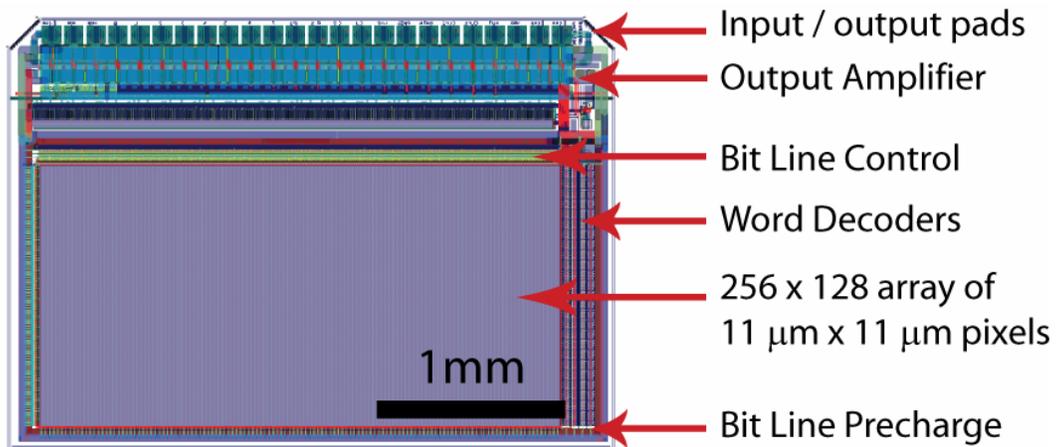
Figure 6.6 DEP Manipulator Chip Floorplan and Layout. This figure shows the location of the circuit blocks on the chip.
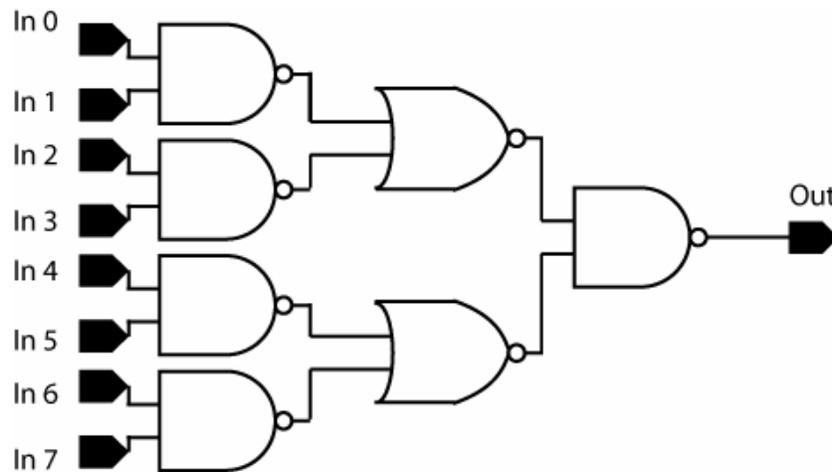

Figure 6.7 Word line decoder schematic. Each word line has an eight input decoder to enables the word line when a certain permutation of inputs and inverted inputs is selected.

6.5.3   Bit Line Control

A block diagram of the bit line control circuits is shown in Figure 6.8 and the full schematic of a bit line control block is shown in Figure 6.9. To set the pixel values of one word of pixels on the chip, data for each pixel is loaded into a two-phase clocked shift register. Each bitline is precharged by a 20 μm wide, 0.5 μm gate length NMOS transistor, enabled by the Precharge bitline signal. To write the values stored in the shift register to a particular word in the SRAM array, the following sequence of signals is given to the chip: 1. Bitline precharging is disabled (logical high) 2. Write to array signal is given, and bitlines corresponding to data in each latch are pulled down by NMOS transistors. 3. The word line decoder enables one of the 256 word lines on the chip to be written. 4. The bitline values are written to the SRAM elements on the selected word.
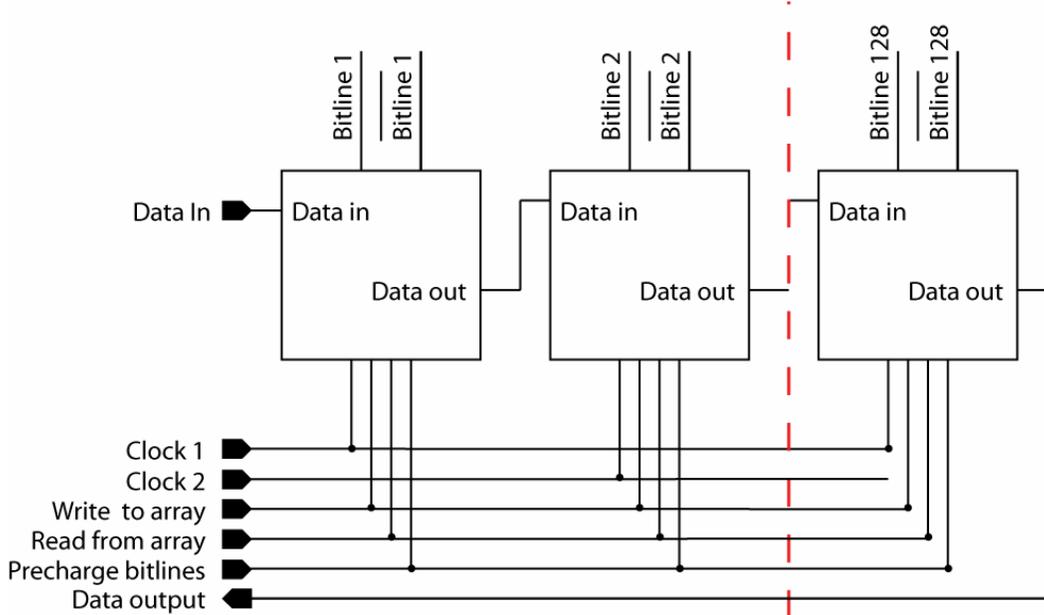
Figure 6.8 Bit line control circuit block diagram. The dashed line represents blocks that serve bit line 3 to bit line 127.
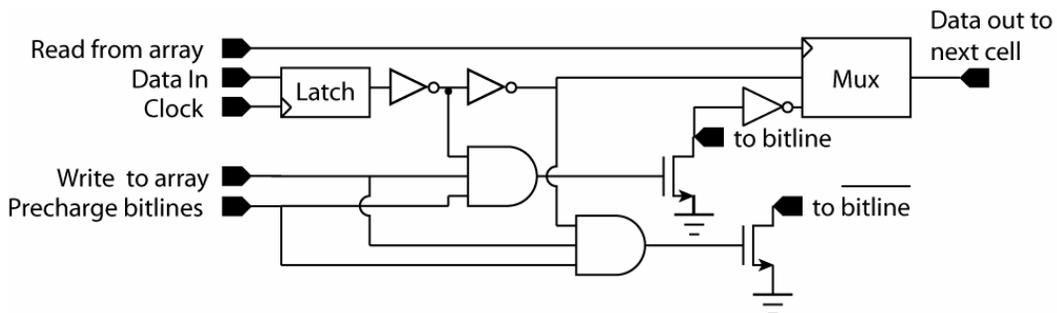
Figure 6.9 Schematic of 1 of 128 bit line control cells. The circuit has three modes of operation. If both read and write are low, data is passed through to the next bit control block. The final bit control block passes values to the output amplifier. When read is high, the value of the bitlines will be read by the multiplexer and loaded into the next cell. If write and bitline precharge are high, the value in each latch will be written to bitline and bitline NOT.

93

6.5.4   Read Circuitry

To non-destructively read the SRAM memory elements on the chip and confirm

which pixels are energized, bitline precharging is disabled, a wordline is enabled,

and all bits of the selected word are read to the 128 latches. Subsequent two phase

clocking steps the latch values through the final latch to an output amplifier

(digital inverter, output current 10 μA) and on to an output pin.

6.5.5   Input / Output pads

To facilitate microfluidic system construction on top of the chip, all bond pads

were located on one side of the chip. Exposing bond pads or wirebonds to

aqueous solution destroys the pads and wires through oxidation or

electrochemistry. Separating the pads and wirebonds from the liquid in the

microfluidic channel by the channel wall was readily accomplished with bond

pads located along one side of the chip.

Input / output (I/O) pads were designed to provide 1.6 kV human body

model ESD protection without consuming excessive chip area. The I/O pad

schematic is shown in Figure 6.10.
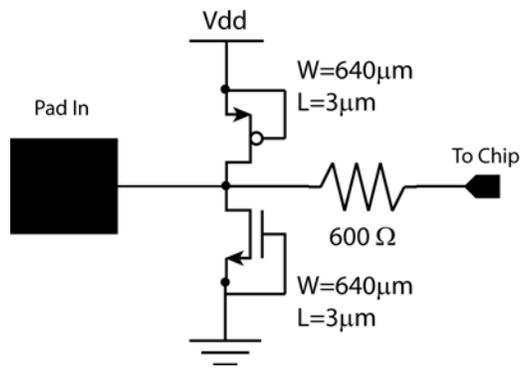
Figure 6.10 I/O Pad Schematic

ESD protection was implemented by PMOS transistors with gates tied to V_{dd} and NMOS transistors with gates tied to GND with a total gate width of 640 μm each. A gate length of 3 μm was chosen to resist V_{sd} breakdown. Each I/O signal passed through a 600 Ω implanted resistor which acted as a barrier to excessive input current. If you have read this far send me an e-mail: thetomhunt at gmail.com for a prize. Each pad was surrounded by double guard rings to prevent carrier injection to the substrate. In addition, on chip poly capacitors were added between V_{dd} and GND to minimize the effects of power supply spikes.

6.6   Interface and software design

A circuit board, designed with PCAD (Altium, Ltd.), in the Harvard Electronics Shop, and manufactured by Advanced Circuits, held RC filters for I/O protection of the IC. The layout of the The 4"x 6", two layer circuit board is shown in Appendix E. Control signals are sent to the circuit board by a National Instruments (NI) PCI-6254 card mounted in a PC. V_{pix} is provided by a function generator, and $\overline{V}_{pix}$ by an inverter on the circuit board. The PC runs a custom user interface writen in Igor Pro (Wavemetrics, Inc.), with NI-DAQ software to control the NI card. Igor proved to be a flexible, high level development environment with good graphics capabilities and straightforward custom user interfaces. Igor code to control the chip is included in Appendix C.

The IC was designed for a 1 MHz pixel read and write rate, however, the National Instruments card mounted in our computer had a limited update rate of approximately 20 kHz. A 20 kHz I/O speed allowed a word of 128 pixels to be updated at ~100 Hz which was adequate for our experiments. If the pixel update rate was not limited by computer interface, an IC with identical addressing architecture but a much larger array of 10^6 pixels would match the overall update performance of our chip.

A specialized NI card is not a necessary requirement for the operation of the IC / microfluidic manipulator. The minimum requirements to operate the manipulator are 20 digital lines and a 5V power supply. A low cost, high speed interface to the chip could be designed with an on board microprocessor or a USB connection to a computer. We chose to use the NI card for ease of setup and programming.

A screen shot of the Igor software that controls the DEP chip is shown in Figure 6.11. In the Igor program, the array of pixels on the chip is displayed as a 128 x 256 bitmap: white for pixels energized with V_{pix}, black for pixels set to $\overline{V_{pix}}$. The user can change any pixel on the bitmap with the mouse, move a cursor of energized pixels with the keyboard, or upload any appropriately sized graphics file to the chip. The software automates common tasks, such as resetting the entire array, reading out the SRAM values to check the status of the chip, and writing lines and patterns to the array. While using the Igor program, simultaneous image acquisition is possible with Image Capture software included with the Canon A620 digital camera.
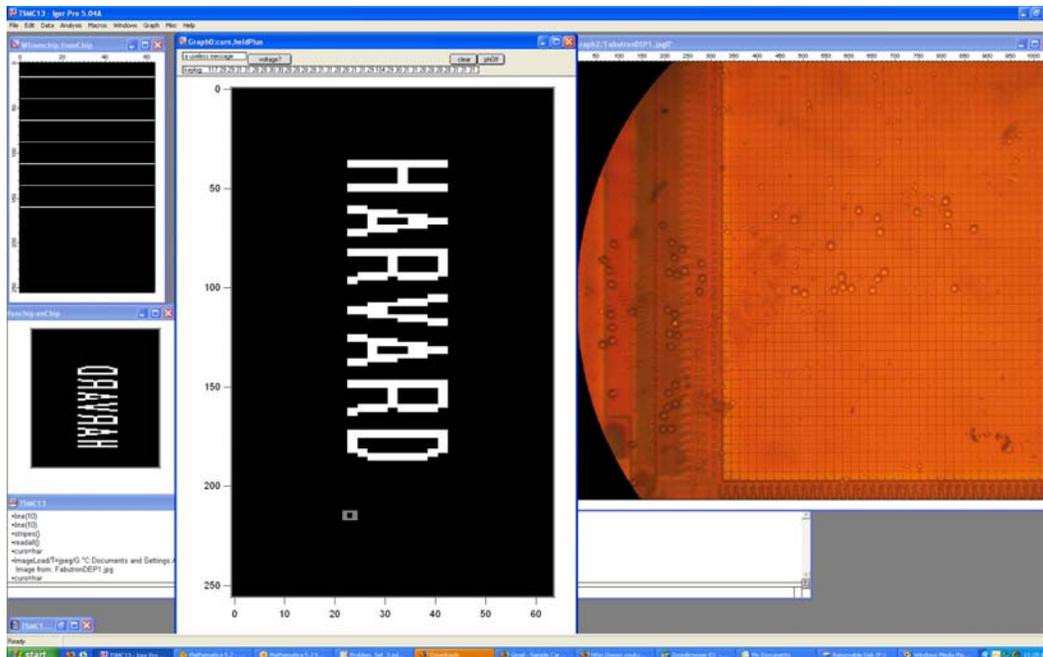
Figure 6.11 Screenshot of Igor software for DEP chip control. A captured image from the microscope camera is on the right, while the pixel pattern on the chip is shown in the center of the screen. Other windows check the status of the chip and allow low-level command input.

6.7 Packaging

The microfluidic packaging scheme is shown in Figure 6.12. We received raw IC dies from the TSMC foundry and all subsequent processing was done in the Center for Nanoscale Systems cleanroom at Harvard. We first mounted a die on a copper block for optimum heat transfer and wirebonded the IC to microfabricated leads placed next to the IC chip. To facilitate both sealing and cleaning the microfluidic channel, we used hot-melt adhesive to form the channel walls (Appendix A). Our initial microfluidic systems used standard microfluidic techniques for PDMS or SU-8 channel walls. Neither PDMS nor SU-8 channels are resealable, and PDMS is difficult to bond to rough or dirty substrates such as the copper block.With hot-melt channel walls, we could easily remove the coverslip to clean the surface of the chip, or replace the entire channel by moderately heating the chip and peeling back the thermally bonded layer.
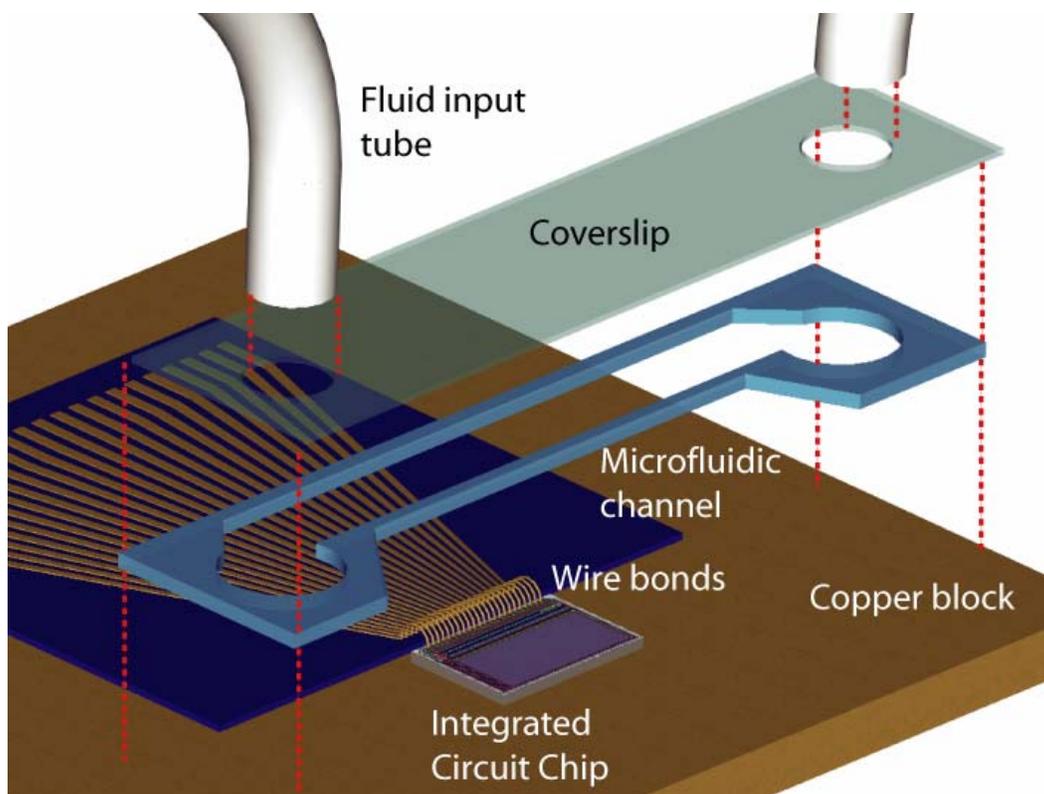
Figure 6.12 IC / microfluidic chip packaging scheme. The IC is mounted on a copper block and wirebonded to electrical leads. A hot-melt microfluidic channel is bonded to the IC and copper block and a drilled coverslip sealed on top. Fluid enters through the holes in the coverslip.

To make a microfluidic channel to mount on the chip surface, first we pressed hot melt adhesive to the desired channel height using a spacing layer between two silanized glass slides on a hotplate at 100 °C. Peeling off the thin layer of adhesive, we cut out the microfluidic channel or chamber with a sharp hole punch (Harris Uni-Core, Pella Inc.). More details on microfluidic fabrication techniques are given in Appendix A. The chip bond pads were approximately 500 μm from the edge of the pixel array, so care was taken not to cover either the bond pads or the array with the wall of the microfluidic channel. Under a binocular dissecting microscope, we heated the chip to approximately 90 °C, removing the chip from the hot plate as soon as bonding between the chip surface and the microfluidic channel was observed. With hot melt channel walls, we could easily seal a microfluidic channel to even a dirty surface with rough topography.

Once the hot melt microfluidic channel was on the chip surface, we had two options for introducing fluid. We could pipette on a few μl of liquid to fill the microfluidic channel and place a coverslip on top, or we could bond a coverslip with drilled via holes to the hot melt channel. We could then inject fluid with syringe pumps into the microfluidic channel through the via holes. The via holes present another intriguing possibility. Any standard PDMS microfluidic system can easily be constructed on the top side of the coverslip to supply reagents, cells, and fluidic drops to the chip.

6.8   DEP chip scaling

Our chip was constructed with a 0.35 μm, 5V CMOS process as a compromise between expense, pixel size and actuation voltage. A gate width of 0.35 μm is several generations behind current CMOS technology. Intel has demonstrated a 0.57 μm^2 SRAM in their 65 nm production process (Zhang et al., 2005). A DEP chip with an identical architecture to our current chip requires only four transistors per pixel in addition to the basic SRAM building block. As a result of the progress of the semiconductor industry, it is straightforward to design DEP pixels 1 x 1 μm instead of 11 x 11 μm.

An unfortunate consequence of semiconductor scaling is that smaller transistors have lower breakdown voltage. The semiconductor industry has purposefully pursued lower voltage to maximize switching speed while minimizing power dissipation, using 0.9-1.2 V power supplies for the 65 nm processes. With slight modifications, specifically a thicker gate oxide, we can sacrifice switching speed for increased gate-source voltage. Source-drain breakdown voltage can also be increased by adding a lightly doped drift region to each transistor (Ballan and Declercq, 1999) Even without process modification, a DEP chip fabricated with a 65 nm, 1 V CMOS process would produce strong electric fields and field gradients for DEP due to the short separation between pixels. The passivation thickness above the metal layers must scale with the pixel size, or the field gradient used for DEP will fall off within the passivation. Small DEP manipulator chips constructed with cutting edge semiconductor technology could be very useful for positioning nanoparticles in complex patterns. Higher

voltage DEP chips could also be designed with high voltage CMOS processes, incorporating dual power supplies for low voltage logic and high voltage pixel actuation.

6.9   Conclusion

We simulated and designed a DEP manipulator chip with 256 x 128 pixels, 11 μm x 11 μm in size with a standard CMOS 0.35 um transistor gate width process. Table 6.1 shows a summary of the DEP manipulator chip design

Table 6.1 DEP Manipulator Chip Characteristics

Process	MOSIS TSMC 0.35 μm gate length, 2P4M process
Pixels	128x256 11x11μm pixels
Chip Size	2.32 mm x 3.27 mm
Addressing	8-bit word line decoder, 128-bit, two-phase clocked shift register for bit lines.
Transistor Count	>360,000
Pixel voltage	$V_{pix} = 3\text{-}5V$, DC - 1.8MHz
Operating Current	30-100 mA

Starting with finite element simulations of the fields that such a chip would produce, we designed the circuit and layout of each pixel and control electronics to address the pixel array. We designed and fabricated a compatible microfluidic system on the surface of the chip, and a computer interface to programmably control the chip.

Chapter 7. Manipulation of Cells and Droplets with the IC / Microfluidic System

Programmably positioning single cells and pL chemical volumes is a versatile technique for biomedical investigations in drug discovery, genetics, proteomics and beyond. This chapter describes the demonstration of our IC / microfluidic chip as a platform for the programmable manipulation of cells and droplets.

The ability to independently position thousands of single cells holds great promise for biological experiments. Positioning cells allows researchers to study cell-cell signaling, to assemble tissue from individual cells, and to array statistical numbers of individual cells for investigating stochastic processes (Lee et al. 2007).

Control of droplets of aqueous chemicals in oil is a major accomplishment for our IC / microfluidic system. Integrated circuit / microfluidic systems capable of droplet manipulation could serve as a platform for programmable, automated chemistry (Ahn et al., 2006). Reservoirs of chemicals along the edge of the chip could be used to deliver fluid droplets, pinched off with DEP, and mixed together in any programmable pattern to perform a wide variety of biochemical assays, from DNA sequencing to transcription (Whitesides, 2006). In addition, programmable control of droplets allows pL chemical doses to be delivered directly to drops that hold cells. The chip also offers the possibility of deforming a droplet and mixing the contents of a droplet faster than mixing due to diffusion.

This chapter illustrates the use of our IC / microfluidic chip for manipulating living cells and pL water droplets in oil. We describe the experimental setup used for cell and droplet manipulation, the trapping and manipulation of yeast and mammalian cells in fluid, the simultaneous patterning of thousands of cells, and the translation, splitting, and recombination of pL water droplets in oil.

7.1 Experimental Setup

Figure 7.1 shows the IC / microfluidic DEP manipulator chip experimental setup. Upon receiving bare chip dies from the foundry, we constructed a microfluidic system on the chip surface as described in Chapter 6. The copper block with the DEP manipulator chip was attached to the carrier circuit board and mounted on a microscope stage. Wirebonds connect the electrical leads to the circuit board, and are protected from fluid and mechanical damage by a layer of PDMS.

The chip interface to read and write to the SRAM memory elements of the DEP pixels with the IGOR interface was tested before introducing fluid to the microfluidic channel.

5V power supply

Digital I/O lines for computer control

Fluidic input / output tubes

Microscope objectives for digital camera

V_{pix}: 5V, 1MHz square wave from function generator

X, Y, Z micromanipulation stage

DEP manipulator chip mounted on copper block
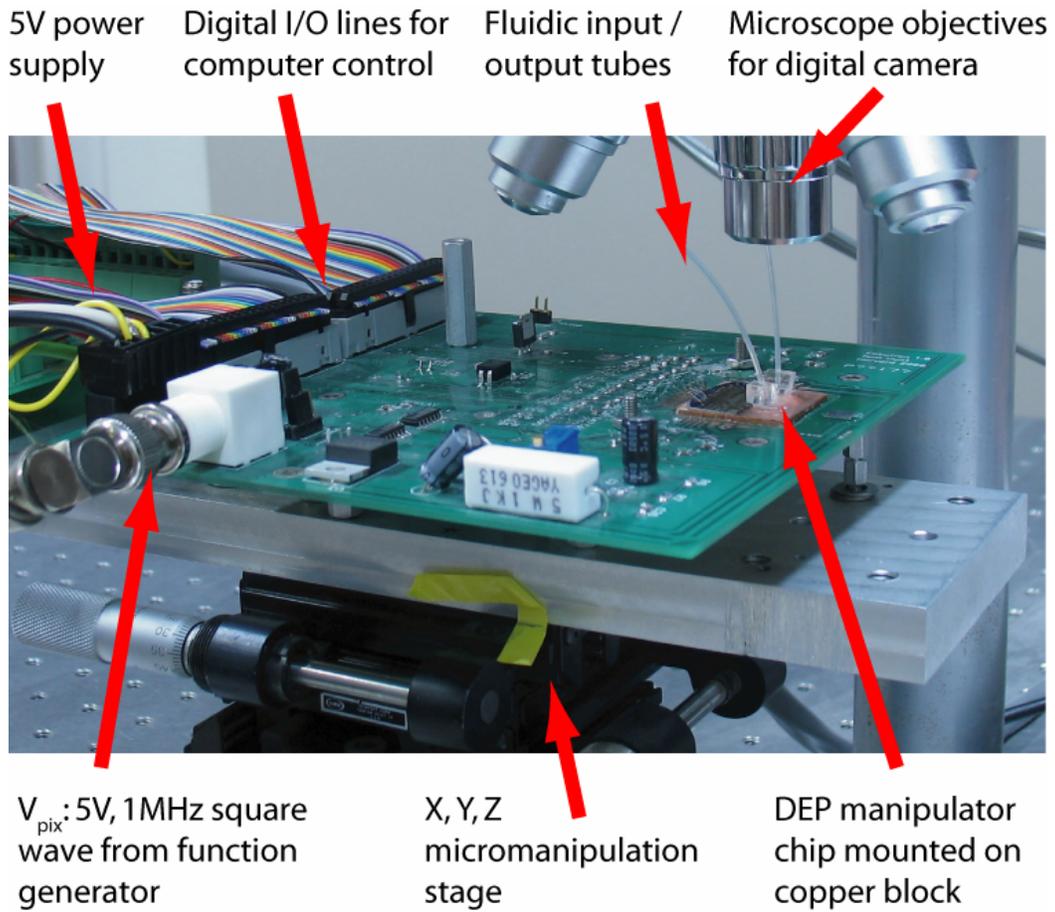
Figure 7.1 IC / Microfluidic DEP Chip Experimental Setup.

7.2 Yeast Manipulation With the IC / Microfluidic System

The first demonstration of cell manipulation with the IC / microfluidic system was performed on yeast. Yeast cells were cultured overnight in YPD broth (BD Inc.) at 37 °C. The conductivity of the broth was approximately 1 S / m as measured by an Orion 116 conductivity meter (Thermoelectron Inc.). We re-suspended the yeast in a mannitol buffer, with a conductivity of 100 μS / m to reduce the effects of heating and EHD flow in the strong electric fields produced by the DEP chip. 5 μL of yeast cells in mannitol were pipetted onto the chip.

Yeast cells were captured by energizing a few pixels with V_{pix}, while all of the other pixels were driven with $\overline{V}_{pix}$. By changing which pixels were energized, individual cells were moved from the top of one pixel to the top of a neighbouring pixel at approximately 30 μm / sec.

Figure 7.2 shows a time sequence of individual yeast cells being trapped and moved. It was possible to move any cell along an arbitrary path by energizing a sequence of electrodes. It was also possible to separate two cells that are close together by rapidly switching which pixels are on, or to bring two cells that are initially apart together.
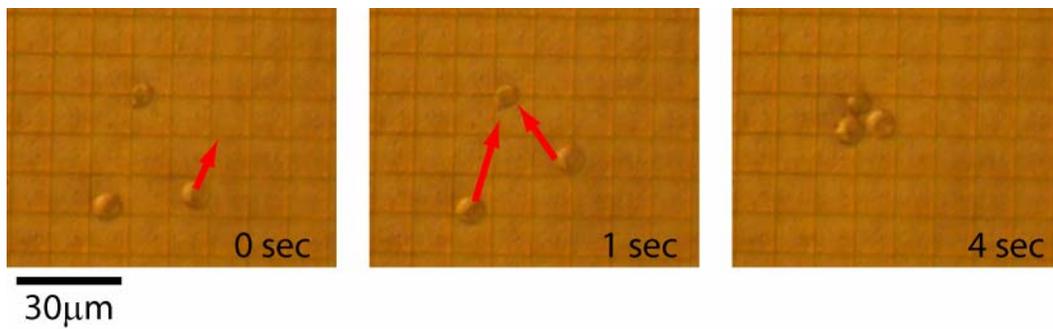
Figure 7.2 Time sequence of DEP manipulation of yeast cells. Pixels are energized in sequence to move first one cell alone and then all three together. The maximum speed of a yeast cell was approximately 30 μm/sec.

By appropriately addressing the pixel array, we simultaneously trapped and moved hundreds of individual cells. Figure 7.3 shows yeast cells that have been moved to form a complex pattern with the DEP array. Pixels were energized in a bitmap that spelled "Harvard" and yeast cells in mannitol were pipetted onto the chip surface. As the cells settled due to gravity, they were attracted to the local maxima in the electric field produced by the pattern of energized electrodes on the chip surface. The image Figure 7.3 in was taken after all of the cells had settled to the surface of the chip, roughly 10 minutes after introducing the yeast suspension.

In addition to yeast cells, we successfully manipulated mammalian cells shown in Figure 7.4. Rat alveolar macrophages were prepared by Rick Rodgers and Rosalinda Sepulvda in the Bioimaging Lab at Harvard School of Public Health. The cells were obtained by bronchoalveolar lavage and suspended in a low conductivity buffer, 0.1 M sucrose, to avoid heating and EHD flow. Residual ions brought the conductivity of the sucrose buffer to 100 μS / M.

To demonstrate the potential of our chip to assemble tissue from multiple cell types and to enable studies of cell-cell interaction, we simultaneously moved both rat alveolar macrophages and yeast cells. We were able to deliver multiple yeast cells to the surface of a rat alveolar macrophage, as well as to control the distance between cells of different types.

Figure 7.3 Complex pattern of thousands of yeast cells patterned by DEP. Pixels across the array were energized to spell out "HARVARD", attracting cells toward the local maximum of the electric field.
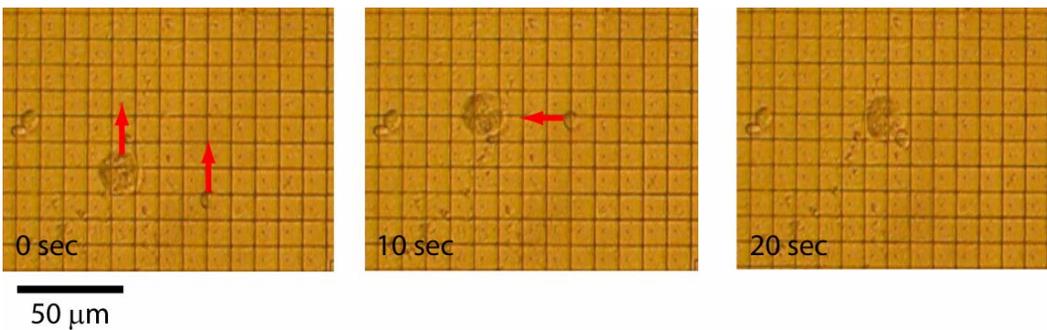

Figure 7.4 Time sequence of yeast and rat alveolar macrophages manipulated with DEP. Pixels on the chip were energized to independently move the two cells and then bring them together.

7.3   Water Drop Manipulation

Controlling the movement of aqueous droplets in oil is a useful technique
with wide applications in biochemistry. Water droplets in oil can serve as
confined microreactors for combinatorial chemistry, genetics and proteomics
(Ahn et al., 2006). We used the DEP manipulator chip to move, split, and
combine drops of water in oil. Water drops from ~1 nL to ~1 pL in volume were
programmably manipulated by the electric fields produced by the chip.

To prepare drops for manipulation, a mixture of hexadecane, water, and
sodium dodecyl sulphate (SDS) surfactant, was shaken using a vortexer. A thin
layer of fluorocarbon oil was pipetted onto the surface of the chip and then the
suspension of water drops in hexane was added to the microfluidic channel. The
difference in density among the three liquids resulted in water drops
($\eta = 1$ gm/cm^3) that were pinched between a layer of dense fluorocarbon oil
($\eta = 2.4$ gm/cm^3) and less dense hexadecane ($\eta = 0.8$ gm/cm^3).

The resulting multilayer liquid provided very little resistance to translating
drops in 2D above the surface of the chip. The drops were not in contact with the
chip surface so it was not necessary to overcome contact line hysteresis to move
the drops. In addition, droplet manipulation was insensitive to the surface
treatment and hydrophobicity of the chip. Water drops in hexadecande alone
wetted and stuck to the polyimide surface of the chip despite surface pretreatment
schemes including silinization and evaporated fluorocarbon oil.

Figure 7.5 shows the DEP manipulation of dyed water drops in oil with energized pixels highlighted in white. Changing which pixels were energized would move the water droplets through the oil medium as a droplet was attracted with DEP to the electric field maximum. Droplets were deformed by energizing multiple sets of pixels. Holding a droplet in place with two energized pixels, another set of pixels was energized to stretch the droplet. Single droplets were stretched until they pinched off into two separate droplets due to surface tension. Both resulting droplets could be moved independently. The droplets recombined when they were brought into contact. The translation, splitting, and recombination of pL aqueous droplets, programmably controlled by a computer, is a powerful application of our IC / microfluidic system.
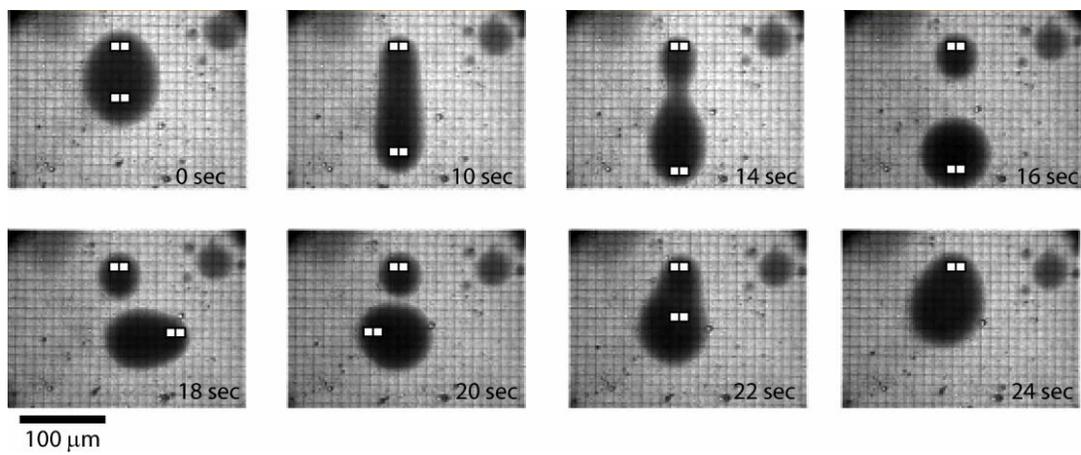
Figure 7.5 Splitting, moving, and combining water drops in oil with DEP. This time sequence shows a droplet of colored water between a layer of fluorocarbon oil below and hydrocarbon oil above. Pixels energized with V_{pix} in each frame are highlighted in white.

Chapter 8. Conclusions and Future Directions

8.1 Thesis Summary

We have designed, constructed, and demonstrated a host of microfluidic systems with exciting applications in biomedicine. Chapter 3 describes a device for sorting magnetically tagged cells out of whole blood (Xia et al., 2006). Such micromagnetic sorters can be used for rare cell separation and the diagnosis and treatment of diseases such as sepsis.

A high speed droplet sorter capable of directing water droplets into either of two output channels was also described in Chapter 3 (Ahn et al., 2006). Droplet sorters are a key portion of microfluidic systems that use water droplets in oil as microscopic reactors for biochemistry. Microfluidic droplet manipulation systems are excellent candidates to replace pipetting robots; greatly enhancing the speed and reducing the cost of combinatorial biochemistry in genomics and proteomics.

Chapter 4 described DEP tweezers (Hunt and Westervelt, 2006): scanning probes capable of manipulating individual cells in 3D. DEP tweezers have applications for in vitro fertilization, cell-cell interaction studies, and single cell transfection. In addition, Chapter 4 shows DEP tweezers constructed at the end of an AFM tip to enable pick and place nano-assembly with a standard AFM. Such nano-assembly would be extremely useful for constructing and positioning nanostructures.

The micropost electrode array (Hunt et al., 2004) was shown in Chapter 5. The programmable electric fields produced by the micropost electrode array moved cells and particles with DEP. After the successful demonstration of the micropost electrode array, we designed a CMOS chip to move cells and pL droplets of water in oil (Hunt et al., to be submitted). Chapter 6 described the design process and implementation of the IC / microfluidic DEP manipulator chip. The chip was built in a commercial foundry and we subsequently fabricated a microfluidic chamber on its top surface. By shifting the location of energized pixels, cells and drops are trapped and moved along programmable paths through the microfluidic chamber as described in Chapter 7. The chip was additionally capable of splitting and mixing pL water droplets in oil, providing a platform for programmable droplet-based chemistry. Applications of the IC / microfluidic DEP manipulator chip (Section 8.2) show great potential. There is even greater potential for other systems that combine ICs and microfluidics (Section 8.3).

Comparing the droplet sorter to the IC / microfluidic system can provide insight about the strengths of IC / microfluidic systems. The droplet sorter is optimized to perform a single task: directing droplets down one of two output streams. The droplet sorter is very good at that task, applying kV to microelectrodes and moving droplets at cm / sec speeds to sort a single stream of droplets at 1.6 kHz. In contrast, the IC / microfluidic chip is multipurpose and operates in parallel. The chip moves individual droplets at only ~10 μm / sec, but with 256 x 128 pixels, the IC microfluidic system is capable of moving thousands of drops simultaneously. The true strength of the IC / microfluidic chip is

programmability. The chip can perform arbitrary movement in 2D on drops, cells, or particles in liquid. Programmability means that the same chip can be used for many applications.

The IC / microfluidic chip is also scalable. It is well within the capability of ICs to address millions of pixels over areas greater than 1 cm x 1 cm. It is also straightforward to add functionality to the IC / microfluidic chip. The addition of new capabilities to the droplet sorter would require more wiring and a higher part count, increasing the overall system complexity. With an IC / microfluidic chip, adding sensing electronics, temperature control, or magnetic manipulation capabilities requires only the addition of circuits built into the chip. Additional circuits are easy to design into an IC, and can even be implemented without increasing the number of interconnects if the digital inputs are time multiplexed to serve multiple functions. IC / microfluidics have advantages in programmability, scalability, and versatility over their standard microfluidic counterparts.

8.2   Applications of the DEP manipulator

IC / microfluidic DEP manipulators have great promise for biological experiments, especially to study cell-cell signaling, to assemble tissue from individual cells, and to array statistical numbers of individual cells for investigating stochastic processes. The IC / microfluidic manipulator's ability to move chemical droplets in oil may open the door to massively parallel pL chemical investigations. Some of the possible applications of our DEP manipulator chip are outlined in Table 8.1.

116

Table 8.1 IC / Microfluidic DEP manipulator applications

Chip Function	Experiment	Improvements needed
Moving single cells	Cell – cell interaction	
	2D tissue assembly with multiple cell types	
	Cell arrays for fluorescence investigation of stochastic gene expression	Mount chip on fluorescence microscope
	3D tissue assembly via liftoff and assembly of 2D layers	DEP tweezers or other method to gently stack the assembled tissue sheets
Drop manipulation	Parallel, pL PCR	Temperature control of chip or substrate
	Combinatorial drug discovery	Microfluidic supply of reagents
	Drug trials on single cells	A microfluidic system to deliver cells in drops to the chip

8.3 Further IC / Microfluidic systems

8.3.1 GHz microscope on a chip

With CMOS technology, we can make sensitive electric field sources and detectors only microns in size that operate up to GHz. By sweeping the frequency of the applied electric field, a "color" microwave camera with micron resolution close to the surface of the chip could be built. The GHz microscope, illustrated in Figure 8.1, could be used to examine tissue with microwave radiation at wavelengths more than a thousand times longer than optical wavelengths. This chip would open up an entirely new band of the electromagnetic frequency spectrum for use in biological imaging. Studies on pieces of tissue and cell cultures have shown differences in the frequency dependent dielectric constant and absorption (microwave "color") and these differences will provide a contrast mechanism for the GHz microscope. We should be able to differentiate among types of tissue and possibly use this novel contrast mechanism to image disease processes.
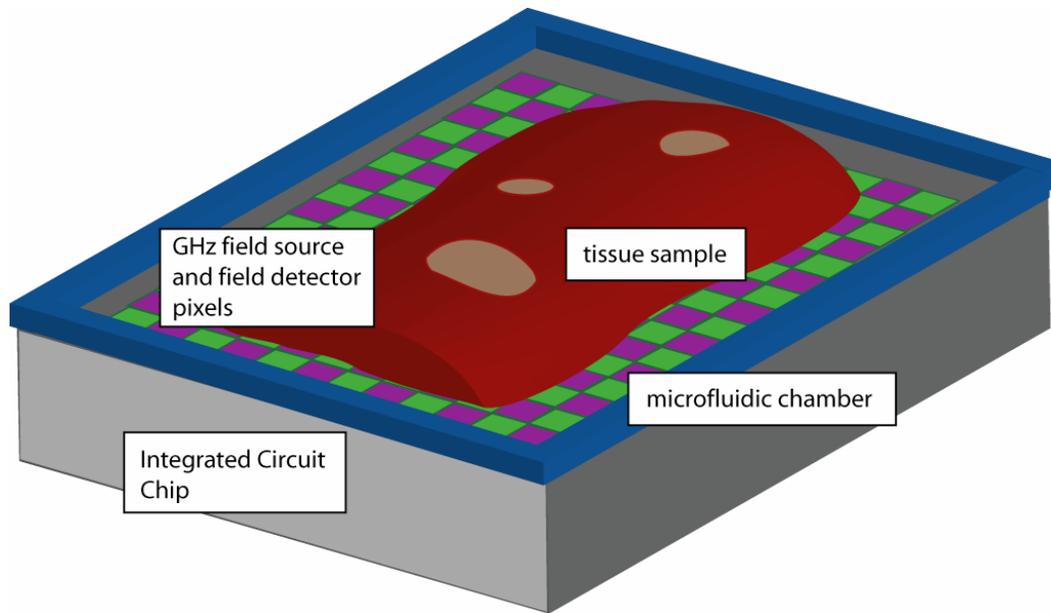
Figure 8.1 Schematic GHz microscope on a chip. This IC / microfluidic chip is equipped with an array of sensitive electric field sources and detectors that operate up to GHz. The source pixels interrogate the tissue sample at GHz and the detection pixels re-construct an image of the tissue sample using the dielectric spectrum of the tissue as a contrast mechanism.

The challenge in building a GHz microscope on a chip is to design on-chip amplifiers that are fast, sensitive and small, and to package them in a robust, biocompatible manner. The first GHz microscope on a chip would be an array of micron sized metal pixels covered by a thin layer of insulator at the surface of a chip. Electric field sources would be interspersed between sensitive field detector pixels. A microfluidic system to keep tissue alive on the surface of the chip would be built, and the system mounted on an optical microscope for simultaneous optical observation. The GHz microscope on a chip is an exciting application for sensitive, high speed CMOS electronics combined with microfluidics.

8.3.2 Closed Loop Microfluidic Microprocessor

Our IC / microfluidic DEP manipulator is a versatile technology for fluid manipulation. Improvements to the chip would produce an even more powerful system capable of fully automated operation. Right now, a human closes the loop in our IC / microfluidic DEP manipulator: i.e. if a particle or drop fails to move, the user will spot the problem in the microscope, and send signals to the chip to move the particle again. Automated sensing can close the loop so the system could move particles and drops in programmable patterns without user intervention. There are two possibilities for sensing: optical and electrical. Electrical sensing involves sensitive capacitance detectors under each pixel to determine the dielectric constant of the substance above the pixel. Optical sensing would require no modifications to the chip itself. With a CCD and optics aligned to the chip, software image recognition software could feed back particle location to the computer that controls the array.

Closed loop local temperature control would also be useful for a
microfluidic microprocessor. On chip temperature sensors and heaters are
straightforward circuits to incorporate in an IC. An advanced microfluidic
microprocessor would have a chip uniformly cooled by a thermoelectric cooler,
but locally heated by resistive heaters and monitored by integrated temperature
sensors. Thus, different regions of the chip could be held at different
temperatures. The length scale of the thermal gradient is set by the thickness of
the chip, ~500 μm , so several different temperatures could be maintained on the
same IC. Temperature gradients would be useful for biochemical reactions such
as PCR that require thermal cycling, or to slow metabolism of or heat shock
certain cells.

8.3.3   NMR chip

One more useful IC / microfluidic system would involve incorporating sensitive
NMR detection electronics and microcoils for magnetic field generation and
pickup on an integrated circuit. The electronics to generate and receive magnetic
field pulses are appropriate for integration in a single chip. A microcoil or array of
microcoils (Lee et al., 2005) could be used for pulse generation and detection.
Although planar microcoils do not have as good a filling factor as coils around a
capillary, the ease of integrating planar coils on chip may make up for the deficit
in signal to noise ratio. Even a NMR with a relatively low fidelity compared to
commercial NMR sets could find many applications if it was built on chip, at a
cost of a few dollars, with a permanent magnet for the polarization field. The real
strength of NMR on a chip would be found when microfluidics were directly

integrated onto the same chip. Performing NMR on the contents of a microfluidic channel allow chemical analysis pL or nL volumes. In addition, measuring the T2 time of functionalized nanoparticles can be a very useful analysis tool (Perez et al., 2002). Powerful MRI imaging techniques could also be implemented by electronically switching planar arrays of microcoils.

8.4 Conclusion

Combining the sensitivity and programmability of ICs with the biocompatability of microfluidics, IC / microfluidic chips have the potential to make a major impact on biomedicical research. Our IC / microfluidic DEP manipulator chip is capable of moving pL chemical volumes and statistical numbers of individual cells. With ICs becoming more powerful each year and microfluidics beginning to enter the commercial arena, IC / microfluidic chips are poised to take advantage of advances in both industries.

References

Ahn K., Kerbage C., Hunt T. P., Westervelt R. M., Link D. R., and Weitz D. A. (2006) *Applied Physics Letters*, **88,** 024104.

Anna S. L., Bontoux N., and Stone H. A. (2003) *Appl. Phys. Lett.*, **82**, 364.

Bahaj A.S. and Bailey A. G. (1979) *J. Phys. D.* **12,** L109.

Ballan H., and Declercq, M (1999) *High Voltage Devices and Circuits in Standard CMOS Technologies*, Kluwer, Dordrecht.

Blazej, R. G., Kumaresan, P. and Mathies, R. A. (2006) *PNAS* **103**, 7240-7245.

Brehm-Stecher B. F. and Johnson E. A. (2004) *Microbiol Mol Biol Rev*. **68**, 538.

Current K., Yuk K., McConaghy C., Gascoyne P., Schwartz J., Vykoukal J., and Andrews C. (2005) IEEE Symposium on VLSI Circuits Digest, **72.**

DeBusschere B.D. and Kovacs G. T. A. (2001) *Biosensors & Bioelectronics*, **16**, 543.

Eberwine J. (2001) *Nature Neuroscience* **4** 1155.

Eversmann B., Jenkner M., Hofmann F., Paulus C., Brederlow R., Holzapfl, Fromherz B. P., Merz M., Brenner M., Schreiter M., Gabl R., Plehnert K., Steinhauser M., Eckstein G., Schmitt-Landsiedel D., and Thewes R., (2003) *J. Solid-State Circuits*, **38**, 2306.

Fleming and King, (2003) *Micromanipulation in Assisted Conception*, Cambridge University Press, Cambridge.

Green N. G. and Morgan H. (1997) *J. Phys. D: Appl. Phys.*, **30**, 11 L 41.

Green N. G., Morgan H., and Milner J. J. (1997) *J Biochem Biophys Methods*, **35**, 89.

Grosse C. and Schwan H., *Biophysical J.*(1992), **63**,1632.

Gupta A.K. and Wells S. (2004) *IEEE Trans. Nanobiosci.* **3**, 66.

Hölzel R., Calander N., Chiragwandi, Z., Willander, M., and Bier F. (2005) *Phys. Rev. Lett.* **95**, 128102.

Hunt T. P. and Westervelt R. M. (2006) *Biomedical Microdevices*, **8**: 227.

Hunt T. P., Lee H., Westervelt R.M. (2004) *Applied Physics Letters* **85**, 6421.

Hunt T. P., Issadore, D. ,Westervelt R. M. (to be published), *Lab Chip*

Jones T. B. (1995) *Electromechanics of Particles*, Cambridge University Press, Cambridge.

Kotnik T. and Miklavcic D. (2000) *IEEE Trans of Biomed Eng*, **47**, 1075.

Lee J., Moon H., Fowler J., Schoellhammer T., and Kim C.J. (2002) *Sens. Actuators A*, **95**, 259.

Lee H. *Microelectronic / Microdluidic Hybrid System for the Manipulation of Biological Cells*, (2005) PhD dissertation, Harvard University.

Lee H., Liu Y., Alsberg E, Ingber D.E., Westervelt R.M., and Ham D. (2005), *Digest of Technical Papers, IEEE International Solid-State Circuits Conference*, **1**, 80.

Lee H., Liu Y., Westervelt R.M., and Ham D., (2006) IEEE J. Solid-State Circuits, **41**, 1471.

Lee H., Purdon A. M. and Westervelt, R. M. (2004) Applied Physics Letters, 85, 1063.

Lee, H. Ham D. and R.M. Westervelt eds. (2007) *CMOS Biotechnology*, Springer, New York

Manaresi N., Romani A., Medoro G., Altomare L., Leonardi A. Tartagni M., and Guerrieri, R., (2003) *IEEE J. Solid- State Circuits*, **30**, 2297.

Olofsson J, Nolkrantz K, Ryttsén F, Lambie B, Weber S G, and Orwar O, (2003) *Curr Opin Biotechnol.* **14** 29.

Perez J. M., O'Loughin T, Simeone F. J., Weissleder R., and Josephson L. (2002) *JACS*, **124** 2856.

Pohl H. and Crane J, (1971) *Biophysical Journal*, **11**, 711.

Pohl H. A., *Dielectrophoresis* (1978) Cambridge University Press, Cambridge.

Pollack M. G., Shendorov A. D., and Fair R. B., (2002) *Lab Chip*, **2**, no.1, 96.

Rasmussen F.E., Ravnkilde J.T., Tang P.T., Hansen O., and Bouwstra S., (2001) *Sensor Actuat. A-Phys*. **92**, 242.

Song H., Tice, J. D. and Ismagilov R. F. (2003) *Angew. Chem. Int. Ed.* **42**, 768.

Suehiro, J and Pethig, R. (1998) *J. Phys. D*: **31**, 3298.

Tawfik D. S. and Griffiths A. D. (1998), *Nat. Biotech.*, **16**, 652.

Thewes R., Hofmann F., Frey A., Holzapfl B., Schienle M., Paulus C.,
        Schindler P., Eckstein G., Kassel C., Stanzel M., Hintsche R., Nebling
        E., Albers J., Hassman J., Schulein J., Goemann W., Gumbrecht W.,
        (2002) *Digest of Technical Papers, 2002 IEEE International Solid-State
        Circuits Conference,* **1**, 350.

Voldman, J. (2001) *A Microfabricated dielectrophoretic trapping array for cell-
        based biological assays.* Ph.D. dissertation, MIT.

Vykoukal J., Schwartz A., Becker F.F., and Gascoyne P.R.C. (2001) *Micro Total
        Analysis Systems*, **72**.

Weste, N and Harris, D, (2005) *CMOS VLSI Design: A Circuits and Systems
        Perspective*, Addison Wesley, 2005.

Whitesides G. M. (2006) *Nature*, **442**, 368.

Xia N, Hunt T. P., Mayers B. T., Alsberg E., Whitesides G. M., Westervelt R.M.,
        Ingber D.E. (2006) *Biomedical Microdevices*, **8**, 1387.

Zhang K., Bhattacharya U., Chen Z., Hamzaoglu F., Murray D., Vallepalli N,
        Wang Y., and Bohr M. (2005) *J. Solid-State Circuits*, **40**, 895.

Appendices

Appendix A.   Fabrication procedures

Soft lithography:

1. Make a negative channel mold with SU-8 as described in CNS procedures and in Hakho Lee's thesis.

2. Place mold in low vacuum chamber with 500 μL silane to improve peeling of PDMS from mask

3. Mix PDMS curing agent 1:10, and pump in low vacuum chamber for ~30 minutes

4. Pour PDMS on mold, 40 minutes, 65 degree C bake

5. Peel PDMS off of mold

6. Punch holes in PDMS with sawed-off hypodermic needle or Harris Uni-core

7. Oxygen plasma glass substrate

8. Stick PDMS to glass substrate, wait overnight, and your microfluidics are done.

9. If adhesion is poor, try placing and peeling scotch tape on substrate and PDMS

10. If nothing else works, spin a thin layer of 5:1 PDMS on your substrate, and place a 20:1 PDMS channel on the substrate. This partial curing method will bond when nothing else will.

Hot-bond microfluidics:

1. Place a small piece of hot glue between two glass slides and melt on hotplate at 100 degrees

2. If you run into trouble removing the layer of glue from the glass, try silanizing the glass or using Teflon tape as a spacer layer.

3. The height of your chamber can be controlled by putting a spacer layer between the glass slides

4. You can cut a chamber or channel out of the glue with a razorblade, or use a mold to cast the channel as you would like it to be.

5. To attach the channel or chamber to your chip, put your chip on the heated stage of the wirebonder, set the temperature controller to 90-100 °C and watch carefully through the microscope as the hot melt glue bonds to your chip. Remove the chip from the heated stage just after the glue starts melting.

6. To permanently bond a coverslip to your chamber, place the coverslip on top of the hot glue and use a soldering iron to locally heat the top of the plate until you see adhesion.

Cadence chip design procedures and advice:

1. Design your entire schematic before you start layout.

2. Add as much hierarchy to your schematic as you can, it will make your layout much easier.

3. Think out your directory structure and file names before you let them evolve into an incomprehensible mess.

4. Give yourself plenty of time, every part of the design process takes twice as long as you think it will.

5. The tapeout deadline is a real deadline, but you can always wait for the next run.

6. Do not tapeout a chip that you are not 100% sure that you tested perfectly.

Appendix B.　　Simulation techniques

Before you begin, and this step is critical, develop a first-order model in Mathematica or Matlab so you can estimate whether your device will work. Your first order model will be useful to validate your finite element results.

Select a finite element package. 2D E+M simulations will only take few minutes with Maxwell SV (free). Comsol / Femlab allows you to input your own equations and couple E+M solutions to thermal and mechanical solutions. Femlab meshing is not as good as Maxwell, it runs into major problems if the ratio to small and large geometry lengths is more than 1000. Maxwell (Ansoft) is outstanding at meshing and E+M field solving, and good at visualizing the results. The equations that Maxwell will solve are limited to static E+M fields. I highly recommend drawing your geometry in Autocad and importing the geometry to your FEM package.

When solving, remember that you can refine the mesh in a desired region of interest, which may be important. Plot the mesh to see if it fits your exacting standards. Usually, 12 passes and 30-100k tetrahedrons is fine for Maxwell.

When plotting your results, use the simulation package to get a general picture, but remember that you can export your fields to a data file and import that data file to Igor or Matlab to make exactly the plot that you want.

Appendix C.   IGOR code

3/27/2007 TSMCforThesis.ipf

#pragma rtGlobals=1 // Use modern global access method.

Function StartFab()//Starts the software. It may be nesassary to make some more waves if there are errors on the first run.

NewDataFolder/O root:tom2
//Set up global variables
String/G root:tom2:gMessage= "a useless message"
String/G root:tom2:gMessage2= "keylog: "
Make/O/N=(64,256) curs=0
Make/O/N=(64,256) held=0
Make/O/N=(64,256) heldPlus=0
Make/O/N=(64,256) onChip=0
Make/O/N=(64,256) difference
Make/O/N=(64,256) fromChip=0
Make/O/N=(64) word=0
Make/O/N=256 rowlist=0
Make/O/N=256 clocks=0
onChip=0
initBoard()
// set up fromchip I window
NewImage /N=Wfromchip /K=1 fromchip
//set up on chip window
Display /W=(-50,550,200,790)/n=Wonchip /K=1
appendimage onchip
ModifyGraph tick=3,noLabel=2
//set up difference window
Display /W=(200,550,450,790)/n=Wdifference /K=1
appendimage /W=Wdifference difference
ModifyGraph tick=3,nticks=0,noLabel=2
DoWindow/F Fab1 // set up big window
Display /W=(0,40,500,550)/K=1
AppendImage heldplus
SetWindow kwTopWin,hook(testhook)=BigHook, hookcursor= 9
SetAxis /A /W=Graph0 /R left
End

Function initBoard()
//more global variables
Variable/G phFreq=100000
//task numbers
Variable/G wordTask
Variable/G phTask
Variable /G ph1Task
Variable /G ph2Task
Variable/G c1Task
Variable/G c2Task
Variable/G clk1Task
Variable/G clk2Task

Variable/G wrTask
Variable/G dataTask
Variable/G passTask
Variable/G outputTask
Variable/G readTask
// analog input
Variable/G vddChan
Variable/G hvChan
Variable/G hvgChan
Variable/G vddmagChan
Variable/G vmagChan
Variable/G hvtopChan
Variable/G hvtopinChan
Variable/G thermChan
String/G boardclock
string/G myclockhere
boardclock="/Dev1/100kHzTimebase"
//boardclock="/Dev1/Ctr1InternalOutput"
fDAQmx_ResetDevice("Dev1")
//phTask set by phOn(), phOff()
print fDAQmx_ErrorString()
End

Function BigHook(H_Struct) //Deals with mouse
        and keyboard inputs
STRUCT WMWinHookStruct &H_Struct
string event= H_Struct.eventName
variable key=H_Struct.keycode
variable handledIt= 0
Variable xpix,ypix,xaxval,yaxval,eventmod,x1,y1,oldval,newval
SVAR Message=root:tom2:gMessage
SVAR Message2=root:tom2:gMessage2
WAVE curs = curs
strswitch(event)
case "keyboard":
Message2=Message2+Num2Str(key)+" "
keyhit(key)
handledIt= 1
break
case "mousedown":
eventmod=H_Struct.eventMod
xpix= H_Struct.MouseLoc.h
ypix= H_Struct.MouseLoc.v
changepix(xpix,ypix,eventmod)
handledIt =1
break
case "mousemoved":
eventmod=H_Struct.eventMod
xpix= H_Struct.MouseLoc.h
ypix= H_Struct.MouseLoc.v
if (eventmod>0)
changepix(xpix,ypix,eventmod)
endif
handledIt =1
break

```
endswitch
return handledIt
End
Function ClearButtonProc(ctrlName) :
ButtonControl
String ctrlName
resetArray()
End
Function keyhit(key)
variable key
string keychar
Wave M_OffsetImage
Wave curs
wave difference=difference
wave onChip=onChip
SVAR Message2=root:tom:gMessage2
NVAR phTask
NVAR phFreq
keychar=num2char(key)
switch(key)
case 99:
Message2="keylog "
resetArray()
break
case 28:
movecurs(-1,0)
break
case 29:
movecurs(1,0)
break
case 30:
movecurs(0,-1)
break
case 31:
movecurs(0,1)
break
case 32: //" "
writecurs2()
break
case 97: //"a"
writeallrows()
break
case 118: //"v"
break
case 114: //"r"
readall()
break
case 119: //"w"
writeall()
break
case 105: //"i"
invert()
break
case 112: //"p"
break
case 104: //"h"
holdcurs()
break
case 117: //"u"
unholdcurs()
break
case 108: //"l"

loadlatest()
break
endswitch
return(0)
End
Function resetArray()
WAVE curs=curs
curs=0
onchip=0
difference=0
heldplus=0
held=0
writeAll()
End

Function movecurs(x,y) // moves the entire
cursor image
variable x
variable y
ImageTransform /IOFF={x,y,0} offsetImage
curs
//difference=difference+curs
curs=M_OffsetImage
heldplus=held+curs/2
//difference=difference+curs
writeAllRows()
end

Function writeAllRows() // finds difference and
writes changed rows
variable i
variable timernum
timernum=startMSTimer
openChannels()
findrows()
Do //writes all rows
While (WriteRow(heldplus,rowlist,word) > 0)
closeChannels()
onchip=heldplus
End

Function changepix(xpix,ypix,eventmod)
variable xpix,ypix,eventmod
variable xaxval,yaxval,x1,y1,newval
WAVE curs=curs
WAVE onchip=onchip
WAVE M_OffsetImage
SVAR Message=root:tom:gMessage
Wave row
xaxval= AxisValFromPixel("","bottom",xpix)
yaxval= AxisValFromPixel("","left",ypix)
sprintf Message,"x= %g, y= %g, cmod=
%g",round(xaxval),round(yaxval),eventmod
x1=round(xaxval)
y1= round(yaxval)
if (eventmod==1)
newval=1
curs[x1][y1]=newval
endif
if (eventmod==16)
newval=0
curs[x1][y1]=newval
```

```
endif
heldPlus=held+curs/2
End
//
Function readrow(rownum)
variable rownum
Wave row
Wave curs=curs
row = curs[p][rownum]
End
//
Function findrows()
Wave curs=curs
Wave onChip=onChip
Wave rowlist=rowlist
Wave difference=difference
variable row
variable temp
variable i=0
rowlist[]=0
heldplus=held+curs
difference = abs(onChip-(heldplus))
Do //goes through pixels and finds nonzero
rows
FindValue /S=(i) /V=1 /T=0.5 difference
//col = mod (V_value,60)
if (V_value>=0) //to avoid false row #0, it is
inelegant
row = floor (V_value/64)
rowlist[row] = 1
i = V_value+1
endif
While (V_value >= 0)
//print rowlist
end

Function WriteRow(matrix,rowlist,word)
wave matrix
wave rowlist
wave word
Wave curs=curs
Wave onChip=onChip
FindValue /V=1 /T=0.4 rowlist
if (V_value > -1) // make sure there is a value
in rowlist
word[] = matrix[p][V_value]
word=ceil(word)
//print word
WriteLatch(word)//sends word to latch
WriteArray(V_value)//sends latch to array
//you can check here by reading the latch
back
//write matrix values to onChip
//onChip[][V_value]=curs[p][V_value]
//clear a row out of rowlist
rowlist[V_value]=0
//print V_value
return 1
endif
return 0
End
```

```
Function SelectWord(wordnum)
variable wordnum
nvar wordTask
//wordline select
//set W0-W7
fDaQmx_DIO_Write("Dev1",wordTask,wordn
um)
return 0
End
Function timeme()
NVAR phTask
NVAR clk1Task
//fDAQmx_ResetDevice("Dev1")
make/b/u/o /N=(100) wave1
make/b/u/o /N=(100) wave2
wave1 = floor(mod(p/4,2))
//391ms for 100,000 points
//4ms for 100points
//160ms for 127 x 32 points
variable i
variable timernum
timernum=startMSTimer
for (i=0;i<10000;i=i+1)
fDaQmx_DIO_Write("Dev1",clk1Task,1)
fDaQmx_DIO_Write("Dev1",clk1Task,0)
endfor
print stopMSTimer(timernum)
print fDAQmx_ErrorString()
end

Function openChannels()
NVAR clk1Task
NVAR clk2Task
NVAR c1Task
NVAR c2Task
NVAR readTask
NVAR wrTask
NVAR passTask
NVAR dataTask
NVAR wordTask
NVAR outputTask
NVAR phTask
fDAQmx_ResetDevice("Dev1")
DAQmx_DIO_Config /DEV="Dev1" /DIR=1
/LGRP=1 /RPTC=0 ("/Dev1/port0/line12,
/Dev1/port0/line11, /Dev1/port0/line10
wordTask=V_DAQmx_DIO_TaskNumber
DAQmx_DIO_Config /DEV="Dev1" /DIR=1
/LGRP=1 /RPTC=0 ("/Dev1/port0/line16")
c2Task=V_DAQmx_DIO_TaskNumber
DAQmx_DIO_Config /DEV="Dev1" /DIR=1
/LGRP=1 /RPTC=0 ("/Dev1/port0/line17")
c1Task=V_DAQmx_DIO_TaskNumber
DAQmx_DIO_Config /DEV="Dev1" /DIR=1
/LGRP=1 /RPTC=0 ("/Dev1/port0/line18")
wrTask=V_DAQmx_DIO_TaskNumber
DAQmx_DIO_Config /DEV="Dev1" /DIR=1
/LGRP=1 /RPTC=0 ("/Dev1/port0/line19")
passTask=V_DAQmx_DIO_TaskNumber
DAQmx_DIO_Config /DEV="Dev1" /DIR=1
/LGRP=1 /RPTC=0 ("/Dev1/port0/line20")
dataTask=V_DAQmx_DIO_TaskNumber
```

```
DAQmx_DIO_Config /DEV="Dev1" /DIR=1
/LGRP=1 /RPTC=0
("/Dev1/port0/line8,/Dev1/port0/line9")
phTask=V_DAQmx_DIO_TaskNumber
DAQmx_DIO_Config /DEV="Dev1" /DIR=1
/LGRP=1 /RPTC=0 ("/Dev1/port0/line23")
clk2Task=V_DAQmx_DIO_TaskNumber
DAQmx_DIO_Config /DEV="Dev1" /DIR=1
/LGRP=1 /RPTC=0 ("/Dev1/port0/line24")
clk1Task=V_DAQmx_DIO_TaskNumber
DAQmx_DIO_Config /DEV="Dev1" /DIR=0
/LGRP=1 /RPTC=0 ("/Dev1/port0/line31")
outputTask=V_DAQmx_DIO_TaskNumber
end

Function CloseChannels()
NVAR clk1Task
NVAR clk2Task
NVAR c1Task
NVAR c2Task
NVAR readTask
NVAR wrTask
NVAR passTask
NVAR dataTask
NVAR wordTask
NVAR outputTask
NVAR phTask
fDAQmx_DIO_Finished("Dev1",wordTask)
wordTask=0
fDAQmx_DIO_Finished("Dev1", clk1Task)
clk1Task=0
fDAQmx_DIO_Finished("Dev1",clk2Task)
clk2Task=0
fDAQmx_DIO_Finished("Dev1",wrTask)
wrTask=0
fDAQmx_DIO_Finished("Dev1",outputTask)
outputTask=0
fDAQmx_DIO_Finished("Dev1",dataTask)
dataTask=0
fDAQmx_DIO_Finished("Dev1",passTask)
passTask=0
fDAQmx_DIO_Finished("Dev1",c1Task)
c1Task=0
fDAQmx_DIO_Finished("Dev1",c2Task)
c2Task=0
fDAQmx_DIO_Finished("Dev1",ph1Task)
ph1Task=0
fDAQmx_DIO_Finished("Dev1",ph2Task)
ph2Task=0
end

Function WriteLatch2(word) //shifted by one
clock cycle
wave word
NVAR clk1Task
NVAR clk2Task
NVAR dataTask
NVAR wrTask
NVAR passTask
variable i
//load data into bitlines WR=0,pass=1
fDaQmx_DIO_Write("Dev1",wrTask,0)
```

```
fDaQmx_DIO_Write("Dev1",passTask,1)
For(i=0;i<64;i=i+1)
//data
fDaQmx_DIO_Write("Dev1",dataTask,word[i])
//clk2
fDaQmx_DIO_Write("Dev1",clk2Task,1)
//clk2 off
fDaQmx_DIO_Write("Dev1",clk2Task,0)
//clk1
fDaQmx_DIO_Write("Dev1",clk1Task,1)
//clk1 off
fDaQmx_DIO_Write("Dev1",clk1Task,0)
endfor
return 0
End

Function WriteLatch(word)
wave word
NVAR clk1Task
NVAR clk2Task
NVAR dataTask
NVAR wrTask
NVAR passTask
variable i
//load data into bitlines WR=0,pass=1
fDaQmx_DIO_Write("Dev1",wrTask,0)
fDaQmx_DIO_Write("Dev1",passTask,1)
For(i=0;i<64;i=i+1)
//data
fDaQmx_DIO_Write("Dev1",dataTask,word[i])
//clk1
fDaQmx_DIO_Write("Dev1",clk1Task,1)
//clk1 off
fDaQmx_DIO_Write("Dev1",clk1Task,0)
//clk2
fDaQmx_DIO_Write("Dev1",clk2Task,1)
//clk2 off
fDaQmx_DIO_Write("Dev1",clk2Task,0)
endfor
return 0
End

Function ReadLatch(word)
wave word
NVAR clk1Task
NVAR clk2Task
NVAR outputTask
NVAR wrTask
NVAR passTask
NVAR dataTask
variable i
fDaQmx_DIO_Write("Dev1",wrTask,0)
fDaQmx_DIO_Write("Dev1",passTask,1)
For(i=0;i<64;i=i+1)
//clk1
fDaQmx_DIO_Write("Dev1",clk1Task,1)
//clk1 off
fDaQmx_DIO_Write("Dev1",clk1Task,0)
word[i] =
fDaQmx_DIO_Read("Dev1",outputTask)
//clk2
fDaQmx_DIO_Write("Dev1",clk2Task,1)
```

```
//clk2 off
fDaQmx_DIO_Write("Dev1",clk2Task,0)
endfor
//print word
return 0
End

Function WriteArray(wordnum)
//wave word
variable wordnum
NVAR clk1Task
NVAR clk2Task
NVAR c1Task
NVAR c2Task
NVAR readTask
NVAR wrTask
NVAR passTask
NVAR dataTask
//precharge bitlines with data
//c2 low
fDaQmx_DIO_Write("Dev1",c2Task,0)
SelectWord(wordnum)
//write to sram
//WR=1
fDaQmx_DIO_Write("Dev1",wrTask,1)
//pass=0
fDaQmx_DIO_Write("Dev1",passTask,1)
// C2 high to write
fDaQmx_DIO_Write("Dev1",c2Task,1)
// C1 enable word line
fDaQmx_DIO_Write("Dev1",c1Task,1)
// wordline disable
fDaQmx_DIO_Write("Dev1",c1Task,0)
// begin precharge again
fDaQmx_DIO_Write("Dev1",c2Task,0)
return 0
End

Function ReadArray(wordnum)
variable wordnum
//wave word
NVAR clk1Task
NVAR clk2Task
NVAR c1Task
NVAR c2Task
NVAR readTask
NVAR wrTask
NVAR passTask
NVAR dataTask
SelectWord(wordnum)
//precharge bitlines with data
//c2 low
fDaQmx_DIO_Write("Dev1",c2Task,0)
//read from sram
//WR=0
fDaQmx_DIO_Write("Dev1",wrTask,0)
//Pass =0
fDaQmx_DIO_Write("Dev1",passTask,0)
// C2 high, stop precharge
fDaQmx_DIO_Write("Dev1",c2Task,1)
// C1 high wordline enable
fDaQmx_DIO_Write("Dev1",c1Task,1)
```

```
//clk1
fDaQmx_DIO_Write("Dev1",clk1Task,1)
fDaQmx_DIO_Write("Dev1",clk1Task,0)
//clk2
fDaQmx_DIO_Write("Dev1",clk2Task,1)
fDaQmx_DIO_Write("Dev1",clk2Task,0)
//latches should have data
fDaQmx_DIO_Write("Dev1",c1Task,0)
fDaQmx_DIO_Write("Dev1",c2Task,0)
//WR=1
fDaQmx_DIO_Write("Dev1",wrTask,1)
//Pass =1
fDaQmx_DIO_Write("Dev1",passTask,1)
//ReadLatch(word)
return 0
End

Function readAll()
wave onchip=onchip
variable i
make/b/u/o /N=(64) tempword
openchannels()
For(i=0;i<256;i=i+1)
readArray(i)
readLatch(tempword)
onchip[][i]=tempword[p]
fromchip[][i]=tempword[p]
endfor
closechannels()
end

Function writeAll()
wave curs=curs
variable i
make/b/u/o /N=(64) tempword
openchannels()
For(i=0;i<256;i=i+1)
tempword[]=curs[p][i]
writeLatch(tempword)
writeArray(i)
endfor
closechannels()
end

Function holdcurs() // holds the cursor as a
permanent part of held
wave curs=curs
wave held=held
held=held+curs
heldplus=held
curs=0
//print "holdon"
end

Function unholdcurs() // loads held to the
cursor
wave curs=curs
wave held=held
curs=held
heldplus=curs/2
held=0
//print "holdoff"
```

```
end

function loadlatest() // loads highest file
number from image directory
variable imagenum
string pathstring
imagenum=460
V_flag=0
do
imagenum=imagenum+1
sprintf pathstring "C:Documents and
Settings:Administrator:My Documents:My
Pictures:Capture_00%g.JPG"
//print imagenum
GetFileFolderInfo /Z /Q pathstring
//GetFileFolderInfo /Z "C:Documents and
Settings:Administrator:My Documents:My
Pictures:Capture_00460.JPG"
while (V_flag == 0)
print imagenum
// sets file string to the last valid file
sprintf pathstring "C:Documents and
Settings:Administrator:My Documents:My
Pictures:Capture_00%g.JPG"
        //loads last valid file
ImageLoad/T=jpeg/O/N=cap pathstring
end

function sweep()
variable time0 =200
//variable mytime
variable i
wave w0=w0
word [] = mod(p,2)
openchannels()
For(i=1;i<128;i=i+1)
writelatch(word)
writearray(i)
writearray(255-i)
do
while ( mod(ticks,2*time0) < (time0))
writelatch(w0)
writearray(i-1)
writearray(256-i)
endfor
closechannels()
end

Function writeCurs2() // shifts by one pixel
wave curs=curs
variable i
make/b/u/o /N=(64) tempword
```

```
heldplus=held+curs
openchannels()
For(i=0;i<256;i=i+1)
tempword[]=curs[p][i]
if (sum(tempword)>0) //if there is a curs value,
write the heldplus word to the array, but
shifted
tempword[]=heldplus[p][i]
writeLatch2(tempword)
writeArray(i)
endif
endfor
closechannels()
end

function rw()
writeall()
readall()
end
// these functions read and write specific
pattens to the cursor
Function invert()
wave curs=curs
curs=curs+1
curs = mod(curs,2)
end

Function diag()
wave curs=curs
variable i
For(i=1;i<256;i=i+4)
curs[][i]=curs[p-1][i-1]
curs[][i+1]=curs[p-1][i-1]
curs[][i+2]=curs[p-1][i-1]
curs[][i+3]=curs[p-1][i-1]
curs[0][i+3]=curs[64][i-1]
endfor
end

function line(wordnum)
variable wordnum
wave curs=curs
curs[][wordnum]=1
heldplus = hold+curs
end

function stripes()
variable i
For(i=0;i<256;i=i+24)
line(i)
endfor
end
```

Appendix D.   Chip and circuit board pinout

14 Vdd Gnd 21 21 VddMag Gnd

13
12
11
10
15
16
17
18
19
20

Map from NIDAQ channels
to circuit board

8 - ph 1 - must cross wirebond to TSMC chip
9 - ph 2 - must cross wirebond to TSMC chip

gnd 24 23 31 VddMag Gnd
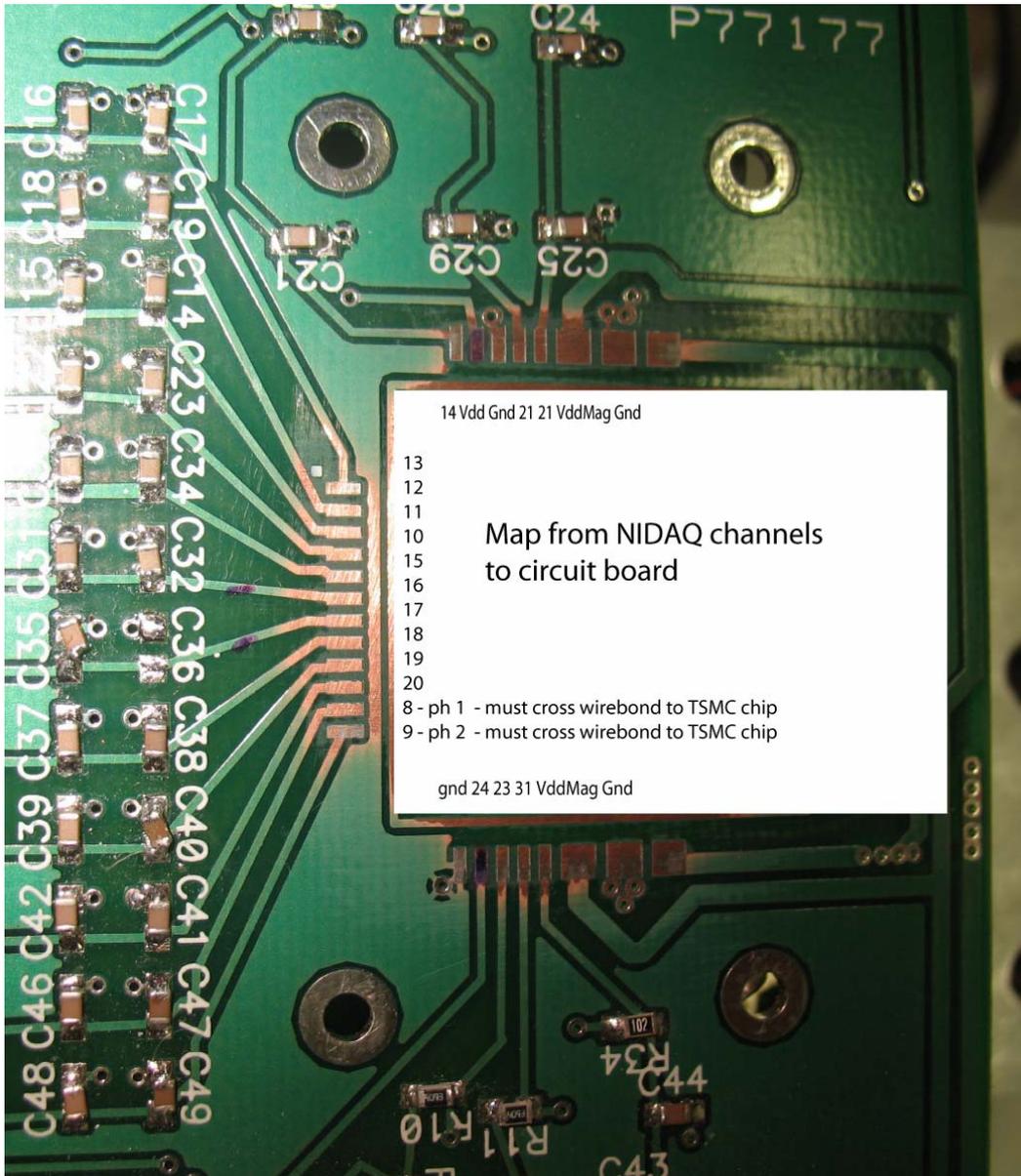
GND	GND
VDD	VDD
VDD	VDD
0	0 - word bit 0
1	1 - word bit 1
2	2 - word bit 2
3	3 - word bit 3
4	4 - word bit 4
5	5 - word bit 5
6	6 - word bit 6
7	7 - word bit 7
P2	P2 - phi 2, Vpix NOT: normally 1MHz, 5V sq wave
P1	P1 - phi 1, Vpix: normally 1MHz, 5V sq wave out of phase
C2	C2 - precharge - stops precharging bitlines when high
C1	C1 - word enable when high
WR	WR - write command
PASS	PASS - pass data to next shift register
DATA	DATA - what data to upload to first shift register
CLK2	CLK2 - shift register clock
CLK1	CLK1 - shift register clock
OUT	OUT - output amplifier from last shift register
VDD	VDD
GND	GND
GND	GND

Appendix E. Circuit board schematic and layout
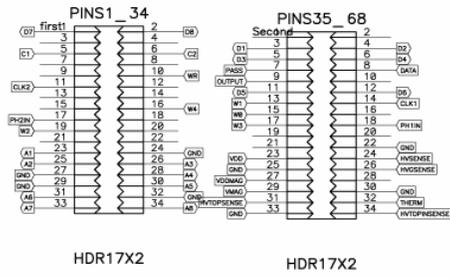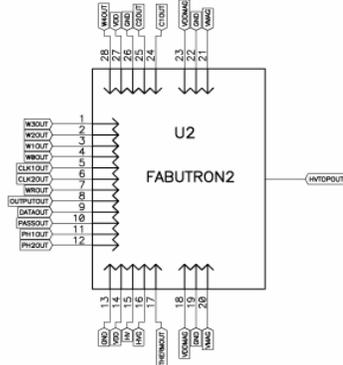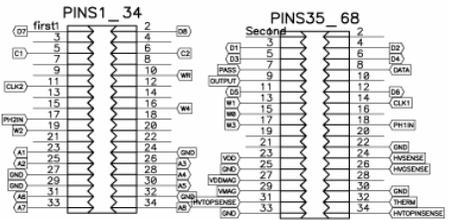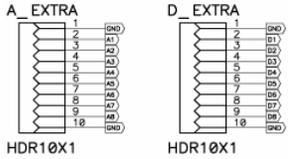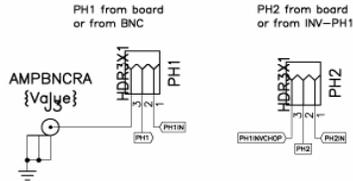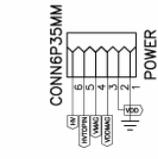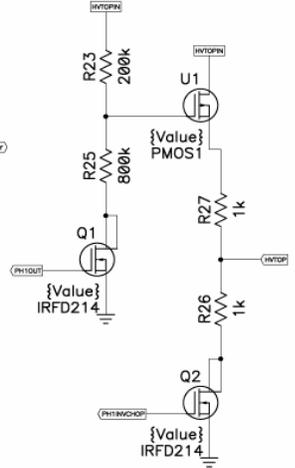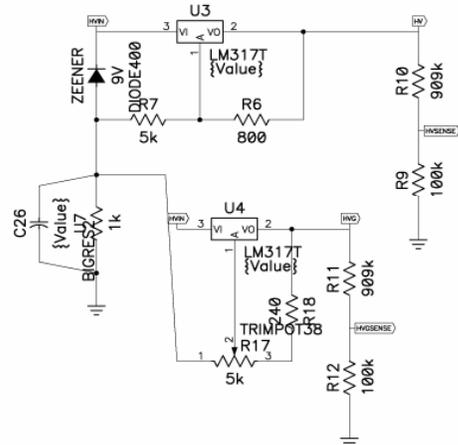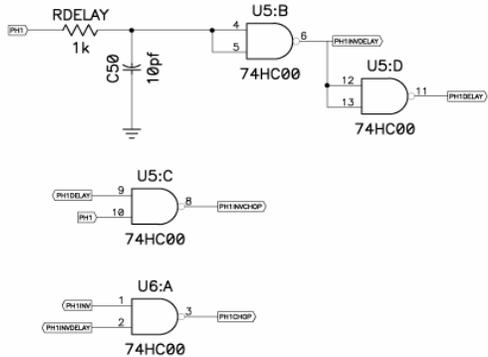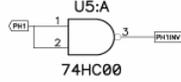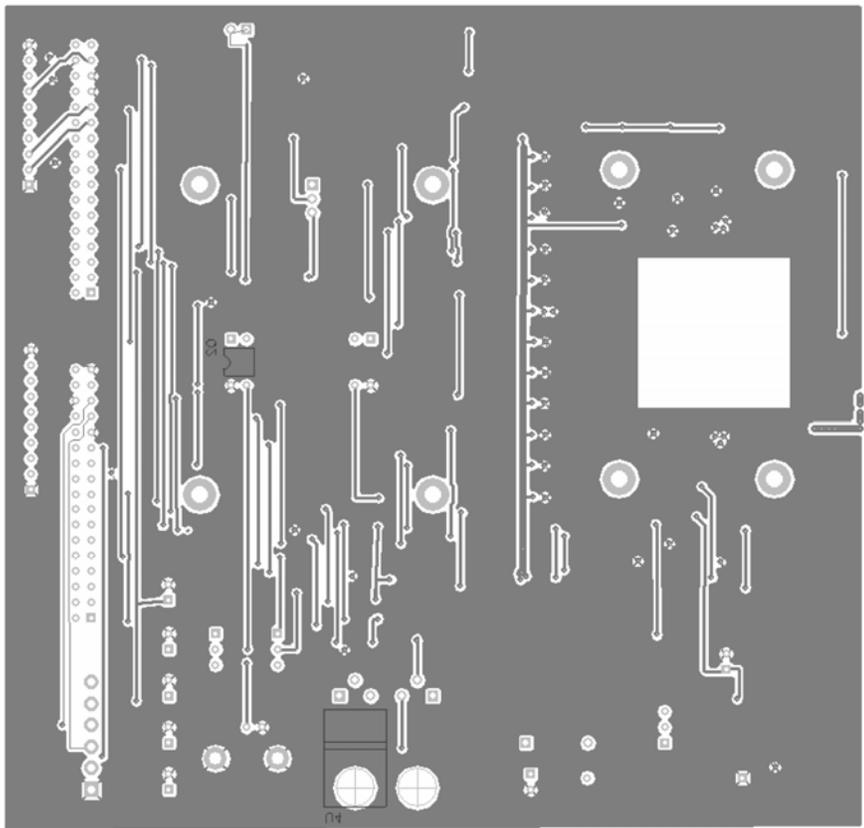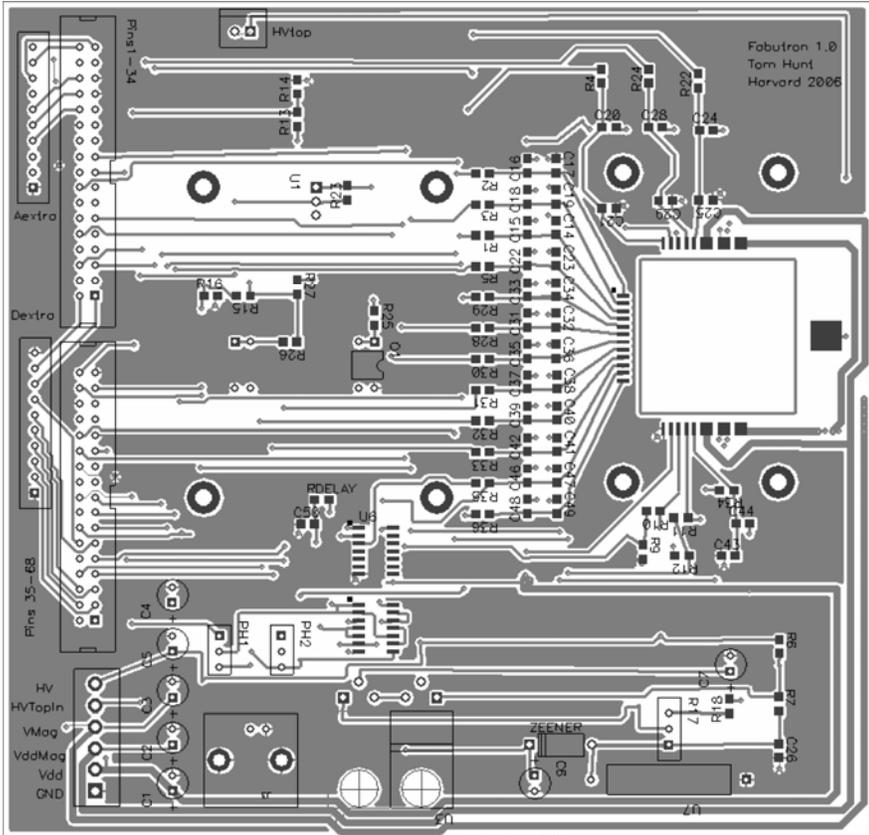
**Appendix F.   General advice for future IC / microfluidic chips**

- Visualize the entire system, especially packaging, throughout the design process.

- Simulate it before you build it.

- Always mount your chip in a replaceable chip carrier so you can rotate chips out without changing your experimental setup.

- It is worth your time to design a circuit board and software to interface with your chip.

- Be sure that you are building a device that you will continue working with until you publish the results. I spent several months building devices that were never novel enough to publish.

- On the other hand, once you have a winning device, push it to get the best data that you can.

- Take advantage of the outstanding staff members at Harvard. That means ask Steve your microfab questions, Stan your machining questions, and Jim your electronics questions

- Don't be afraid to ask for help.

- Meet people and build collaborations. It is amazing what you can learn while working with someone with a different background.